44th AIAA Aerospace Sciences Meeting and Exhibit
9 - 12 January 2006, Reno, Nevada

AIAA 2006-713

Review and Assessment of Turbulence Models for Hypersonic Flows: 2D/Axisymmetric Cases

Christopher J. Roy[a,*] and Frederick G. Blottner[b]

[a]*Aerospace Engineering Department, Auburn University, 211 Aerospace Engineering Building, Auburn, AL 36849-5338 USA*

[b]*Consultant, Albuquerque, NM USA*

*Corresponding author. Tel.: +1-334-844-5187; fax: +1-334-844-6803

E-mail addresses: cjroy@eng.auburn.edu (C. Roy)

Abstract

Turbulence modeling remains a major source of uncertainty in the computational prediction of aerodynamic forces and heating for hypersonic vehicles. The first goal of this paper is to update the previous comprehensive review published in 1991 by Settles and Dodson (G. S. Settles and L. J. Dodson, "Hypersonic Shock/Boundary-Layer Interaction Database," NASA CR 177577, April 1991). In their review, Settles and Dodson developed a methodology for assessing experiments appropriate for turbulence model validation and critically surveyed the existing hypersonic experimental database. We limit the scope of our current effort by considering only two-dimensional/axisymmetric flows in the hypersonic speed regime where calorically perfect gas models are appropriate. We extend the prior database of recommended hypersonic experiments by adding three new cases. The first two cases, the flat plate/cylinder and the sharp cone, are canonical test cases which are amenable to theory-based correlations, and these correlations are discussed in detail. The third case added is the two-dimensional shock impinging on a flat plate boundary layer. The second goal is to review and assess the validation usage of various turbulence models on the existing experimental database. Here we limit the scope to one- and two-equation turbulence models where integration to the wall is used (i.e., we omit studies involving wall functions). In order to preserve a models prior validation history, we omitted corrections to the standard turbulence models in cases where the impact of such corrections on low-speed flows had not been adequately addressed (either through a re-validation of the models on a wide range of low-speed test cases or theoretical arguments). A methodology for validating turbulence models is given, and turbulence model comparisons from various authors are compiled and presented in graphical form. Conclusions are drawn for those models which have been applied to a sufficiently wide range of two-dimensional/axisymmetric hypersonic flows, and recommendations for future experimental and modeling efforts are given.

1. Introduction

1.1. Background

Turbulence plays a key role in determining the aerodynamic forces and heating for hypersonic vehicles. However, experimental data for turbulence model validation are difficult to obtain. There are very few flight tests in the open literature, and these tests generally provide only small amounts of data, usually with large experimental uncertainties. There are many more ground-based wind tunnel tests on simplified geometries in hypersonic flow. These ground tests generally provide much more data than the flight tests, and usually with smaller experimental uncertainties. However, due to the extremely high velocities found in hypersonic flow, the hypersonic ground tests generally do not match the same freestream enthalpy levels typical of hypersonic flight. The validation of turbulence models with wind tunnel data thus generally involves significant extrapolation to flight enthalpies. Because of these difficulties in obtaining validation data for turbulent, hypersonic flows, designers are forced to rely heavily on computational fluid dynamics and the associated models for turbulence, chemistry, ablation, etc.

The current effort builds on the reviews by Settles and Dodson [1-4] conducted in the early 1990s. Differences between the Settles and Dodson reviews and the current work are that the current effort:

1. has different scope since only hypersonic flows (including those without shock waves) are considered,

2. includes new experimental data since 1994,

3. addresses the steps required for performing the turbulence model validation, and

4. takes the additional step of reviewing and assessing turbulence models as applied to the existing hypersonic experimental database.

The current article can be considered both an update to the Settles and Dodson work, as well as an extension which includes the steps of validating the turbulence models. Finally, we soften the Settles and Dodson requirement that the upstream boundary layer be fully characterized in cases where the predictive capabilities of the turbulence model are judged to be sufficiently good (i.e., flat plates/cylinders with natural transition).

1.2. Scope

The validation of turbulence models should necessarily include a wide range of flows. However, the extremely wide range of turbulent flows and available experimental data are enormous, so we are forced to limit the scope of this article. Furthermore, while we have endeavored to include all appropriate experimental and computational studies, it is inevitable that some qualified studies will be overlooked. We apologize in advance for such omissions.

Herein we consider only hypersonic flows, where the freestream Mach number is (somewhat arbitrarily) limited to values greater than or equal to five. In addition, only wall-bounded flows are considered, thus eliminating flows such as hypersonic mixing layers and jets. While there are

ongoing research efforts in advanced turbulence models such as Reynolds stress models and large eddy simulation, the most complex models currently employed in design studies (where a large number of parametric cases must be considered) are one- and two-equation turbulence models. We therefore limit the current study to these models. We also limit this study to models where integration of the governing equations to the wall is performed, thereby eliminating the use of wall functions. This choice was primarily driven by the fact that a majority of the cases of interest for hypersonic flows include shock-boundary layer interactions, where the assumptions inherent in the use of wall functions are difficult to justify. We further limit our scope to cases where the transition from laminar to turbulent flow occurs naturally, and where this transition location is specified in the experimental description. The focus here is not on the prediction of transition, which itself is a difficult challenge for hypersonic flows. Finally, the effects of surface roughness, ablation, chemical reactions, real gases, and body rotation are all neglected as the existing experimental database does not yet adequately address these phenomena.

In most cases, turbulence models are expected to be valid for a wide range of problems and not "tuned" for a very limited class of turbulent flows (this latter approach more closely resembles model calibration or parameter fitting than a true prediction). Therefore the testing of a turbulence model for high speed flows should include the evaluation of the model for all speeds and various flow geometries to determine its limitations. Here we limit our study to include only those models which have a well-established validation history over a wide range of flow conditions including low-speed flows. We therefore will not discuss efforts where the researchers propose model improvements, but do not address the effects of these model improvements on the prior model validation heritage. We strongly recommend that future high-speed turbulence modelers test their compressible flow model improvements on a standard set of incompressible flow as well, or at least give arguments as to why their corrections will not impact low-speed flows.

1.3. Molecular transport for hypersonic flows

Due to the difficulties of reproducing high enthalpy environments in ground-based facilities, the freestream static temperatures are often quite low, sometimes on the order of 50 K or below. In addition, the most common test gases are air and nitrogen. For these reasons, the model should be sure to use appropriate molecular models for viscosity and thermal conductivity. At standard temperatures, Sutherland's law can be used for the absolute molecular viscosity of air, and is given by

$$\mu = 1.458 \times 10^{-6} T^{3/2} / (T + 110.4) \quad \text{Units are kg/m/s} \tag{1}$$

where T is given in Kelvin. For air at lower temperatures (say below 100 K) and for nitrogen, Keyes model for viscosity should be used:

$$\begin{gathered} \mu = a_0 \times 10^{-6} \sqrt{T} / (1 + a_1 T_1 / T) \qquad T_1 = 10^{-a_2/T} \\ \text{Air:} \quad a_0 = 1.488 \qquad a_1 = 122.1 \qquad a_2 = 5.0 \\ \text{Nitrogen:} \quad a_0 = 1.418 \qquad a_1 = 116.4 \qquad a_2 = 5.0 \end{gathered} \tag{2}$$

The thermal conductivity can then be determined from the Prandtl number and the specific heat at constant pressure.

1.4. Turbulence

1.4.1. Physics

The Navier-Stokes equations contain all of the physics necessary to simulate turbulent flows. However, due to the wide range of length and time scales associated with simulating the turbulence at Reynolds numbers typical of flight vehicles, this direct simulation approach for turbulence is well beyond the capabilities even of today's fastest computers. Engineers are thus forced to rely on turbulence models, which account for the effects of the turbulence rather than simulate it directly. The simplest turbulence modeling approach is Reynolds-Averaged Navier-Stokes (RANS), where all of the turbulent length and time scales are modeled via temporal filtering of the Navier-Stokes equations.

1.4.2. Averaging procedures

The following development utilizes both Reynolds (overbar) and Favre (overtilde) averaging [5]. For Reynolds (or time) averaging, the instantaneous variables (f) are decomposed into mean ($\bar{f}$) and fluctuating (f') components

$$f = \bar{f} + f'$$

The mean is found from an average in time for steady problems or an ensemble average for transient problems. The average in time is

$$\bar{f} = \frac{1}{T}\int_{t}^{t+T} f(x_i, t)dt \tag{3}$$

where T is some time scale much larger than the turbulent time scales, but much smaller than any large-scale unsteadiness inherent in the problem of interest. For Favre (or density-weighted) averaging, the instantaneous variables (f) are broken down into density-weighted mean ($\tilde{f}$) and fluctuating (f'') components

$$f = \tilde{f} + f''$$

For the density-weighted mean, we thus have

$$\tilde{f} = \frac{1}{\bar{\rho}T}\int_{t}^{t+T} \rho(x_i, t)f(x_i, t)dt = \overline{\rho f} / \bar{\rho} \tag{4}$$

1.4.3. Compressibility effects

Typically turbulence models have been developed for incompressible flows and then extended without much change to compressible flows. This approach in many cases is not adequate. For complex turbulent flows, Coakley et al. [86] have recommended corrections to apply to the two-equation $k-\varepsilon$ and $k-\omega$ turbulent eddy viscosity models. In addition, Aupoix and Viala [87] have proposed corrections to the $k-\varepsilon$ model for compressible flows. The authors have used flat plate flows and mixing layers to assess the compressible corrections introduced. Significant efforts to assess turbulence models for compressible flows have occurred at NASA Ames Research Center. The results of these investigations have been published by Horstman [88], Horstman [89], Coakley and Huang [84], Huang and Coakley [90], Coakley et al.[86], Bardina et al. [91], and Bardina et al. [92]. See Appendix A for additional discussion of the compressibility effects for hypersonic flows.

2. Turbulence models

2.1. One-equation models (eddy-viscosity transport models)

2.1.1. Spalart-Allmaras (SA)

A transport equation for determining the eddy viscosity with near-wall effects included has been developed by Spalart and Allmaras [7], [8]. The accuracy of the predictions with the Spalart-Allmaras model is fairly insensitive to the y^+ spacing at the wall relative to the two-equation models, at least for high-speed flows [9]. Our experience with this model suggests that it has a good combination of accuracy and robustness for attached flows. While stable for large y^+ values, the maximum for accurate solutions should be roughly $y^+ \leq 1$.

2.1.2. Goldberg (UG)

Goldberg has developed a one-equation turbulence model [158], [97].

2.1.3. Menter one-equation model (MTR)

Menter has developed a one-equation turbulence model [6].

2.2. Two-equation models

2.2.1. Jones and Launder high Reynolds number k-ε (kεJL)

The basic *k*-ε model was developed by Jones and Launder [10] in 1972, and is valid for high Reynolds number flows only. Damping functions or wall functions must be used in order to handle wall-bounded flows.

2.2.2. Launder and Sharma (standard) k-ε (kεLS)

The standard *k*-ε formulation is appropriate for high Reynolds number flows only. In order to apply this model to wall-bounded flows, damping terms may be added to allow this model to be

integrated to the wall. The standard model was revised by Launder and Sharma [11] in 1974. The *k*-ε model is generally good for free shear flows, but will not be as accurate for wall-bounded flows as the *k*-ω models, especially in the presence of adverse pressure gradients. It is recommended that the y^+ values at the wall be kept below one.

2.2.3. Chien k-ε (kεCH)

Chien has developed a low Reynolds number k-ε model [82].

2.2.4. Nagano and Hishida k-ε (kεNH)

Nagano and Hishida have developed a low Reynolds number k-ε model [126].

2.2.5. Rodi k-ε (kεR)

Rodi has developed a low Reynolds number k-ε model [160].

2.2.6. So k-ε (kεSO)

So has developed a low Reynolds number k-ε model [83].

2.2.7. Huang and Coakley k-ε (kεHC)

Coakley and Huang have developed a low Reynolds number k-ε model [84].

2.2.8. Wilcox 1988 k-ω (kω88)

The Wilcox 1988 k-ω model [132] is generally better than the *k*-ε model for wall-bounded flows, especially in the presence of adverse pressure gradients. It is recommended that the y^+ values at the wall be kept well below one. One problem with this original Wilcox *k*-ω model is the sensitivity of the results to the freestream ω levels.

2.2.9. Wilcox 1988 k-ω low Reynolds number (kω88LR)

Wilcox has also developed a low Reynolds number version [132] of his 1988 k-ω model.

2.2.10. Wilcox (1998) k-ω (kω98)

In 1998, Wilcox updated his original *k*-ω turbulence model to more accurately predict free shear flows [5]. This updated version will be referred to as the Wilcox (1998) *k*-ω model. The Wilcox (1998) *k*-ω model is generally better than the *k*-ε model for wall-bounded flows, especially in the presence of adverse pressure gradients. It is recommended that the y^+ values at the wall be kept well below one. While the sensitivity of the results to the freestream ω levels is indeed reduced in the 1998 version of the model [5], some sensitivity effects remain for high-speed flows [12].

2.2.11. Menter Shear Stress Transport k-ω (SST)

The Menter *k*-ω model is a blending of the *k*-ω model near walls and a transformed *k*-ε model in shear layers and the freestream [13]. The Shear Stress Transport (SST) version has obtained good results for a wide range of flows.

2.2.12. Menter Baseline k-ω (BSL)

The Menter *k*-ω model is a blending of the *k*-ω model near walls and a transformed *k*-ε model in shear layers and the freestream [13]. The baseline (BSL) version has also obtained good results for a wide range of flows.

2.2.13. Smith k-*l* (k*l*)

Smith has developed a two-equation k-*l* model [105], [163].

2.2.14. Robinson and Hassan k-ζ (kζ)

It is generally acknowledged that the failure of the standard *k*-ε model to accurately predict a wide variety of flows is due to inadequate modeling of the dissipation equation. Robinson and Hassan [14], [15], have developed a new two-equation turbulence model based on the vorticity variance (enstrophy) equation which has demonstrated good predictive capability for a wide-variety of flows. A number of modeled terms in the enstrophy equation are included with the goal of incorporating additional physics into the equation governing the dissipation of turbulent kinetic energy. One major advantage of implementing the *k*-ζ model into a Navier-Stokes code is that the model does not rely on damping or wall functions.

2.2.15. Coakley q-ω (qω)

Coakley has developed a two-equation k-*l* model [85].

2.3. Physical freestream turbulence quantities

One method for determining the freestream turbulence properties is as follows. For the two-equation models, the specification of a freestream turbulence intensity (*Tu*) can be used to determine the turbulent kinetic energy in the freestream from

$$k = \frac{1.2}{2}(TuV_\infty)^2 \tag{5}$$

where *Tu*=0.1 corresponds to a freestream turbulence intensity of 10%. However, the experimental measurement of ε (or ω, ζ, etc.) is extremely difficult. As a result, the dissipation variable is often determined by specifying the ratio of turbulent to laminar viscosity, μ_t/μ, i.e.,

$$\varepsilon = \frac{C_\mu \rho k^2/\mu}{\mu_t/\mu} \tag{6}$$

or

$$\omega = \frac{\rho k/\mu}{\mu_t/\mu} \tag{7}$$

For one-equation eddy viscosity turbulence models, the transported variable is simply found from the μ_t/μ ratio.

2.3.1. Effects on transition

High freestream turbulence intensity levels can lead to early transition from laminar to turbulent flow. This phenomenon is often referred to as bypass transition (since the natural transition mechanisms are bypassed) or more recently as transition due to a High Disturbance Environment (HDE) [16]. While some turbulence models also provide a transition prediction capability, the transition process is complex, especially for high-speed flows, and its modeling is beyond the scope of the current work.

2.3.2. Effects on turbulence

Experimental evidence [17], [18] suggests that surface properties (e.g., shear stress) in the fully-developed turbulent region are generally not affected by freestream turbulence intensity, at least in the case of low-speed flows. Thus it is expected that there should be little or no effect of the freestream turbulence levels on the mean flow predictions.

2.4. Smooth wall boundary conditions

For the Spalart-Allmaras model, the transported eddy viscosity is zero at solid walls. For the two-equation models, the turbulent kinetic energy k is specified to be zero at the surface. Similarly, the specific dissipation rate ε is often set to zero at solid surfaces. For the k-ω models, the omega value for the first cell off the wall ω_1 may be set to

$$\omega_1 = \frac{6\nu}{\beta_0(\Delta y)^2} \tag{8}$$

where Δy is the distance from the cell center to the wall and $\beta_0 = 9/125$ for the Wilcox model and $\beta_0 = 3/40$ for the Menter model. The wall value for omega is then set to

$$\omega_w = 10\frac{6\nu_w}{\beta_0(\Delta y)^2} \tag{9}$$

The interior ghost cell value for ω is then set so that the second derivative of ω at the wall is zero, i.e.,

$$\left.\frac{\partial^2 \omega}{\partial y^2}\right|_w = 0 \tag{10}$$

3. Turbulence model validation methodology

The turbulence model validation methodology presented herein is influenced heavily by the work of Marvin [19] and Marvin and Huang [20]. The proposed validation framework [12] includes guidelines for documentation, model sensitivities, and model validation. In addition, it is recommended that a significant effort be made to estimate the numerical accuracy of the simulations as part of the validation procedure. Listed below are six criteria for assessing the models. The first three criteria (3.1-3.3) focus on the thorough documentation of the model evaluation efforts. Details of the flow case and the models used must be given in enough detail so that the results are reproducible by other researchers. The last three criteria (3.4-3.6) list the specific standards for evaluating the models. The turbulence models should be evaluated by first establishing the numerical accuracy of the simulations, then by examining model sensitivities, and then finally by validation comparisons to experimental data.

3.1. Cases examined

Details of (or references to) the specific flow problem examined should be given including flowfield geometry and relevant physics (e.g., ideal gas versus equilibrium thermochemistry, transport properties, etc.). All required boundary conditions should be listed including inflow and outflow conditions, wall boundary conditions for temperature, incoming boundary layer thickness, freestream turbulence intensities, a measure of the freestream turbulence dissipation rate, etc. One of the difficulties encountered in the specification of computational boundary conditions is that the level of information required may not be fully characterized in the experiment. For example, a large number of otherwise excellent hypersonic validation data sets fail to report the thickness of the turbulent boundary layer upstream of the interaction region; this information is especially important when the boundary layer is tripped to force transition to turbulence. It should be clearly stated whether the flow is fully turbulent or transitional. Finally, the data available for model validation should be given (e.g., feature location, surface quantities, turbulent field profiles, etc.).

3.2. Turbulence models examined

It should be clearly stated which form of the turbulence model is employed. It is strongly recommended that the standard model constants be used so as to build on prior turbulence model validation efforts. Where applicable, the form of the low Reynolds number wall damping functions used should be stated. The treatment of the near-wall regions should also be listed (i.e., integration to the wall versus wall functions).

3.3. Model implementation issues

The form of the governing equations should be given. For example, different results may be found when employing the full Navier-Stokes, thin-layer Navier-Stokes, parabolized Navier-Stokes, viscous shock layer equations, or boundary layer equations. The boundary conditions employed in the simulation, including both flow properties and turbulence quantities, should be specified. Finally, any limiting of the turbulence quantities should be discussed. For example, limiting of the ratio of production to dissipation of turbulent kinetic energy to some ratio (e.g., P/

$\rho\varepsilon \leq 5$) is often used. In addition, realizeability constraints on the turbulence variables and/or normal turbulent stresses [21] should also be discussed.

3.4. Efforts to establish numerical accuracy

The numerical accuracy of the simulations is an important factor to consider when comparing to experimental data; for example, if the numerical accuracy of pressure distributions are estimated to be ±20%, then agreement with experimental data within 5% does not mean the model is accurate within 5%. The first step towards determining the accuracy of the simulations is code verification, i.e., building confidence that the code is solving the governing equations correctly. Code verification can be performed by comparison of the code results to exact solutions to the governing equations, highly accurate numerical benchmark solutions, or by the method of manufactured solutions [22], [23]. Once one has confidence that the code is verified, then the accuracy of the individual solutions must be verified. Solution accuracy includes assessing the errors due to incomplete iterative convergence [12], temporal convergence for unsteady problems, and grid convergence. Methods for estimating the grid convergence errors based on systematic grid refinement [24] tend to be the most reliable and are applicable to any type of discretization including finite-difference, finite-volume, and finite-element. Grid convergence error estimates for hypersonic flows are complicated by the presence of shock waves, which tend to reduce the spatial order of accuracy to first order on sufficiently refined meshes [25], [26], regardless of the nominal order of the spatial discretization scheme.

3.4.1. Grid convergence

Grid (or spatial) convergence for steady-state solutions can be estimated by performing computations on two or more meshes. The Richardson extrapolation procedure [22] can be used to obtain an estimate of the exact solution from the relation

$$f_{RE} = f_1 + \frac{f_1 - f_2}{3} \tag{11}$$

where 1 denotes the fine mesh and 2 the coarse mesh. This relation assumes that the numerical scheme is second-order, that both mesh levels are in the asymptotic grid convergence range, and that a mesh refinement factor of two (i.e., grid doubling) is used. A more general expression for the Richardson extrapolated value is given by

$$f_{RE} = f_1 + \frac{f_1 - f_2}{r^p - 1} \tag{12}$$

where r is the grid refinement factor and p is the order of accuracy (either formal or observed). The formal order of accuracy can be found from a truncation error analysis of the discretization method. If solutions are available on three meshes, then the observed order of accuracy can be calculated from

$$p = \frac{\ln\left(\frac{f_3 - f_2}{f_2 - f_1}\right)}{\ln(r)} \tag{13}$$

where 2 now denotes the medium mesh and 3 the coarse mesh. Here it is assumed that the refinement factor between the coarse and medium mesh is equal to that between the medium and fine mesh.

The accuracy of the solutions can be estimated using the exact solution approximated by f_{RE} which gives the solution error as

$$\% \text{ Error of } f_k = 100\% \times \frac{f_k - f_{RE}}{f_{RE}} \tag{14}$$

where k = 1, 2, etc. is the mesh level. Since it is equally possible that the true exact solution is above or below this estimate, it is generally recommended that some factor of safety be included in the error estimate. Roache combines the concept of a factor of safety along with absolute values to produce an error band rather than an error estimate. The resulting error (or numerical uncertainty) estimate is referred to as the Grid Convergence Index, or GCI [24]. The GCI thus produces an error (or uncertainty) band around the fine mesh solution and is given by

$$GCI = \frac{F_s}{r^p - 1}\left|\frac{f_2 - f_1}{f_1}\right| \tag{15}$$

When solutions from only two meshes are available, Roache recommends a factor of safety of three. For three meshes where the observed order of accuracy agrees with the formal order of accuracy, a much less conservative value of F_s = 1.25 is suggested.

3.4.2. Iterative convergence

When implicit or relaxation methods are employed, an additional error source arises due to iterative convergence. The numerical error due to incomplete iterative convergence is usually assessed by evaluating norms of the residuals, where the residual is defined by substituting the current solution into the discretized governing equations. For steady-state flows, the residual is calculated with the steady-state terms only, even if the temporal terms are included to speed up the convergence process. The residuals will approach zero as the steady-state solution is reached and the current solution satisfies the discretized form of the steady equations. These residuals can generally be driven to zero within machine round-off tolerance; however, this extreme level of iterative convergence is generally not necessary. Many studies (e.g., [12], [27]) suggest that for computational fluid dynamics simulations, the residual reduction levels correlate quite well with the actual iterative error in the flow properties.

3.5. Turbulence model sensitivities

Model sensitivity studies should be performed to determine practical guidelines for model use. A systematic study of the effects of the freestream turbulence levels on the numerical predictions should be performed. The normal spacing at the wall (y^+) should also be varied in order to test model robustness and accuracy for both integration to the wall and wall functions. In addition to establishing the solution accuracy, a mesh refinement study can also be used to determine a given turbulence model's sensitivity to the mesh density.

The sensitivity to the freestream turbulence levels can manifest in two forms: changes in the location of transition from laminar to turbulent flow and changes in the eddy viscosity levels in the turbulent region. The former may actually be a desirable characteristic when bypass transition is being modeled, while the latter is generally undesirable. Experimental evidence [28], [29] suggests that surface properties (e.g., shear stress) in the fully-developed turbulent region are generally not affected by freestream turbulence intensity, at least in the case of low-speed flows.

3.6. Turbulence model validation results

Model validation results should be presented in a quantitative manner rather than qualitatively. For example, the percent difference between the predictions and experiment should be plotted or explicitly stated. Whenever possible, experimental error bounds should be given for all measurements used for validation. These error bounds should include contributions from instrument uncertainty, experimental run-to-run uncertainty, physical model alignment uncertainty, flowfield nonuniformities, etc. Bias errors are generally difficult to quantify, so if possible, multiple measurement techniques should be employed and, furthermore, tests in multiple facilities should be performed. Techniques are available for converting some experimental bias errors into random uncertainties [166].

4. Validation data

The validation of turbulence models must rely on real-world observations, i.e., experimental data, to establish model accuracy. The experimental data have been mainly obtained from wind tunnels, where detailed measurements can be performed, rather than in flight. There is a long history of high speed turbulent wind tunnel flow experiments. Compilation of experimental data for compressible turbulent boundary layers up to approximately 1980 is given in AGARD reports by Fernholz and Finley [30], [31], [32]. For high speed compressible turbulence, an experimental database has been developed by Settles and Dodson [1], [2], [3], [4] for three-dimensional shock-wave boundary layer interactive flows, attached boundary layers, and free shear flows. The hypersonic portions of these databases are described below along with other more limited reviews. In addition, a discussion is provided on the role of both correlations and Direct Numerical Simulation (DNS) data in turbulence model validation.

4.1. AGARD experimental review

There has been a significant effort by Fernholz and Finley [30], [31], [32] to document available experimental data for compressible turbulent flow up to about 1980. A total of 77 experiments are reviewed with 59 given in Ref. [30] and 18 given in Ref. [31]. A further compilation of compressible boundary layer data is given in Ref. [32]. The number of hypersonic experiments is limited. In addition, these reports do not provide a clear recommendation for a limited list of experiments that should be used for validation of turbulence models.

4.2. Experimental reviews by Settles and Dodson

A very careful assessment of validation experiments for compressible turbulent flow was performed by Settles and Dodson in the early 1990s [1], [2], [3], [4]. The list of the eight **necessary criteria** is given below (in abbreviated form) in the order in which they were applied.

1. *Baseline applicable:* Supersonic or hypersonic turbulent flow with shock wave/boundary layer interaction
2. *Simplicity:* Experimental geometries sufficiently simple that they may be readily modeled by CFD methods
3. *Specific applicability:* Must provide useful experimental data for testing turbulent modeling
4. *Well-defined experimental boundary conditions:* Sufficient boundary condition data must be supplied to allow CFD solutions to be performed without any assumptions
5. *Well-defined experimental error bounds:* Must provide an analysis of the accuracy and repeatability of the data
6. *Consistency criterion:* all data must be consistent
7. *Adequate documentation of data:* data must be available in tabulated form and capable of being put into machine-readable form
8. *Adequate spatial resolution of data:* sufficient data must be presented such that key features of the flow are clearly resolved

In addition to the above necessary criteria, the following **desirable criteria** were also used in the evaluation of the experiments:

1. *Turbulent data:* Turbulent properties (Reynolds stress, etc.) of the flow field are given
2. *Realistic test conditions:* Flow conditions and boundary conditions typical of actual hypersonic flight
3. *Non-intrusive instrumentation:* Preference is given to this type of experimental data
4. *Redundant measurements:* Preference is given to experiments in which redundant data are taken

5. *Flow structure and physics:* Preference is given to those experiments which reveal flow structure and physical mechanisms

The initial study [1] examined 105 experimental studies of shock wave interactions with turbulent boundary layers at Mach 3 or higher. There are 5 experiments at hypersonic conditions that were considered as acceptable while 7 experiments at supersonic conditions that were considered as acceptable. The second study [2] examined 39 experiments of attached boundary layers with pressure gradients and 45 supersonic turbulent mixing layer experiments. The authors recommended 9 experiments as acceptable for attached boundary layers with pressure gradients and 3 experiments as acceptable for supersonic turbulent mixing layers. The last report [3] has reviewed 7 additional experiments and has corrections to 3 of the previous reviewed experiments. A summary of the supersonic and hypersonic shock/boundary-layer interaction experiments has been published in Ref. [4].

All of the references to the acceptable supersonic experiments are not included in the list of references of this review but are available in Ref. [4]. For hypersonic flow conditions, 7 experiments on 6 flow geometries are classified as acceptable for validation of turbulence models. The data for all of the acceptable experiments is tabulated in the Settles and Dodson reports and available in electronic format. The Settles and Dodson flow geometries have been numbered with the first four being two-dimensional or axisymmetric and the next four being three-dimensional experiments. Additional flow geometries or flow problems will be discussed in this paper, with a total of 12 validation cases being recommended. The Settles and Dodson flow geometries are as follows:

(1) 2D Compression Corner

For a freestream Mach number of 9, the wall pressure and heat flux have been determined in the experiment of Coleman and Stollery [33].

(2) Cylinder with Conical Flare

For a freestream Mach number of 7, the wall pressure and heat flux have been measured and flow field surveys have been made in the experiment of Kussoy and Horstman [34].

(3) Cone with Conical Flare

For a freestream Mach number of 11 and 13, the wall pressure and heat flux have been measured in the experiment of Holden et al. [35] and Holden [36].

(4) Axisymmetric Impinging Shock

For a freestream Mach number of 7, the wall pressure, skin friction and heat flux have been measured and flow field surveys have been made in the experiment of Kussoy and Horstman [37].

(5) Flat Plate with Two Fins (Crossing Shocks)

For a freestream Mach number of 8.3, the wall pressure and heat flux have been measured and surveys in the flow field have been made in the experiment of Kussoy and Horstman [38].

(6) Flat Plate with 3D Fin

For a freestream Mach number of 6, the wall pressure and heat flux have been measured in the experiment of Law [39]. For a freestream Mach number of 8.2, the wall pressure and heat flux have been measured and surveys in the flow field have been made in the experiment of Kussoy and Horstman [40] and [41]. For hypersonic flow at Mach 4.9, the Rodi and Dolling experiments [241] are also acceptable.

(7) Cylinder with Skewed Flare

For hypersonic flow, Settles and Dodson have no available experiments.

(8) 3D Compression Corner with Sweep

For hypersonic flow, Settles and Dodson have no available experiments.

4.3. ERCOFTAC database

A comprehensive database of European work is being developed on the web at the following location: http://ercoftac.mech.surrey.ac.uk/ and has the name, European Research Community on Flow, Turbulence and Combustion (ERCOFTAC). A complete review of this database has not yet been performed, but most of the databases are presently very limited as this effort is in the early stages of development.

4.4. Holden database

A review of the hypersonic experiments that have been performed at Calspan has been made by Holden and reported in Ref. [42]. There are numerous experiments that have been performed that are of interest:

(1) Sharp and blunted cones at Mach 11 with laminar, transitional and turbulent flow have been investigated. This work is documented by Holden [43].

(2) Flow over a cone/flare model at Mach 11 to 16 has been investigate. Earlier experiments on this flow geometry is one of the Settles and Dodson acceptable experiments. This work is documented by Holden [44].

(3) 2D compression corner [42]

(4) Flat plate with 3D fin [36], [42]

(5) Flat plate [42], [45], [46]

(6) 2D impinging shock [42], [47], [48]

4.5. Other limited reviews

It has been nearly 15 years since a comprehensive review has been performed on the new experiments in hypersonic flow. There have been several limited reviews of hypersonic experiments at the California Institute of Technology by Hornung [49] and hypersonic flow research in Europe by Groenig and Olivier [50].

4.6. Theoretical correlations

Theory-based correlations exist for two of the simpler geometries discussed herein: the flat plate and the sharp cone. Theoretical results which correlate well with a large number of experimental data sets will mitigate the experimental bias errors that vary from facility to facility as well as bias errors associated with a given measurement technique.

4.6.1. Correlations for the flat plate

The turbulence properties of interest are the wall skin friction, heat transfer, and profiles of velocity and temperature across the boundary layer. A detailed discussion of the theoretical correlations for the flat plate can be found in Appendix B. The main results are summarized below.

Correlation of Skin Friction Data

The transformation theories transform the experimental compressible skin friction and momentum thickness Reynolds number to incompressible values as follows for the Van Driest II theory [115]

$$\begin{aligned} C_{fvD} &= F_c C_f \qquad F_c \text{ skin friction transformation function} \\ Re_{\theta vD} &= F_\theta Re_\theta \qquad F_\theta \text{ momentum thickness Reynolds No. transformation function} \end{aligned} \tag{16}$$

Therefore if the theory is accurate, the transformed skin friction C_{fvD} and momentum thickness Reynolds number $Re_{\theta vD}$ should be the same as the incompressible values.

$$C_{fvD} \approx C_{f,\,i} \qquad Re_{\theta vD} \approx Re_{\theta,\,i}$$

The transformation functions are given by

$$\begin{aligned} F_c &= rm/(\sin^{-1}\alpha + \cos^{-1}\beta)^2 \\ F_\theta &= \mu_e/\mu_w \qquad F_s = F_\theta/F_c \end{aligned} \tag{17}$$

where

$$m = M_e^2(\gamma - 1)/2 \qquad F = T_w/T_e$$

$$r = \text{Recovery factor} = 0.9$$

$$A = \sqrt{rm/F} \qquad B = (1 + rm - F)/F$$

$$\alpha = (2A^2 - B)/\sqrt{4A^2 + B^2}$$

$$\beta = B/\sqrt{4A^2 + B^2}$$

The local incompressible skin friction is evaluated from Karman-Schoenherr relation which is considered the most accurate fit to the incompressible experimental data:

$$C_{f,i} = \frac{1}{\log(2Re_\theta|_{inc})[17.075\log(2Re_\theta|_{inc}) + 14.832]} \tag{18}$$

Squire [72] estimates that the accuracy of the Van Driest II correlation is within ±3% for the flat plate. Based on the sometimes erratic agreement between experiments and the correlation, we feel that this error estimate is somewhat optimistic.

Correlation of Heat Transfer

Reynolds analogy is used to predict the wall heat flux, which is expressed at the Stanton number

$$St = q_w/[\rho_e u_e(H_w - H_{aw})] \tag{19}$$

Reynolds analogy is written in terms of the compressible skin friction

$$2St/C_f = R_{af} = \text{ Reynolds analogy factor} \tag{20}$$

Experiments indicate that $0.9 < R_{af} < 1.3$. While there are insufficient reliable experimental data to establish the Reynold analogy factor, for hypersonic flows the best choice is $R_{af} \cong 1$. Additional work is needed to establish the appropriate value for the Reynolds analogy factor.

Mean Velocity Profiles

In the log-law region, similarity of the compressible velocity $\tilde{u}$ is obtained with the Van Driest velocity transformation. The transformed Van Driest expression uses the inner turbulence variables

$$u^+ = \tilde{u}/u_\tau \qquad y^+ = \bar{\rho}_w y u_\tau/\mu_w \qquad u_\tau = \sqrt{\tau_w/\bar{\rho}_w} \qquad l_m^+ = \kappa y^+ D_f$$

and is given as

$$u_c^+ = \frac{\tilde{u}_c}{u_\tau} = \frac{(\tilde{u}_e/u_\tau)}{A}\left\{\text{asin}\left[\frac{2A^2(\tilde{u}/\tilde{u}_e) - B}{\sqrt{B^2 + 4A^2}}\right] - \text{asin}\left(\frac{-B}{\sqrt{B^2 + 4A^2}}\right)\right\} = \frac{1}{\kappa}\ln(y^+) + C \tag{21}$$

where A and B are defined as

$$A^2 = \beta u_e^2/T_w = Pr_T u_e^2/2c_p T_w \qquad B = -\frac{\alpha u_e}{T_w} = \left(\frac{T_e}{T_w}\right) - 1 + A^2 = -\frac{Pr_T u_e q_w}{c_p T_w \tau_w}$$

Huang, Bradshaw, and Coakley [71] have obtain the transformed velocity from the wall to the edge of the boundary by taking into account the viscous sublayer and by including a wake function. This procedure gives the skin friction, velocity, and temperature profiles as a function of the Reynolds number. It has been developed as a seven step procedure with iteration of the solution until converged. See Appendix B for details.

Mean Temperature Profiles

The general form of the mean temperature across the zero pressure gradient turbulent compressible boundary layer as a function of the mean turbulent velocity and turbulent kinetic energy is

$$T = T_w - \alpha\tilde{u} - \beta\tilde{u}^2 - \gamma_T k \tag{22}$$

Huang, Bradshaw, and Coakley [71] (HBC) have developed the temperature equation by neglecting the convective terms in the momentum and energy equations. Their analysis (see Appendix B) yields the following relations for the variables in Eq. (22)

$$\alpha = (Pr_T/c_p)(q_w/\tau_w) \qquad \beta = Pr_T/2c_p \qquad \gamma_T = Pr_T/c_p \tag{23}$$

4.6.2. Correlation for the sharp cone

In the correlation of the cone properties, there are three items that are needed.

1) *Transformation of compressible boundary layer equations (Dorodnitsyn and Howarth) and properties to incompressible equations and properties:* This item has been discussed in the section concerned with the flat plate case (Section 4.6.1). The Van Driest II theory [115] is considered the best transformation for the correlation of the surface skin friction and heat transfer properties, but the Huang, Bradshaw, and Coakley approach should also be considered.
2) *Reynolds analog factor:* For the prediction of the heat transfer for flat plates, Reynolds analogy is used and has been discussed in the flat plate section (Section 4.6.1).
3) *Transformation of cone boundary layer equations (Mangler-Dorodnitsyn-Howarth) and properties to flat plate equations and properties:* The cone to flat plate transformation for the compressible properties is the new item that is needed to correlate the sharp cone properties.

Theories for cone to flat plate Mangler transformation are usually of the form

$$(C_f)_{Cone}/(C_f)_{FlatPlate} = (St)_{Cone}/(St)_{FlatPlate} = G(Re, M_e, T_e/T_e)$$

The Mangler transformation parameter G for compressible flow could be a function of the boundary layer edge Reynolds number based on x or θ, M_e, and T_w/T_e. In Appendix C is a brief indication of some of the contributions to this issue.

One of the problems with the sharp cone is the lack of a theoretical correlation of the experimental data to use as a benchmark solution. For laminar flow, the skin friction and heat transfer for a flat plate are multiplied by $\sqrt{3}$ to obtain the cone values. There does not appear to be a well establish approach to transform the turbulent flat plate results to the cone. Van Driest [74] has suggested an approximate approach that has been developed further in Ref. [75] using the von Karman momentum integral relation. The flat plate skin friction and wall heat flux are multiplied by a scale factor S_f that gives the *Cone Rule* as follows:

$$(C_f)_{cone} = S_f\,(C_f)_{plate} \qquad (q_w)_{cone} = S_f\,(q_w)_{plate}$$
$$S_f = \sqrt{3} = 1.732 \text{ for laminar flow} \qquad S_f \approx 1.13 \text{ for turbulent flow} \tag{24}$$

In the development of the cone rule it has been assume that the skin friction is a function of the momentum thickness and is expressed in the following form for both the flat plate and cone:

$$C_f = C_0 Re_\theta^{-m} \qquad C_f = \left(\frac{C_0 \rho_e u_e}{\mu_e}\right)\theta^{-m} \qquad \frac{1}{8} \le m \le \frac{1}{4} \qquad C_0 = \text{Constant} \tag{25}$$

A correlation of the heat transfer on axisymmetric flight vehicles with flat plate relations has been investigated by Zoby and Sullivan [76] and an additional correlation including ground data has been investigated by Zoby and Graves [77]. The former includes six references for experimental data on sharp cones where the Mach number varies from 2.0 to 4.2. An assessment of the theoretical correlations for sharp cones was given in Ref. [78].

4.7. Direct numerical simulation database

The numerical solution of the unsteady Navier-Stokes equations with refined grids as formulated in the Direct Numerical Simulation (DNS) and Large Eddy Simulations (LES) methods have potential of providing an accurate numerical simulation database with limited or no turbulence modeling assumptions. As computer speed and memory size have increased, the accuracy and capabilities of these computational fluid dynamic approaches have increased and will increase in the future. Next a brief indication is given of the turbulent flat plate and sharp cone flow problems that are being solved with the DNS and LES methods.

Martin [189]

Martin [189] has started to develop a DNS database of hypersonic turbulent boundary layer flows over a flat plate. She provides a review of previous DNS solutions that have been obtained for high speed compressible flows. The list includes a review of other work as well as her previous papers with co-workers. Martin has obtained DNS solutions for perfect gas and reacting air flows over a flat plate. Martin [189] presented DNS solutions for perfect gas flow with the gas viscosity modeled with a power law dependence on temperature. The simulations use freestream conditions corresponding to an altitude of 20 km and the Mach number varies from 3 to 8. The wall temperature is specified to be nearly the adiabatic temperature. At Mach 8, the wall temperature is 2713 K and would result in significant dissociation of the oxygen in air. The perfect gas model is not adequate to simulate these physical flow conditions. From the simulation solutions obtained, the mean flow velocity across the boundary layer has been determined, then transformed with the Van Driest transformation to incompressible form, and presented in figures for the cases simulated. No information is presented on the wall skin friction and heat transfer. This work is important as it is starting to provide useful DNS solutions at hypersonic flow conditions. However, there is a need to extend this work by obtaining simulations with a gas model that are more appropriate for the flow conditions.

Yan et al. [188]

Yan et al. [188] have obtained LES solutions with the Monotonically Integrated LES (MILES) technique for flat plate flow at Mach number 2.88 and 4. Both adiabatic and isothermal wall boundary conditions are used. The authors have provided a list of researchers that have studied compressible LES with no work performed at hypersonic flow conditions. The authors velocity profile predictions are compared to the law of the wall analysis and experimental data of Zheltovodov at Mach 2.9 and 3.74. LES temperature profiles are also compared to experimental data. The comparison for velocity and temperature at Mach 2.9 are good but the comparison at Mach 4 is poor. The interesting results of this investigation are concerned with heat transfer and Reynolds analogy. The authors indicate that Reynolds analog factor is $R_{af} = 2St/C_f = 1/Pr_{tm} = 1.124$ where the mean Prandtl number $Pr_{tm} = 0.89$. At Mach 4, LES solution gives $R_{af} = 1.23$ while the experimental value is $R_{af} = 1.12$. The Reynolds analog factors differ by 10%. The simulations obtained in this article indicate the potential of the LES technique to help valid turbulence models; however, the subgrid scale model required in LES is a limitation of this approach.

Pruett and Chang [229]

The Pruett and Chang [229] investigations are concerned with DNS of hypersonic boundary layer flows on sharp cones and cone-flare models. The initial work in 1995 is an approximate simulation of the geometry and flow conditions in the wind tunnel experiment of Stetson et al. [216]. A 7 deg. half-angle cone in a Mach 8 flow is simulated. The inviscid flow at the edge of the boundary layer is specified and the wall temperature is specified as the laminar adiabatic wall temperature, which is given in Figure 11 as 611 K. The free-stream properties are estimated from the Sims tables, which give the total temperature as 733 K, static temperature 53 K, and the unit Reynolds number as 3.407×10^6/m. Pruett and Chang [230] in 1998 published an investigation of DNS of hypersonic boundary layer flow on a flared cone. The DNS solution is for the quiet (low freestream turbulence) wind tunnel experiment of Lachowicz et al. [227], where the free-stream turbulence has been reduced significantly. The axial length of the cone-flared model is 0.51 m and the sharp cone axial length is 0.254 m. The free-stream flow conditions for the simulation are specified as Mach number 8, static temperature 55 K, total temperature 450 K, and unit Reynolds number 8.85×10^6/m. In both of the above DNS the air viscosity is determined with Sutherland viscosity law and a perfect gas model is used. Although the Pruett and Chang DNS computations do not provide useful information on fully developed turbulent flow on the conical part of the models, the numerical simulations indicate the future potential for providing valuable data for validation of compressible turbulence models.

Summary

For flows without chemical reactions and for flight conditions, the wall temperature needs to be sufficient low. The maximum gas temperature occurs in the boundary layer due to viscous dissipation and can be sufficiently high to produce vibrational excitation. Complete simulation without chemical reactions requires a vibrational nonequilibrium model. The solutions from the complete model can be bounded by using perfect gas and thermally perfect gas models, which makes DNS solutions with these models valuable. The gas models need a more appropriate

viscosity model than Sutherland viscosity law. For hypersonic wind tunnel conditions, the stagnation temperature is sufficient high to have vibrational excitation while the freestream temperature in the test section is low. The model requirements are the same as for flight conditions as vibrational nonequilibrium effects can be important. Keyes viscosity model should be used due to the low gas temperatures. The desired database should include a matrix of accurate solutions which depend on Mach number, boundary layer momentum thickness Reynolds number, and wall temperature. A series of solutions should be obtained with only one of the variables varying and with the other two variables held constant. These solutions would provide a database that can be used to validate the Van Driest transformation approach to correlate compressible turbulent skin friction and heat transfer (Stanton number) and to determine the Reynolds factor in the Reynolds analogy. In addition, the DNS method should be extended to flow over sharp cones. The database would help to determine the Mangler transformation required to transform compressible turbulent flow for the axisymmetric case to the two-dimensional case.

5. Turbulence model validation

5.1. Overview

The various turbulence models that are assessed in the current work are listed in Table 1. Recall that we focus only on one- and two-equation turbulence models where integration to the wall is employed (no wall functions) and which have also been previously validated for a wide range of non-hypersonic flows.

A listing of hypersonic validation experiments is presented in Table 2 along with the turbulence models from Table 1 which have been used with each experiment for validation purposes. The flow geometries in Table 2 include the accepted experiments of Settles and Dodson as cases 1 to 8. Cases 9 to 11 could also become standard benchmark case for hypersonic turbulent flows. Cases 9 and 11 have received extensive validation usage. For the sharp circular cone (case 10), an accurate correlation of the sharp cone database similar to Van Driest II is needed.

Table 1: Turbulence Model Notation

Turbulence Model	Notation
One-Equation Models	
Spalart-Allmaras [7], [8]	SA
Goldberg [158]	UG
Menter [6]	MTR
Two-Equation Models	
k-ε Jones-Launder [10]	kεJL
k-ε Launder-Sharma [11]	kεLS
k-ε Chien [82]	kεCH
k-ε Nagano and Hishida [126]	kεNH
k-ε Rodi [160]	kεR
k-ε So [83] [146]	kεSO
k-ε Huang-Coakley [84]	kεHC
k-ω Wilcox (1988) [132]	kω88
k-ω Wilcox (1988) low Reynolds number[132]	kω88LR
k-ω Wilcox (1998) [5]	kω88
k-ω Menter with SST [13]	SST
k-ω Menter with BSL [13]	BSL
k-*l* Smith [105], [163]	k*l*
k-ζ Robinson-Hassan [14], [15]	kζ
q-ω Coakley [85]	qω

Table 2: Summary of Hypersonic Experiments and Validation Usage

Case No.	Flow Geometry	Experiments	Validation Usage	Turbulence Models Assessed
1	2D Compression Corner	[33][159][95] [48]	[90][84][86] [98] [158][97] [99] [96] None	qω, kω88, kεLS, kεCH, kεSO, kεHC kεJL, kεR UG, SA, MTR kω88LR, SA, SST kζ
2	Cylinder with Conical Flare	[34] [56][57]	[89], [98] [84][90][86] None	kεJL, kεR qω, kω88, kεLS, kεCH, kεSO, kεHC
3	Cone with Conical Flare	[44]	[98]	kεJL, kεR
4	Axisymmetric Impinging Shock	[37][164][102] [101]	[90][86] [98] [100] None	kω88, kεLS kεJL, kεR qω
5	Flat Plate with Two Fins (Crossing Shocks)	TBD	TBD	TBD
6	Flat Plate with 3D Fin	TBD	TBD	TBD
7	Cylinder with Skewed Flare	TBD	TBD	TBD
8	3D Compression Corner with Sweep	TBD	TBD	TBD

Table 2: Summary of Hypersonic Experiments and Validation Usage

Case No.	Flow Geometry	Experiments	Validation Usage	Turbulence Models Assessed
9	Flat Plate/Cylinder	VDII [115]	[130] [91] [99] [12]	Various kω88, kεLS, SST, SA kω88, SST, SA SA, kω98, kεNH, BSL
		HBC [71]	[167] [91]	kω88, kεLS kω88, kεLS, SST, SA
		AVC [87]	[87]	kω88, kεLS
		[179][180][63] [181][182][183] [61] [40][38] [128][184] [48][187][42][46]	[131][203]	kω88, kεCH, k*l*, SA
10	Sharp Circular Cone	VDII [115] & White [75]	[12]	SA, kω98, kεNH, BSL
		[119], [120]	[121][122]	kζ
			[12]	SA, kω98, kεNH, BSL
		[210][211]	None?	
		[214]	None?	
		[52][217][218][220]	None?	
		[48][43][42][225][46][44]	None?	
11	2D Impinging Shock	[40]	[98] [105] see fig. 11, ref. [100]	kεJL, kεR k*l*

5.2. Zero pressure gradient cases

5.2.1. Flat plate/cylinder (case 9): experimental studies

The uniform viscous flow over a thin flat plate is considered, where a laminar to turbulent boundary layer develops along the surface. In the present case the freestream flow is supersonic or hypersonic and the inflow boundary condition is near the leading edge of the plate. For Navier-Stokes solutions, there are many choices for the computational grid. It is recommended that a

parabolic grid be used as described in Roy and Blottner [9]. The boundary conditions for a parabolic grid are well defined and are continuous without a singularity at the leading edge. Boundary layer flows with zero pressure gradient are often included in this database, but upstream history effects can significantly influence the data results, with the nonequilibrium turbulence effects sometimes persisting 1000's of boundary layer thicknesses downstream [48]. For this reason, studies conducted on wind tunnel walls have been omitted from this review.

An extensive database of compressible turbulent flows in a standard form has been performed by Fernholz and Finley [30], [32]. This database is limited to two-dimensional flows where flow profile data are available in tabular form. Assessment of the data quality or significance of the data has not been performed. Tabulated data is given for the edge and wall flow properties and survey properties across the boundary layer. The hypersonic database given in the Fernholz and Finley reports include a number of experiments where either real gas effects were an issue, a fully turbulent boundary layer was not established after the transition process, or the wind tunnel side wall was used to generate the boundary layer (thus bringing the equilibrium nature of the turbulent boundary layer into question). As a result, the Fernholz and Finley reports are of only limited value. The two experiments which will be included from this database those of Hopkins and Keener and Horstman-Owen (discussed in detail below).

Hopkins and Keener [179], [180], [63] (Fernholz & Finley cases 6601, 7203 and 7204)

The initial work by Hopkins and Keener [179] was concerned with measuring the properties of the turbulent boundary layer on the *side wall* of the NASA Ames 8x7 foot *supersonic* wind tunnel at Mach 2.4 to 3.4. The next investigations was performed in the NASA Ames 3.5 ft. *hypersonic* wind tunnel. Hopkins and Keener [180] measured the local skin friction, total-temperature profiles, and pitot-pressure profiles on the hypersonic *wind tunnel wall*. Although the pressure gradient is small near the measurement location, there appears to be significant upstream history effects in this experiment. Keener and Hopkins [63] investigated the wind tunnel air flow over a *flat plate* at Mach 6.2 - 6.5. The total temperature of the freestream was 764 K to 1028 K and the temperature at the edge of the boundary layer was 73 K or greater. The analysis of the air flow properties included corrections for calorically imperfect gas effects. The boundary layer properties were investigated with forced and natural transition. Surface properties measured: pressure, temperature, wall shear stress. Properties measured across boundary layer: static and pitot pressure, total temperature.

Horstman-Owen [181], [182], [183] (Fernholz & Finley case 7205)

This investigation was performed for air flow over an *axisymmetric cone-ogive-cylinder* at Mach 7.2 in the NASA Ames 3.5 ft. hypersonic wind tunnel. The total temperature of the freestream air was 667 K and the temperature at the edge of the boundary layer was 59 K. Natural transition occurred along the body and the boundary layer became an equilibrium, constant pressure flow downstream on the body. The transverse curvature effects are considered to be negligible for this geometry. Fluctuating properties of the flow were also measured and $\langle u' \rangle / u_\tau = 0.17$ at $y/\delta = 1.1$, which gives an indication of the turbulent intensity in the freestream flow. Surface properties measured: pressure, temperature, wall shear stress. Properties measured across boundary layer: pitot pressure, total temperature.

Additional experiments, that have not been included in the Fernholz and Finley database, follow below.

Coleman-Elfstrom-Stollery [61] (see also Refs. [33], [159], and [95])

The compressible turbulent boundary layer on a *flat plate* was studied at a freestream Mach number of 9 in the Imperial College No. 2 gun tunnel. The total temperature of the freestream air was 1070 K. The local boundary layer edge Mach number was varied (Mach 3, 5, and 9) by changing the incidence of the plate from 0 to 26.5 deg. Both natural and tripped boundary layer flows were investigated. Theory based on Spalding-Chi skin friction and Reynolds analogy was used to predict the Stanton number for the three Mach numbers. There was an increased discrepancy between measurements of heat transfer and the prediction of the theory as the Mach number was increased. Surface properties measured: static pressure and heat transfer. Properties measured across boundary layer: pitot pressure.

Kussoy-Horstman [40], [38]

The experiments were conducted with flow over a water-cooled *flat plate* in the NASA Ames 3.5-ft. hypersonic wind tunnel at Mach 8.2. The flat plate without a sharp fin is the database that is being considered. The plate surface was maintained at a constant surface temperature of $300 \pm 5K$. In the first experiment [40], the properties of the boundary layer 1.87 m from the leading edge were determined. In the second experiment [38], the properties of the boundary layer 1.62 m from the leading edge were determined. Natural transition occurred between 0.5 m and 1.0 m from the leading edge. A fully developed, equilibrium boundary layer was established at the measurement location. Tabulated results are presented for boundary layer surface and edge properties. Tabulated results for the velocity, density and temperature profiles are also given for the measurement location. Surface properties measured: static pressure and heat transfer. Properties measured across boundary layer: pitot pressure, static pressure, and total temperature.

Hopkins et al. [128], [184], [62]

The initial experiments were performed by Hopkins et al. [128] on simple shapes for turbulent boundary layers with nearly zero pressure gradient in the NASA Ames 3.5-ft. hypersonic wind tunnel. Local skin friction and heat transfer data were measured on flat plates (Mach 6.5 and 7.4), cones (edge Mach 4.9, 5.0, and 6.6), and the wind tunnel wall (Mach 7.4). Skin-friction data are given in tabulated form. The next experiments were performed by Hopkins et al. [184] on a sharp leading edge flat plate in the same Ames facility. Flat plate skin friction was measured directly with an edge Mach number of 6.5. The skin friction experimental database at various moment thickness Reynolds numbers and adiabatic wall temperature ratios are given in tabulated form. Hopkins et al. [62] conducted further flat plate experiments in the same Ames facility. This study provides additional results to those previously reported by Keener and Hopkins [63], but at a higher Reynolds number. The model was injected into the airstream at various angles of attack, which resulted in local Mach numbers at the measuring station of 5.9, 6.4, 6.9, 7.4, and 7.8. No boundary layer trips were used. The model surface temperature was nearly isothermal. Direct measurements of skin friction and velocity profiles were made for the various Mach numbers and for $T_w/T_{aw} = 0.3$ and 0.5. Real gas corrections as given in NACA Report 1135 were used in the

analysis of the data. Tabulated results of the database are given in the article. Surface properties measured: wall shear stress with a skin-friction balance. Properties measured across boundary layer: pitot pressure.

Holden [48], [187], [42], [46]

Experiments [48] were conducted on a flat plate in the Calspan 48 inch and 96 inch shock tunnels at Mach numbers 6.8 to 13. Steady flow was established in these facilities in 1 or 2 ms. The investigation measured the wall shear stress and the heat flux. The wall skin friction and heat transfer results were transformed with the Van Driest method and compared in figures to the incompressible results. The experimental data is approximately within 30% of the incompressible results, which is more scatter than expected from experimental results. This paper provides no details on the flow conditions, which makes the results of limited value. Another experiment [187] was conducted in the Calspan tunnels on a flat plate with a constant curvature surface downstream with a freestream Mach number of 8. The upstream part of the database on the flat plate could be useful, but needs further evaluation. A brief summary of experiments performed on flat plates is given by Holden and Moselle [42]. An electronic database [46] of results from the many experiments performed by Holden is now available on the internet to qualified users. A further evaluation of the usefulness of the Holden flat plate database needs to be performed.

5.2.2. Flat plate/cylinder (case 9): assessment of theoretical correlations and models

The assessment of correlations and models for turbulence is concerned with the comparison of the resulting predictions with experimental data. The turbulence properties of interest are the wall skin friction, heat transfer, and profiles of velocity and temperature across the boundary layer. The flat plate problem is unique since analytic analyses of the turbulent boundary layer flow have been performed which result in correlations of the experimental results.The following investigators have used experimental data to assess the accuracy of theoretical correlations and/or turbulence models for the turbulent boundary layer with zero pressure gradient.

Van Driest [73], [190]

In the initial article [73] (Van Driest I) a theory is developed for predicting properties of compressible turbulent boundary layer flows with the Prandtl mixing length model, but no comparison of theory to experimental data is given. In the second article [115] (Van Driest II) the theory is modified to incorporate the von Kármán mixing length turbulence model. The turbulent Prandtl number is still assumed to be one, but in the temperature relation the recovery factor is introduced. The usual approach of plotting normalized skin friction as a function of Mach number was used by Van Driest and he compared the two theories to experimental data. The experimental database included experimental data of Coles [194], Chapman-Kester [192], Sommer-Short [195], and Korkegi [196]. With this supersonic/hypersonic database, no conclusion could be made on which of the two Van Driest theories provided the best prediction of skin friction.

Peterson [197]

Peterson [197] compares seven theories for predicting the skin friction with an experimental database for turbulent boundary layer flows with zero pressure-gradient. The theories transform the

experimental skin friction and Reynolds number to incompressible (transformed) values. The theoretical prediction of the incompressible skin friction as a function of incompressible Reynolds number is obtained from the Karman-Schoenherr formula, which is considered the most accurate fit of the incompressible experimental database. Peterson uses an experimental compressible skin friction database obtained from 21 references and the data from the references are tabulated. For hypersonic flow, there are two references for an adiabatic wall, (Korkegi [196] and Matting et al. [198]) and there are three references for a non-adiabatic wall (Winkler-Cha [173], Sommer-Short [195], and Hill [171], [172]). The significance of this paper is the author uses the transformations of the various theories to correlate all of the experimental data at different Mach numbers, wall temperature ratios, and Reynolds numbers into a single curve. Also, Peterson recognizes the work of Wilson [199] where he developed a skin friction transformation for zero heat transfer with the von Karman mixing-length law. Van Driest [73] developed a skin friction transformation with the Prandtl mixing-length (now referred to as Van Driest I). Van Driest [190] extended the theory of Wilson to the case with heat transfer (Van Driest II of more appropriately Peterson refers to this theory as Wilson-Van Driest).

Hopkins et al. [128], [184], [129], [63]

Hopkins et al. [128] investigated the accuracy of the correlation theories of Sommer and Short, Spalding and Chi, Van Driest II, and Coles for the local skin friction. The prediction of heat transfer for these theories was also investigated. Hopkins et al. [184] investigated eight local skin-friction transformation theories of Van Driest II, Spalding-Chi, Sommer-Short, Eckert, Moore, Harkness, Coles, and Baronti-Libby. These theories were assessed against the Mach 6.5 experimental database of the authors. It was concluded that the methods of Van Driest II and Coles predict the skin friction within about 5%. The other six theories under-predicted the skin friction from 10% to 25% for this experimental data set. The survey article by Hopkins and Inouye [129] is based on the original NASA Technical Note [128] and includes additional skin-friction and heat-transfer data. Four theories are investigated further and these theories are described in the survey article. The incompressible skin-friction formula of Kármán-Schoenherr is used to determine the skin friction as a function of the momentum thickness Reynolds number. The hypersonic database for the *adiabatic flat plate* is only the experiment of Korkegi [196] while the database for the non-adiabatic flat plate is Sommer and Short [195] (hollow-cylinder), Hopkins et al. [128], Hopkins-Keener-Louie [184], Wallace-McLaughlin [200], Young and McLaughlin [201], and Neal [202]. The authors suggested for hypersonic flat plate flows that Van Driest II theory be used to predict turbulent skin friction and heat transfer be obtained with a Reynolds analogy factor equal to one and a recovery factor equal to 0.9. In the ensuing article by Hopkins, Keener, Polek, and Dwyer [62], the four theories for correlating experimental skin-friction data were further investigated. Their experimental data was compared to numerical turbulent boundary layer solutions with an algebraic eddy viscosity model of Cebeci. In addition Baronti-Libby and Van Driest methods for correlating mean velocity profiles were investigated. The authors determined that the Van Driest II, Coles, and numerical turbulent boundary layer solutions give the best predictions of skin friction and are within $\pm 10\ \%$. The authors state, “The Van Driest theory gave the most satisfactory transformations of the velocity-profile data onto the incompressible law-of-the-wall and velocity-defect curves.” Keener and Hopkins [63] have investigated five velocity profile correlation

methods for their Mach 6.5 database: wall reference temperature, T-prime reference temperature, Coles, Baronti-Libby, and Van Driest transformations. It is stated that the use of either the Prandtl mixing length (Van Driest I) or the von Kármán mixing length (Van Driest II) result in identical transformation functions. The Van Driest method gives the best correlation for both the law-of-the-wall and velocity-defect law when compared to Coles' incompressible velocity profile data. The correlations deteriorate with decreasing momentum thickness Reynolds number.

Owen, Horstman, and Kussoy [183]

Boundary layer measurements were made downstream on a cone-ogive-cylinder model at a freestream Mach number of 7.0 [183]. Fluctuating and mean flow measurements were obtained at one location sufficiently far downstream where the pressure gradient is zero. Mean velocity and total temperature boundary layer profiles are given in figures in the paper. The relation between T^* (the total temperature in nondimensional form, see Appendix B) and velocity is linear except in the region close to the wall. The velocity profile was transformed to incompressible form with Van Driest theory and compared to the incompressible velocity correlation curve of Coles. The data are in good agreement with the incompressible law-of-the-wall correlation. In the outer region of the boundary layer, the data are in good agreement with the incompressible velocity-defect correlation.

Fernholz and Finley [31]

The authors investigated the accuracy of some of the cases in the compressible experimental database for the turbulent mean temperature and velocity profiles with comparison to theoretical predictions [31]. The hypersonic cases investigated are as follows:

> **Keener and Hopkins** [63] (Fernholz & Finley case 7204): The *sharp flat plate* experiments have zero pressure gradient with no upstream history effects. The static temperature is in good agreement with the theoretical prediction in the outer part of the boundary layer. The experimental velocity profile database is concluded to be in good agreement the law of the wall and outer law.
>
> **Horstman and Owen** [182] (Fernholz & Finley case 7205): This experiment investigated the turbulent boundary layer flow over an axisymmetric *cone-ogive-cylinder body* where downstream the Mach number is 7.2 at the edge of the boundary layer. The nose of the body might have introduced a slight favorable pressure gradient. However, it is highly probable that the boundary has reached equilibrium at the three measurement stations. Agreement between the velocity profile measurements and the law of the wall is very good. There is good agreement with the outer velocity law. Agreement between measured and theoretical temperature profiles is satisfactory.

Kussoy and Horstman [40], [38]

The first flat plate experiment of Kussoy and Horstman [40] without fins or wedges provide data at Mach 8.2 and at one location, 1.87 m from the sharp leading edge. The experimental mean velocity profile was transformed into incompressible coordinates with Van Driest II theory and compared to Coles' universal law-of-the-wall. Since the data and the theory were in reasonable

agreement, the authors concluded that the turbulent boundary layer is fully developed. The second experiment [38] is for a flat plate at Mach 8.3 with the data obtained at 1.62 m from the leading edge. Again the transformed mean velocity profile is compared to Coles' law-of-the-wall profile in inner variables. The authors conclude the turbulent boundary layer is fully developed. Further analysis of the outer region correlation of the boundary layer also needs evaluation.

Huang, Bradshaw, and Coakley [71], [167]

In the first article [71] a self-consistent transformation method (denoted as HBC) was developed to predict skin friction and velocity profiles of compressible boundary layer flows with zero pressure gradient. The paper is also concerned with the assessment of the authors' HBC transformation by comparing the predictions to the well accepted Van Driest transformation and experimental data. For an adiabatic and non-adiabatic wall, the prediction of skin friction with the two theories was compared to the experimental database used by Hopkins and Inouye [129]. The database was not sufficiently accurate to determine the better theory. The database of Watson [177] was also used to assess the accuracy of the two theories for skin friction. The HBC theory was more accurate than Van Driest II for this case. In addition, the predictions obtained with the HBC transformation method are in good agreement with the experimental velocity and temperature profiles of Kussoy and Horstman [40]. The investigation of Fernholz and Finley [31] has shown that the Van Driest II transformation transforms the compressible velocity profile data into a profile that matches the incompressible law-of-the-wall. In the second paper [167], an assessment of two-equation turbulence models has been performed and it has been determined that the k-ε Launder-Sharma and Wilcox 1988 k-ω models do not give the expected law-of-the-wall behavior. The k-ω model is much less sensitive to density effects than the k-ε model. A density correction to the closure coefficients was developed that improved the accuracy of the two-equation models in the logarithmic part of the turbulent velocity profile.

Aupoix, Viala, and Catris [87], [131], [203]

In the paper by Aupoix and Viala [87] the standard turbulence models are assessed with supersonic and hypersonic boundary layer flow on an adiabatic flat plate. The authors use the following adiabatic wall experimental database to evaluate the local skin friction correlations and to obtain *reference test cases* to evaluate turbulent model predictions (note: these cases are referred to as AVC in Table 2):

Supersonic: Coles [194], Kistler [204], Hasting-Sawyer [205], Mabey et al. [206], [207], Richmond [208].

Hypersonic: Winkler-Cha [173], Moore-Harkness [175], Watson et al. [176], [177],

Laderman and Demetriades [178].

The Van Driest II and HBC approaches correlate the experimental database for adiabatic flat plate flows within a scatter of $\pm 10\%$. The data is not sufficiently accurate to determine which correlation is more accurate. Also the authors investigate the influence of the non-dimensional form of y^+ in the wall damping functions. For high Mach number flows, density gradients influence the logarithmic behavior of the velocity profile and the turbulence models require additional modeling to retain the logarithmic region. A density gradient correction to the

turbulence models is investigated using the approach of Huang et al. [167]. The database given above is used to assess the accuracy of density gradient corrections added to standard turbulence models. The Wilcox 1988 k-ω model is less sensitive to density gradient effects than the k-ε models.

The initial work of Catris and Aupoix was given in an AIAA paper [131] and was later published as Ref. [203] with additional work included. The authors have proposed modifications of the diffusion term in the compressible turbulent transport equations for the various turbulence models. The models investigated are the Chien k-ε model [82], Wilcox k-ω (1988) model [132], the Smith k-*l* model [105], [163], and the Spalart-Allmaras model [7], [8]. The modified turbulence models are assessed for supersonic and hypersonic zero pressure gradient boundary layers where the accuracy of the velocity profile and skin friction are determined with the *reference test cases*. Velocity profile predictions with the various turbulence models are compared to the following flat plate experimental databases: Mabey et al. [206] (Mach 4) and Winkler and Cha [173] (Mach 5.3). Skin friction predictions with the various turbulence models are compared to the following experimental databases: Mabey et al. [207], Winkler and Cha, Watson [177] (Mach 10 - 11.6), and Owen et al. [183] (Mach 7.2). The modified turbulent model solutions generally improve the prediction accuracy.

Bradshaw, Launder, and Lumley [130]

As a part of the Stanford Collaborative Testing of Turbulence Models, one of the entry cases is the compressible flow over a flat plate at a Reynolds number of 10^4 based on momentum thickness. The final problem definition requested turbulence modelers to obtain the following solutions: (Case A) Mach 2, 3, 5, and 8 with an adiabatic wall and (Case B) Mach 5 flow with T_w/T_{aw} equal 0.2, 0.4, 0.6, 0.8, and 1.0. The Van Driest II values of compressible local skin friction and Stanton number with Reynolds analogy factor of 1.16 were determined by Bradshaw as the reference solution for comparison. For Case A, the average of the modeler predictions for skin friction were 1% below reference values at Mach 2 and 4% above reference values at Mach 8. For Case B, the average of the modeler predictions for skin friction were 5.2% high for $T_w/T_{aw} = 0.2$ and 2.5% high at $T_w/T_{aw} = 0.8$. Some further refinement of specification of the viscosity law and equation of state for a perfect gas is needed.

Bardina, Huang, and Coakley [91]

The Mach 5 boundary layer flow over an adiabatic flat plate was investigated at momentum thickness Reynolds numbers of 5,000, 10,000, 20,000, 50,000, and 100,000. The authors performed careful numerical solutions to insure that the solutions for four turbulence models (Launder-Sharma k-ε, Wilcox 1998 k-ω, Menter SST k-ω, and Spalart-Allmaras) had small numerical errors. The Van Driest II transformation theory was used with the von Kármán-Schoenherr incompressible skin friction relation to obtain the compressible skin friction for the numerical predictions. This approach is considered to provide a good fit to experimental flat plate data. The k-ε model showed a significant under-prediction of the skin friction (as much as 20%). In addition, the transformation of Huang, Bradshaw, and Coakley (HBC) gives larger skin friction (5% to 10%) than the Van Driest II transformation. The compressible velocity profiles for the four turbulence models were transformed to incompressible form and compared to the log law of HBC.

The k-ε turbulence model again gave poor results. The Spalart-Allmaras turbulence model gave the best overall predictions for the skin friction and the velocity profile.

Coratekin et al. [99]

The authors have developed a compressible Navier-Stokes code and are concerned with the performance of the numerical scheme and accuracy of three linear turbulence models for hypersonic perfect gas flows [99]. The turbulence models in the code are the following: Wilcox k-ω model (with two compressible corrections - Vuong and Coakley [85], [86] have developed a length scale correction for reattachment boundary layer flows while Coakley and Huang [84], [86] have introduced a correction in flow regions with strong compression effects), Spalart-Allmaras one-equation model, and Menter k-ω SST model. The turbulent boundary layer on an isothermal flat plate at Mach 5 is solved with the code and compared with the Van Driest II [115] correlation of the skin friction. At a given momentum thickness Reynolds number, the turbulent model predictions for skin friction are lower than the values obtained with the Van Driest II theory.

Roy and Blottner [12]

Roy and Blottner [12] examined Mach 8, calorically perfect gas flow over a flat plate using four different turbulence models: Spalart-Allmaras (SA) [7], [8], Nagano and Hishida k-ε (kεNH) [126], Wilcox (1998) k-ω (kω98) [5], and Menter's BSL k-ω (BSL) [13]. The conditions correspond to 15 km altitude, and a wall temperature of 1000 K was used. The plate was 1 m long, and transition was specified at 0.12 m to allow a significant amount of both laminar and fully-developed turbulent flow. The simulation results were compared to the accurate laminar and turbulent results obtained for this case by Van Driest [73], [127]. The validation methodology discussed in Section 3 was used. Multiple grids were run in order to estimate the discretization error. In the fully-developed turbulent region, the discretization error for the Spalart-Allmaras model was approximately 0.5%, while the error for the two-equation models was near 1%. These estimates increase to 0.6% and 1.25% when a safety factor of 1.25 in included. The effects of varying the wall y^+ values between 0.01 and 1.0 were studied, and the models were found to be relatively insensitive to y^+ variations below 0.25. Skin friction profiles in the turbulent region are shown in Fig. 1 for each model. The results appear to reach an approximately constant error relative to the Van Driest correlation by the end of the plate. At this location, the Wilcox (1998) k-ω model underpredicts the Van Driest II curve by 6.7%, while the Spalart-Allmaras, Menter k-ω, and low Reynolds number k-ε overpredict the skin friction by 1.4%, 3.1%, and 6.3%, respectively. Accounting for the grid convergence errors, the skin friction predictions from the Spalart-Allmaras and Menter k-ω models are within the error tolerances, while the low Reynolds number k-ε and Wilcox (1998) k-ω models are not. In addition, the surface shear stress values for the Wilcox (1998) k-ω model showed a sensitivity of up to 4% to the freestream ω values.

5.2.3. Sharp circular cone (case 10): experimental studies

Rumsey et al. [210], [211]

Rumsey and co-workers [210], [211] performed a number of flight test with vehicles with a sharp-cone nose and at various supersonic/hypersonic Mach numbers. The sharp cone database used by Zoby and Sullivan [76] has seven references, with six references from the NASA flight tests. Zoby and Sullivan database only includes data at supersonic Mach numbers. The Rumsey and Lee [210] report has data at Mach 5.15 and has been included as a potential part of the present sharp cone database. The authors present much of the needed database information in figures. The free-stream unit Reynolds number as given in Figure 2 is not consistent with the value determined from the 1976 Standard Atmosphere conditions with the altitude given in Figure 3 (10% difference). The accuracy of this database has not been estimated, but is valuable as limited hypersonic flight data is available.

Stainback, Fischer, and Wagner [213]

The experimental results **[213]** were obtained in the NASA Langley 20-inch hypersonic wind tunnel in air. The authors obtained the Stanton number along the surface of a 10 deg. sharp cone at Mach 6. The study was also concerned with boundary layer transition to turbulent flow and authors measured the unsteady wall pressure. Tabulated test conditions and boundary layer edge properties are given. This database has been used for validation of transition models.

Chien [214]

Chien [214] performed a wind tunnel investigation on the skin friction and heat transfer on a 5 deg. half-angle sharp cone of length 0.656 m at a freestream Mach number of 7.9. The experimental investigation was conducted in the Naval Ordnance Laboratory Hypersonic Wind Tunnel in air. Chien has tabulated the test conditions for 11 runs. The Stanton number as a function of the boundary layer edge properties and surface distance is tabulated for the 11 runs with different free-stream conditions. In addition, surface skin friction measurements were obtained in four of the runs and these values are also tabulated. The measured Stanton numbers are compared to four analytical turbulence models.

Kimmel [119], [120]

The experiment by Kimmel [119], [120] was conducted in the Hypersonic Wind Tunnel B at Arnold Engineering Development Center where six test conditions were used. The investigation is concerned with boundary layer transition on a 7 deg. sharp cone model of length of 1 m at Mach 7.9. In addition, the aft part of the model could be flared or an ogive. Results of this experimental investigation were initially published in the proceedings of an ASME meeting [119] and later published in Ref. [120] with limited changes. The flow conditions are specified with the Mach number and total temperature held constant, while the unit freestream Reynolds number is varied by changing the total pressure. The surface pressure, surface temperature, and wall heat transfer were measured along the model. The heat transfer measurement are given in figures as the Stanton number as a function of s/L or boundary layer edge Reynolds number with length scale s. The

sharp cone results for a free-stream unit Reynolds number 6.6 million per meter can be more readily obtained from this article. Boundary layer edge conditions are not specified.

Hillier et al. [52], [217], [218], [220]

At the Antibes Workshop on Hypersonic Re-entry Flows, which is documented in the books by Desideri et al. [52], the sharp cone is the first hypersonic turbulent flow problems to be solved by participants. Denmann et al. [217] obtained the experimental database in the Imperial College Number 2 Gun Tunnel, where Mach 9.2 nitrogen flow over a 7 deg. cone of length 0.58 m is investigated. The flow in the nozzle is not uniform, but is like a spherical source flow, which give a Mach number gradient along the nozzle. Mallinson et al. [218] have performed further calibration of the gun tunnel flow to determine improved input conditions for hypersonic flow computations. Measurements obtained are pressure and heat transfer (Stanton number) along the cone surface. The pitot pressure is measured across the boundary layer at two locations along the cone. With the assumption that the static pressure is constant across the boundary layer, the Mach number across the boundary layer is obtained from the Rayleigh pitot formula. The wall pressure and Stanton number along the cone surface are given. Lawrence [219] presented at the workshop results that compare his prediction of total pitot pressure across the boundary layer with the experimental data. Hillier et al. [68] have obtained further data for cone geometry with a new test model. The authors present the Stanton number as a function of a Reynolds number (distance along the surface and free-stream properties). In 1993, Abgrall et al. [221] present an update of the European Hypersonic Database and the number one problem in the database is the sharp cone problem.

Holden [48], [43], [42], [225], [46], [44]

Over more than 30 years, Holden has investigated many hypersonic flow problems experimentally and recently created a database of the measured results. Two experiments have been performed that can contribute to the sharp cone database. Holden performed the tests at the experimental facilities at Calspan in the 96-inch shock tunnel. The testing time in this shock tunnel is approximately 25 ms, which makes the change of the model wall temperature very small during a run. The models used in the two tests are as follows:

6 Deg. Sharp Cone: An initial investigation was performed by Holden [48] in 1977 and has limited information provided on the model description and on the free-stream flow properties in the tunnel. Documentation of the next experimental results with the same model is presented in Ref. [43]. This study is mainly concerned with boundary layer transition on 6 deg. sharp and blunt cones at angle of attack in Mach 11 and 13 flows. However, the heat flux as a function of distance along the sharp cone at zero angle of attack is given and the boundary layer has transitioned from laminar to turbulent flow. It appears the distance is along the surface of the cone and measured from the nose-tip junction point, which is not specified. It is estimated that the junction point is 0.15 m from the cone tip and the cone length is 0.71 m. In 1992, Holden [42] reviewed his experiments concerned with hypersonic flow and created a database of work performed from 1965 to 1991. The database includes the sharp cone work reported in the 1985 paper, however little new information is presented on the turbulent boundary flow properties. Holden performed further experiments on this model in 1995 and Ref. [225] is mainly concerned with the transition issue. Tabulated data of free-stream flow

conditions for a list of tunnel runs is given and includes the conditions for Run 2. In addition, tabulated data on the model configuration, angle of attack, free-stream Mach number, and unit Reynolds number for the list of runs is also given. New measured wall pressure and heat flux along the cone surface for the sharp cone at zero angle of attack are given. For these tunnel test runs, the turbulent boundary layer has not become fully turbulent. Described in Ref. [46] is the further development of Holden's hypersonic database. The sharp cone database is available on a CD ROM and on the CUBRC website (http://www.cubrc.org/aerospace/index.html) to qualified applicants. It does not appear that a complete database for experiments performed on 6 deg. sharp cone model is available in the open literature and the information available at Holden's website has not yet been investigated. Tabulation is needed of the skin friction and heat flux along the cone for the various test conditions. The tabulated properties at the edge of the boundary layer are required for the correlation of the skin friction and Stanton number.

6 Deg. Cone with 30 Deg. Flare: The experimental study by Holden was conducted at Mach 11, 13 and 15 and the results documented in a 1991 AIAA paper [44]. Tabulation of the stagnation and free-stream test conditions for the three shock tunnel runs is given. For these flow conditions, the boundary layer is fully turbulent well upstream of the cone/flare junction. The measured wall pressure and heat transfer along the cone/flare model for three runs are given. Holden measured the pitot pressure and total temperature across the boundary layer, and the velocity profiles across the boundary layer have been determined from the measurements. Tabulation of the measured turbulent boundary layer properties are not available in the references reviewed here. Location of the cone/flare junction point is not specified in this paper but is not necessary for the solution on the 6 deg. cone with the reasonable assumption that the upstream effect of the flare can be neglected. However, for the profile data, distance is measured from the cone/flare junction point. In the 1992 and 2003 database papers, Holden et al. do not provide additional information on the cone/flare experiment.

For Holden's experiments, the total temperature is sufficient high that free-stream conditions may include real gas effects due to vibrational excitation. Holden has assumed the gas is in thermodynamic equilibrium in the shock tunnel so vibrational nonequilibrium effects are neglected. This review assumes that the wall temperature of the model is at room temperature of 300 K.

The sharp cone model is defined by the cone half-angle (angle between cone axis and cone surface) and the length L along the cone axis. The axial distance along the center of the cone from the tip is defined as x and distance along the cone surface from the tip is defined as s. The basic flow properties in the freestream are defined by specifying the Mach number, total temperature, and freestream unit Reynolds number, which are tabulated in Table 3 for the current sharp cone experimental database being evaluated. The cone surface temperature is obtained from the specification of the wall to total temperature ratio. The other properties of the freestream flow are obtained from the following perfect gas relations:

$$T_\infty = T_0\left[1+\left(\frac{\gamma-1}{2}\right)M_\infty^2\right]^{-1} \qquad T_w = (T_w/T_0)T_0 \qquad \gamma = 1.4$$

$$a_\infty = \sqrt{\gamma R T_\infty} \qquad u_\infty = a_\infty M_\infty \qquad \rho_\infty = \mu_\infty Re_{u\infty}/u_\infty$$

$$p_\infty = \rho_\infty R T_\infty = p_0\left[1+\left(\frac{\gamma-1}{2}\right)M_\infty^2\right]^{-\gamma/(\gamma-1)}$$

Table 3: Model Geometries and Freestream Conditions for Cone Database

Investigator	Cone half-angle	Cone length (m)	$R_n \times 10^5$ (m)	M_∞	T_0 (K)	$\frac{T_w}{T_0}$	$Re_{u\infty}/m \times 10^{-6}$
Rumsey et al. [210], [211]	7.5°	0.7874		5.15	1265	0.591	31.0
Stainback et al. [213]	10°	≈ 0.5		6	500	0.6	32.9
Chien [214]	5°	0.656		7.90	816	0.351	35.2
Kimmel [119], [120]	7°	1.016	5.0	7.93	722	0.420	6.60
Hillier et al. [52], [217], [218], [220]	7°	0.5783		9.16	1063	0.273	55.0
Holden - Cone Cone/Flare [48], [43], [42], [225], [46], [44]	6° 6°	0.7073 2.667		13.04 10.96	1739 1509	0.173 0.199	15.60 12.07
Pruett (DNS) [229], [230]	7°	1.427 0.254	0 0	8.0 6.0	733 450	0.834 0.865	3.407 8.950

5.2.4. Sharp circular cone (case 10): assessment of theoretical correlations and models

The supersonic/hypersonic flow over a sharp cone at zero angle of attack is of interest as the flow properties at the edge of the boundary layer are approximately constant along the cone. The sharp cone is an extension of the flat plate geometry and is basic to the understanding of turbulent boundary layer flows. One of the problems with the sharp cone is the lack of a theoretical

correlation of the experimental data to use as a Benchmark solution. For laminar flow, the skin friction and heat transfer for a flat plate are multiplied by 3 to obtain the cone values. There does not appear to be a well defined approach to transform the turbulent flat plate results to the cone. However, the flat plate correlation approach for skin friction and heat transfer has been extended to the sharp cone with some approximations. The sharp cone geometry is well suited to wind tunnel testing and avoids the 2D/3D issues involved with flat plate flows. From a computational point of view, this geometry is not ideal because the singularity at the sharp tip can make it difficult to obtain accurate numerical solutions. With the appropriate grid [9], the tip singularity problem can be handled.

In the correlation of the surface skin friction and heat transfer, the flow properties at the edge of the boundary layer are required. For high Reynolds number flows, the boundary layer is thin and the edge properties can be obtained from the inviscid conical flow solutions, where the edge properties are approximated with the wall properties. Tables of the inviscid surface properties as a function of Mach number and cone half-angle have been developed by Sims [209]. (Sims discusses earlier tables developed by Taylor-Maccoll and Kopal.). As interpolation is required with the use of the tables, the wall properties obtained from the numerical solution of the governing ordinary differential equations is a better approach. The conical inviscid perfect gas flow is determined with the cone half-angle θ_c and the freestream Mach number M_∞ specified. The following cone surface properties are obtained from the tables with linear interpolation M_e, T_e/T_∞, and p_e/p_∞ . Then the edge properties are obtained from the relations

$$T_e = T_\infty(T_e/T_\infty) \qquad p_e = p_\infty(p_e/p_\infty) \qquad a_e = \sqrt{\gamma R T_e} \qquad u_e = M_e a_e$$
$$\rho_e/\rho_\infty = (p_e/p_\infty)/(T_e/T_\infty) \qquad \rho_e = p_e/RT_e$$
$$\mu_e = \mu(T_e) \text{ Sutherland or Keyes viscosity}$$
$$Re_{u_e} = \rho_e u_e/\mu_e = \text{ Unit Reynolds number}$$

The shear stress τ_w and heat flux q_w at the surface of the cone are two of the quantities desired from the experiments, turbulence modeling, and the numerical solutions. The wall shear stress is usually written as the non-dimensional skin friction parameter, which is defined in two forms

$$C_{f\infty} = 2\tau_w/\rho_\infty u_\infty^2 \qquad C_{fe} = 2\tau_w/\rho_e u_e^2$$

The wall heat flux is usually written as the non-dimensional Stanton number, which is defined in two forms

$$St_\infty = q_w/\rho_\infty u_\infty c_p(T_{0\infty} - T_w) \qquad c_p = \gamma R/(\gamma - 1)$$
$$St_e = q_w/\rho_e u_e c_p(T_{aw} - T_w) = q_w/\rho_e u_e(H_{aw} - H_w) \qquad H = c_p T + \frac{u^2}{2} \tag{26}$$

The second form of the Stanton number becomes indeterminate when the heat flux is zero. Also the heat transfer coefficient h_c is used and is defined as $q_w = h_c(T_{aw} - T_w)$. The flow properties

across the turbulent boundary layer are also useful in the evaluation and validation of turbulence modeling.

Roy and Blottner [12]

Flow over a sharp cone with a half angle of 7 deg was examined by Roy and Blottner [12] using four different turbulence models: Spalart-Allmaras (SA) [7], [8], Nagano and Hishida k-ε (kεNH) [126], Wilcox (1998) k-ω (kω98) [5], and Menter's BSL k-ω (BSL) [13]. The flow conditions correspond to a wind tunnel test performed by Kimmel [119], [120], where transition occurs at approximately 0.5 m downstream of the nose. The gas is air and the temperatures are such that the perfect gas assumption with $\gamma = 1.4$ is appropriate. The discretization error in surface heating for the Spalart-Allmaras model was estimated to be 0.25% in the turbulent region. The two-equation models had error estimates of less than 1.5% in the turbulent region. The effects of varying the wall y^+ values between 0.01 and 1.0 were studied, and the models were found to be relatively insensitive to y^+ variations below 0.25. In this case, the surface heating values for the Wilcox (1998) k-ω model showed a sensitivity of up to 4% to the freestream ω values.

Skin friction predictions are presented in Fig. 2. Surface heating results versus surface distance Reynolds number are presented in Fig. 3 for the four turbulence models along with laminar boundary layer code results and the turbulent Van Driest cone theory. Note that a) refers to the transformed Van Driest [74], while b) denotes White's cone rule [75]. In addition, experimental data is taken from Kimmel [120] and includes the conservative 10% error bounds suggested by the author. Although the surface heating predictions in the transitional region do not match the experimental data, the predictions in both the laminar and turbulent regions are generally within the experimental error bounds. An enlarged view of the turbulent heating region is presented in Fig. 4. At the end of the cone, the two theoretical correlations agree to within 4%. This difference is well within the accuracy of the correlations which is estimated to be approximately ±5-10%. Taking the theoretical value to be the average of these two curves, the Wilcox (1998) k-ω model is roughly 5.7% below the theory at the end of the cone. Both the Menter k-ω model and the low Reynolds number k-ε model predict heating values approximately 2.5% high, while the Spalart-Allmaras model is 4.3% high. Accounting for the discretization errors, all of the turbulence models are well within the estimated error bounds.

5.3. 2D/axisymmetric cases with adverse pressure gradient

5.3.1. 2D compression corner (case 1)

There are two hypersonic experiments for the 2D compression corner which are deemed acceptable with some caveats. The first experiment was conducted in the Mach 9 nitrogen gun tunnel and includes heat transfer measurements (see Coleman and Stollery [33] and Coleman [159]) and surface pressures from a separate experiment (see Elfstrom [95]). The second experiment was conducted at the Calspan 48 in and 96 in shock tunnels at Mach 8. An overview of the turbulence model validation for this case as discussed below is shown graphically in Figs. 5-8.

Coleman and Stollery/Elfstrom Experiment [33], [159], [95]

Elfstrom [95] reported surface pressure measurements and Coleman and Stollery [33] and Coleman [159] reported surface heat transfer measurements for a Mach 9.22 flow over a 2D wedge/compression corner. The wedge angle was varied between 15 deg. and 38 deg., and includes flows which are nominally attached, incipient separation, and fully separated. It is not fully clear whether or not the pressure [95] and heat transfer [33] measurements had the same upstream length for the flat plate. While this experiment is considered acceptable by Settles and Dodson, there are no numerical uncertainties on the surface quantities given in Refs. [33] and [95], nor are any uncertainties presented in the Settles and Dodson reviews [1], [4]. Note that the experimental uncertainties may be given in Ref. [159] which could not be obtained in time for the current study. Holden [48] points out that the interaction region in the Coleman and Stollery/Elfstrom experiments may be too close to the transition zone, resulting in a different trend of separation zone size versus Reynolds number than seen in equilibrium turbulent boundary layers, which require a distance of approximately 50-100 boundary layer thicknesses between the transition point and the interaction region. Once the oncoming turbulent boundary layer has reached an equilibrium state, the trend appears to be a decrease of separation zone size (and incipient separation point) with increasing Reynolds number, while this experiment showed the opposite trend.

Horstman [98] has used the Coleman and Stollery/Eflstrom experiment (among others) to perform validation computations for two-equation k-ε models. The two turbulence models examined are the high-Reynolds number Jones-Launder k-ε model (kεJL) [10] and the low Reynolds number k-ε model of Rodi (kεR) [160]. A third k-ε model employing various compressibility corrections was also examined, however this model was calibrated using some of the hypersonic validation experiments, thus blurring the line between model prediction and calibration. A y^+ study was performed on a different (unspecified) geometry for this case using surface heat flux, and showed that the kεJL model was sensitive to y^+ values above 0.15, while the kεR model showed some mild sensitivity above 0.5. A grid refinement study was also performed on a few of the test cases (again, which cases were not specified) with no change in the predicted values on grids of 40×100 and 60×150. No sensitivities to the freestream turbulence quantities were discussed. For the 2D compression ramp, the keJL model was found to match the pressure well everywhere except for the constant pressure plateau on the ramp where it is overpredicted by 20%. The heat transfer predicted by this model greatly overpredicts the heating both in the interaction region and in the plateau region, in some regions overpredicting by an order of magnitude or more. The kεR model performed much better, matching the experimental pressure data within 10% and accurately predicting the heat transfer everywhere except within the interaction region, where the model overpredicts the heating by a factor of two.

Coakley, Huang, and co-workers [84], [90], [86] also used the Coleman and Stollery/Eflstrom experiment for turbulence model validation purposes. A number of different two-equation turbulence models were examined including: the q-ω model of Coakley (qω) [85], the 1988 k-ω model of Wilcox (kω88) [132], the k-ε model of Launder and Sharma (kεLS) [11], the k-ε model of Chien (kεCH) [82], the k-ε model of So (kεSO) [83] which includes compressibility extensions given by Zhang et al. [146], and the k-ε model of Huang and Coakley (kεHC) [84]. A number of modeling corrections designed specifically for high-speed separated flows were also investigated

by theses authors, but is unclear how these corrections impact the previous validation efforts for the model, especially at low speeds. These corrected models will therefore not be included in the current review. Grid refinement studies were discussed, but no results were presented and no estimates of the discretization error were given. A wall-spacing study showed that y^+ values greater than one gave errors in the skin friction (>2%) and also gave stability problems with some models; however, varying the y^+ values from 0.1 to 1.0 showed no changes. Sensitivities to the freestream turbulence quantities were not addressed. Only the kεLS and kω88 models were examined for the 15 deg. ramp case, and both models gave good predictions of surface pressure with a slight underprediction in the interaction region. The heat transfer was not predicted as well, with the kεLS model yielding heat transfer levels 25% higher than the data in the interaction region and the kω88 model overpredicting the heating by as much as 50% in the interaction region and in the plateau region on the ramp. All five models were applied to the 34 deg. ramp case, with the keSO and keHC models giving accurate predictions for the surface pressure, while the other three models tend to overpredict the pressure in the interaction region and significantly underpredict the size of the separated region as judged by the initial upstream pressure rise. All five models greatly overpredict the heat transfer in the interaction region by at least a factor of three, and the kw88 model also overpredicts the plateau heating downstream on the ramp by 50%.

Goldberg and co-workers [158], [97] have computed the 38 deg. ramp case of Coleman and Stollery/Elfstrom with three one-equation turbulence models: Goldberg (UG) [158], Spalart-Allmaras (SA) [7],[8], and Menter (MTR) [6]. A mesh refinement study was performed for the UG model only using 200×150 and 250×200 cell meshes with some minor effects on the results. While the effects of changing the y^+ values are not discussed, the y^+ values in all cases are kept near 0.1. No effects of the freestream turbulence levels are examined. The SA and MTR models are shown to underpredict the size of the separation zone, thereby predicting an earlier peak in the pressure. The UG model accurately predicts the pressure and provides fairly good estimates of the wall heating. The SA model also gives good predictions for the surface heating, while the MTR model greatly overpredicts the peak heating levels in the interaction region by as much as a factor of four.

Coratekin et al. [99] have computed the 38 deg. ramp case of Coleman and Stollery/Elfstrom with three turbulence models: a low Reynolds number version of the Wilcox 1988 k-ω model (kω88LR) [132], the Spalart-Allmaras model (SA) [7],[8], and the hybrid k-ω/k-ε model of Menter with the shear stress transport option (SST) [13]. They also examined various compressibility corrections to the kω88LR model, but these corrections have not be evaluated over a wide variety of flowfields and thus will not be included here. A single grid of 128×64 cells is used for this case, with a grid refinement study using three grid levels being performed on a Mach 3, 24 deg. compression corner and assumed to extend to the hypersonic case. The y^+ values employed are not discussed and no sensitivity is performed for the freestream turbulence values. The kω88LR and STT models match the surface pressure levels reasonably well, but underpredict the extent of flow separation as judged by the initial rise in surface pressure. The SA model give good estimates of both the surface pressure and separation extent. The peak surface heat flux levels are overpredicted by a factor of two for all the models, and local values of heat flux are as much as five times the experimental measurements in the interaction region.

Holden Experiment [48]

Due to the concerns regarding the equilibrium nature of the upstream boundary layer, the compression corner experiments conducted by Holden [48] are also included here, although it too fails to report uncertainties on the surface measurements. While no upstream boundary layer profile is measured in this experiment, the surface quantities compared well to the Van Driest II correlations [127]; furthermore, the transition location can be easily determined from the surface skin friction and heat transfer measurements made on a flat plate and reported in the same reference. The freestream Mach number for this case is approximately 8 and the ratio of wall temperature to the freestream stagnation temperature was 0.3. The Reynolds number based on the boundary layer thickness at the interaction location was varied between 100,000 and 10 million. Measurements are reported for surface pressure, skin friction, and heat transfer in the interaction region for wedge angles of 27, 30, 33, and 36 deg. and along the flat plate in a configuration without the wedge. Span effects were also investigated and shown to be negligible. This was the first experiment to show the reversal of the separation zone size and incipient separation with Reynolds number within the same experiment. To our knowledge, this experiment has not been employed for validating turbulence models.

5.3.2. Cylinder with conical flare (case 2)

There are two experiments which meet the Settles and Dodson criteria for the axisymmetric cylinder-flare geometry. The first was included in the Settles and Dodson review and was performed by Kussoy and Horstman [34] at NASA-Ames Research Center. The second is a more recent experiment performed in the supersonic blow-down wind tunnel (HSST) at DRA Fort Halstead, Great Britain and is detailed by Babinsky [57] and Babinsky and Edwards [56]. The former experiment has seen extensive validation usage, while to the authors' knowledge, the latter experiment has not yet been computed in the literature. An overview of the turbulence model validation for this case as discussed below is shown graphically in Figs. 9-12.

Kussoy and Horstman Experiment [34]

Kussoy and Horstman [34] studied the flow over axisymmetric ogive-cylinder-flares at a freestream Mach number of 7 for flare angles between 20 deg. and 35 deg. Data include surface pressure and surface heat transfer both upstream of the shock/boundary layer interaction (see Case 1: flat plate/cylinder flow) and in the interaction region. Pitot-probe surveys through the boundary layer are presented at various axial locations for the 20 deg. flare case only, with the boundary layer surveys upstream of the interaction confirming a fully-developed turbulent boundary layer. Information is given on freestream RMS values for stagnation temperature and mass flux as well as temperature for the water-cooled model surface. The data set includes experimental uncertainty estimates for each measured quantity. Derived boundary layer quantities (displacement thickness, momentum thickness, etc.) are also reported upstream of the interaction. Surface data were taken at 90 deg. locations to confirm that the flow was axisymmetric, and multiple runs were conducted to reduce run-to-run uncertainty. A relatively long model was employed to allow for natural (non-tripped) transition to occur at approximately 0.4 to 0.8 m from the tip, which is at least 0.6 m upstream of the interaction region.

The Kussoy and Horstman cylinder-flare experiments [34] have been used for turbulence model validation purposes by Horstman [98], [89]. A brief synopsis of his results were presented in Ref. [89], while a more detailed discussion is given in Ref. [98]. Horstman examined two different two-equation turbulence models: the low Reynolds number k-ε model of Jones and Launder (kεJL) [10] and the low Reynolds number k-ε model of Rodi (kεR) [160] (a third "compressible" k-ε model is omitted from the present discussion as mentioned in Section 5.3.1). Mesh resolution studies were discussed, however no results were shown and no estimates of the discretization error were reported. The sensitivity to wall-normal mesh spacing was examined and is reported in section 5.3.1 above for the 2D compression corner. For the 20 deg. flare case which was nominally attached flow, both k-ε models gave accurate predictions of the surface pressure. The kεJL model gave reasonable predictions of the heat transfer (within approximately 30%), while the kεR model predicted heat transfer within the experimental uncertainty bounds everywhere except possibly in the recovery region where the heat transfer is underpredicted by as much as 25%. For the 35 deg. flare case with flow separation, the surface pressure was reasonably well predicted by both models, while the heat transfer was over-predicted by an order of magnitude or more by the keJL model and underpredicted by almost a factor of two by the kεR model. The size of the separation zone for this case is under-predicted by over 50% as judged by the initial pressure rise and the peak pressure.

Coakley, Huang, and co-workers [84], [90], [86] also used the Kussoy and Horstman cylinder-flare experiments [34] for turbulence model validation purposes. A number of different two-equation turbulence models were examined including: the q-ω model of Coakley (qω) [85], the 1988 k-ω model of Wilcox (kω88) [132], the k-ε model of Launder and Sharma (kεLS) [11], the k-ε model of Chien (kεCH) [82], the k-ε model of So (kεSO) [83] which includes compressibility extensions given by Zhang et al. [146], and the k-ε model of Huang and Coakley (kεHC) [84]. For a more detailed discussion of this study, see section 5.3.1 above for the 2D compression corner. Only the kεLS and kω88 models were applied to the 20 deg. flare case [84], and both models provided good predictions of the surface pressure. The heat transfer predictions were as much as twice the experimental values. All six models were applied to the 35 deg. flare case [90]. The kεLS, kω88, and qω models gave an adequate prediction of the surface pressure levels, but under-predicted the size of the separation zone by 60%. These models predicted an early peak heating location, with maximum errors of a factor of 6.5, 3, and 4, respectively. The kεHC and kεSO models gave reasonable pressure predictions and only under-predicted the separation zone size by approximately 20%. The peak heating, however, was still over-predicted by a factor of 2.5.

Babinsky and Edwards Experiment [56], [57]

Babinsky and Edwards [56] conducted careful experimental studies of cylinder-flare flows at Mach 5.1 for flare angles between 3 deg. and 20 deg., with additional details presented by Babinsky [57] for flare angles of 15 deg. and 20 deg. The experiments were conducted in the supersonic blow-down wind tunnel (HSST) at DRA Fort Halstead, Great Britain using a Mach 5 nozzle that included a cylindrical centerbody which extended upstream of the test section to the nozzle throat. This centerbody was deemed necessary to allow for the formation of a fully-developed turbulent boundary layer without the use of flow-intrusive boundary layer tripping mechanisms. However, the use of the centerbody led to the presence of non-negligible axial gradients of pitot pressure (10% variation) and Mach number (3% variation) in the test section. Data were presented for

surface pressure, surface heat transfer (via high-resolution liquid crystal thermography), and pitot pressure through the boundary layer at various axial stations. Detailed experimental uncertainties were also provided for each of the measured quantities. Derived quantities presented include velocity profiles, skin friction, boundary layer thickness, and displacement thickness. Conventional theory suggests that for flow angles of 20 deg. and below, no separation will occur. However, investigations using shear stress sensitive liquid crystals showed a small separated region (possibly in the laminar sublayer) for both the 15 and 20 deg. flare cases. The authors suggest that the presence of this small separation zone destroys the similarity between pressure and heat transfer. This experiment has not yet been used for turbulence model validation but is highly recommended.

5.3.3. Cone with conical flare (case 3)

There is only one experiment for the cone/conical flare case that is appropriate for turbulence model validation. Holden [44] performed experiments in Calspan's 96 in shock tunnel at Mach numbers of 11 and 13. This is one of Settles and Dodson's accepted hypersonic experiments; however, there is some discrepancy regarding the references. Settles and Dodson [1],[4] reference a 1984 AIAA Paper [36], a 1986 CUBRC internal report [35], and a 1988 AFOSR technical report [161], all by Holden and co-workers. The initial reporting of these cone/conical flare experiments was not until 1991 in Ref. [44], and this is confirmed by examining Refs. [42] and [162] which are reviews of the experimental hypersonic program conducted at Calspan. In any case, the data presented by Settles and Dodson [1] does appear to be the same data given in Refs. [44] and [162]. It should also be noted that there is also some question regarding the flare angle for this case. Ref. [44] does not make it clear whether the flare angle is measured from the symmetry axis or from the initial cone angle of 6 deg., while Ref. [162] clearly shows that the flare angle should be measured from the symmetry axis. However, Settles and Dodson [1] state that the flare angles should be measured from the 6 deg. forecone, and crude angles measured from Schlieren photographs in [44] and [162] seem to support this conclusion. An overview of the turbulence model validation for this case as discussed below is shown graphically in Figs. 13-14.

Holden Experiment

Holden [44] studied the flow over 6 deg. (half angle) cones with conical flares at freestream Mach numbers of 11 and 13 for flare angles of 30 and 36 deg. The smaller flare angle represents an incipient separated flow case, while the larger angle a fully separated flow. Data include surface pressure and heat transfer as well as pitot pressure and total temperature within the interaction region. Experimental uncertainties are given for the freestream conditions as well as heat transfer coefficient (±5%) and pressure coefficient (±3%).

The Holden cone/conical flare experiment [44] at Mach 11 with a flare angle of 36 deg. has been used for turbulence model validation by Horstman [98] who examined two different two-equation turbulence models: the low Reynolds number k-ε model of Jones and Launder (kεJL) [10] and the low Reynolds number k-ε model of Rodi (kεR) [160] (a third "compressible" k-ε model is omitted from the present discussion as mentioned in Section 5.3.1). Mesh resolution studies were discussed, however no results were shown and no estimates of the discretization error were reported. The sensitivity to wall-normal mesh spacing was examined and is reported in section

5.3.1 above for the 2D compression corner. The surface pressure was reasonably well predicted by the kεR model in the interaction region, with the onset of separation (judged by the initial rise in pressure) occurring slightly downstream of the experimental location. The kεJL model greatly underpredicts the size of the separated zone, and both models fail to capture a secondary peak in the pressure in the vicinity of the downstream plateau region. The kεJL model also overpredicts the peak heating level by nearly a factor of two, but accurately matches the heating in the recovery region downstream of the interaction. The kεR model underpredicts both the peak heating and the heating levels in the recovery region by 50%.

5.3.4. Axisymmetric impinging shock (case 4)

There are two different axisymmetric impinging shock experiments which are deemed acceptable for turbulence model validation. The first is a series of experiments conducted by Kussoy et al. at a Mach number of 7 on a cone-ogive-cylinder model [37], [164], [102]. The second is a more recent experimental investigation by Hillier et al. at Mach 9 on a hollow cylinder model [101]. An overview of the turbulence model validation for this case as discussed below is shown graphically in Figs. 15-16.

Kussoy and Horstman Experiment [37], [164], [102]

Kussoy and Horstman studied the flow over an axisymmetric cone-ogive-cylinder model at a freestream Mach number of 6.9. Axisymmetric cowls of 7.5 and 15 deg. were used to impinge axisymmetric shock waves onto the turbulent boundary layer on the cylinder. Surface data include surface pressure, heat transfer, and skin friction [37], [164]. Pitot pressure, static pressure, and total temperature were surveyed throughout the interaction region [37], [164]. Ref. [102] also presents turbulence intensity and Reynolds stress profiles for these two cases. The cowl length is relatively short, thus the leading shock wave and subsequent expansion fan merge before the shock impinges on the surface. It is therefore strongly recommended that future computations of this experiment also include the viscous boundary layer on the outer cowl itself. The length of the model cylinder is 3.3 m, thus suggesting a fully-developed turbulent boundary layer is formed well ahead of the interaction region. The model surface is water-cooled to maintain a temperature of 300 K. The data set includes experimental uncertainty estimates for each measured quantity, with the exception of the turbulence measurements of Ref. [102]. Derived boundary layer quantities (displacement thickness, momentum thickness, etc.) are also reported upstream of the interaction. Settles and Dodson give the experimental data for the 15 deg. shock generator case [1] in tabular form.

Marvin and Coakley [100] used the Kussoy and Horstman axisymmetric impinging shock experiment [37], [164] with a shock generator angle of 15 deg. for the validation of the q-ω model of Coakley (qω) [85]. The authors fail to report the effects of mesh refinement, variations of the y^+ values, or the effects of varying the freestream turbulence values. Although a negligible amount of flow separation is shown by the experimental data and the qω model, the model significantly underpredicts the size of the interaction region. As a result, the model greatly overpredicts the peak levels of pressure, skin friction, and heat flux (although the scale chosen for the figures does not include the peak values from the model).

The Kussoy and Horstman axisymmetric impinging shock experiment [37], [164] with a shock generator angle of 15 deg. has been used for turbulence model validation by Horstman [98] who

examined two different two-equation turbulence models: the low Reynolds number k-ε model of Jones and Launder (kεJL) [10] and the low Reynolds number k-ε model of Rodi (kεR) [160] (a third "compressible" k-ε model is omitted from the present discussion as mentioned in Section 5.3.1). Mesh resolution studies were discussed, however no results were shown and no estimates of the discretization error were reported. The sensitivity to wall-normal mesh spacing was examined and is reported in section 5.3.1 above for the 2D compression corner. Neither model is able to predict the mild amount of flow separation indicated by the experimental data, and both also underpredict the size of the interaction region. As a result, the peak pressures are overpredicted by 25% and the upstream pressure rise is not captured at all. The peak skin friction levels are overpredicted by a factor of two with the kεR model and a factor of three with the kεJL model. Both models match the surface pressure and skin friction in the recovery region well within the experimental uncertainty bounds. The surface heating levels are overpredicted by 50% with the kεR model and by at least a factor of two with the kεJL model, while the recovery heat flux is underpredicted by 30% with kεJL and 50% by kεR.

Huang and Coakley [90] and Coakley et al. [86] used both shock generator angles of the Kussoy and Horstman experiment [37], [164] for turbulence model validation. Two two-equation turbulence models were examined: the 1988 k-ω model of Wilcox (kω88) [132] and the k-ε model of Launder and Sharma (kεLS) [11]. A mesh refinement study was discussed and the authors state that changing the mesh had no effect of the predictions. While a y^+ sensitivity study was not conducted explicitly, the y^+ values were kept below 0.5 which had been shown to be sufficient for these models in a related study [84]. The effects of changing the freestream turbulence quantities was not assessed in these studies. For the 7.5 deg. shock generator case, both models accurately predict the extent of the interaction region and the surface pressure; however, both models also overpredict the peak heating and skin friction levels by 35% and 70%, respectively. For the 15 deg. shock generator case, the width of the interaction region is underpredicted and the initial pressure rise in the vicinity of the separated flow region is not captured. The peak levels of pressure and skin friction are overpredicted by approximately 30% and 100%, respectively. The kεLS model overpredicts the heating by more than a factor of two, while the kω88 model is 60% higher than the data. The kω88 model overpredicts all three surface quantities by at least a factor of two in the recovery region. The kεLS model accurately captures the wall pressure and skin friction in the recovery region, but underpredicts the heating in the recovery region by 50%.

Hillier et al. Experiment [101]

Hillier et al. studied the flow over an axisymmetric cone-ogive-cylinder model at a freestream Mach number of 8.9 and Reynolds number of 52×10^6/m. An axisymmetric cowl with a quadratic expression for the shock-generating surface is used to impinge an axisymmetric shock wave onto the turbulent boundary layer formed on the cylinder. Surface data include surface pressure and heat transfer. Transition of the boundary layer on the cylinder begins at 80 mm and ends at 170 mm, with the shock interaction occurring at roughly 520 mm. Due to the curved nature of the shock-generating cowl, it is recommended that computations of this experiment also include the viscous boundary layer on the outer cowl itself. The model surface temperature is not reported in the experiment, but should be readily available from the authors. The data set includes experimental

uncertainty estimates for the surface pressure and heat transfer. To our knowledge, this experiment has not been used in the validation of one- or two-equation turbulence models.

5.3.5. 2D impinging shock (case 11)

A 2D impinging shock occurs when an externally generated oblique shock impinges on a flat plate boundary layer. There is only one experimental data set that satisfies the Settles and Dodson criteria. Kussoy and Horstman [40] conducted a careful experimental study of the 2D impinging shock case in the Ames 3.5 ft Hypersonic Wind Tunnel at Mach 8.2. An overview of the turbulence model validation for this case as discussed below is shown graphically in Figs. 17-18.

Kussoy and Horstman Experiment

Kussoy and Horstman [40] studied a 2D oblique shock impinging on a turbulent flat plate boundary layer at a freestream Mach number of 8.2 for effective wedge angles of 5, 8, 9, 10, and 11 deg. Data include surface pressure and heat transfer both upstream of the shock/boundary layer interaction (see Case 9: flat plate/cylinder flow) and in the interaction region. Mean flow surveys through the boundary layer are given for the undisturbed boundary layer (i.e., without the shock generator) in the vicinity of where the shock interaction would occur. Surveys in the interaction are alluded to in the report, but are not presented (these may be included on a computer disk which is mentioned in the report). The model is water-cooled to maintain a surface temperature of 300±5 K. The data set includes extensive experimental uncertainty estimates for each measured quantity, but not for the freestream conditions. A relatively long 2.2 m model was employed to allow for natural (non-tripped) transition to occur approximately 0.5 to 1 m from the leading edge, which is at least 0.5 m upstream of the interaction region. The model length results in a fully developed, equilibrium turbulent boundary layer (confirmed by the flowfield surveys) that is nearly 4 cm high near the interaction region.

The Kussoy and Horstman 2D impinging shock experiment [40] with an effective wedge angle of 10 deg. has been used for turbulence model validation by Horstman [98] who examined two different two-equation turbulence models: the low Reynolds number k-ε model of Jones and Launder (kεJL) [10] and the low Reynolds number k-ε model of Rodi (kεR) [160] (a third "compressible" k-ε model is omitted from the present discussion as mentioned in Section 5.3.1). Mesh resolution studies were discussed, however no results were shown and no estimates of the discretization error were reported. The sensitivity to wall-normal mesh spacing was examined and is reported in section 5.3.1 above for the 2D compression corner. The surface pressure was accurately predicted by both models, with the predictions falling just outside the experimental uncertainty bars over the entire interaction region. The models do appear to slightly underpredict the upstream separation point as judged by the initial rise in the surface pressure. The kεJL model overpredicts the heating by 60% in the interaction region, but accurately matches the heating in the recovery region downstream of the interaction. The kεR model accurately predicts the heating in the interaction region, but underpredicts the heating levels in the recovery region by up to 20%.

The Kussoy and Horstman experiment [40] for 5 and 10 deg. wedge angles was also used by Smith [105] in the validation of a two-equation *k-l* model (*kl*) [105], [163]. A compressibility correction designed specifically for high-speed separated flows[86] was also investigated by the author, but is unclear how this correction impacts the previous validation efforts for the model,

especially at low speeds. Results for the corrected model will therefore not be included here. The transition onset and extent were set to 50 and 100 cm, respectively, (as suggested by the experiment) to achieve the best fit to the undisturbed boundary layer profile. A grid refinement study was performed for the model with the compressibility correction for the 10 deg wedge case with minor effects on the surface properties. The y^+ values in each case are discussed, but no y^+ sensitivity was performed and the effects of varying the freestream turbulence levels were not examined. For the 5 deg. wedge case, the surface pressure is accurately predicted by the model, with a slight underprediction of the upstream extent of the pressure rise. The heat transfer was overpredicted by as much as 30% within the interaction region for this case. The results for the 10 deg. wedge were similar.

6. Recommendations

We recommend that new hypersonic flow experiments be conducted. In addition to surface quantities, these experiments should measure profiles of both mean properties and turbulence statistics (rms velocities, Reynolds stresses, turbulent kinetic energy, etc.) in the interaction region, preferably using non-intrusive measurement techniques. Significant efforts should be made to quantify and reduce the experimental uncertainties in the measurement and freestream quantities. Approaches for converting experimental bias errors into random uncertainties (e.g., Ref. [166]) should also be employed.

On the turbulence modeling side, we recommend that compressibility corrections be implemented in the baseline turbulence models. Some of these corrections (e.g., Catris and Aupoix [131]) vanish as the mean density variations are reduced, thus ensuring prior model validation efforts at low speeds are still valid. For other corrections (e.g., Coakley et al. [86]), the low-speed model validation test cases may need to be revisited. The use of ad hoc model corrections applied to a limited class of flows (i.e., calibration or parameter fitting) should be avoided for turbulence models that will be applied to general hypersonic flows.

Finally, the review and assessment study presented in the current paper should be extended to include 3D hypersonic test cases. We will present such an extension in an upcoming article to be published in the international review journal *Progress in Aerospace Sciences*.

Acknowledgements

The authors would like to thank R. Duggirala and P. Veluri for their aid in preparing the figures presented in this review.

Appendix A: Compressibility Corrections

With the two-equation turbulent turbulence models, the standard form of these equation is not adequate for compressible flows to obtain the logarithmic region of the velocity profile as shown by Huang, Bradshaw, and Coakley [71]. For the $k-\varepsilon$ turbulence, the standard and modified equations developed by Catris and Aupoix [131] are presented. In addition, the modified equation for the eddy viscosity for compressible flow developed by Catris and Aupoix [131] is also presented.

Two-Equation $k-\varepsilon$ Turbulence Models

The standard or classical form of the turbulent kinetic energy equation is

$$\bar{\rho}\frac{Dk}{Dt} = \frac{\partial}{\partial t}(\bar{\rho}k) + \frac{\partial}{\partial x_j}(\bar{\rho}u_j k) = D_k + S_{Pk} - S_{Dk} \tag{1}$$

where the diffusion, production, and destruction terms are

$$D_k = \frac{\partial}{\partial x_j}\left[\left(\mu + \frac{\mu_T}{\sigma_k}\right)\frac{\partial k}{\partial x_j}\right] \qquad S_{Pk} = P_k \qquad S_{Dk} = \bar{\rho}\varepsilon$$

In the above P_k is the turbulent kinetic energy production. Huang, Bradshaw, and Coakley [167] have shown for two-equation turbulence models, that density corrections to the incompressible closure coefficients are required to obtain a logarithmic region of the velocity profile for compressible flows. Catris and Aupoix [131] have modified the turbulent transport equation for two-equation turbulence models. A compressibility correction to the turbulent kinetic energy equation has been developed by Catris and Aupoix, which gives the same form as Eq. (1) except the diffusion term is modified as follows:

$$D_k = \frac{\partial}{\partial x_j}\left[\left(\frac{\mu}{\bar{\rho}} + \frac{\mu_T}{\bar{\rho}\sigma_k}\right)\frac{\partial(\bar{\rho}k)}{\partial x_j}\right]$$

The standard or classical form of the dissipation equation is

$$\bar{\rho}\frac{D\varphi}{Dt} = \frac{\partial}{\partial t}(\bar{\rho}\varphi) + \frac{\partial}{\partial x_j}(\bar{\rho}u_j\varphi) = D_\varepsilon + S_{P\varepsilon} - S_{D\varepsilon} \qquad \varphi = \varepsilon \tag{2}$$

where the diffusion, production, and destruction terms are

$$D_\varepsilon = \frac{\partial}{\partial x_j}\left[(\mu + \mu_T/\sigma_\varepsilon)\frac{\partial\varphi}{\partial x_j}\right] \qquad S_{P\varepsilon} = c_{\varepsilon 1} f_1 P_k \frac{\varphi}{k} \qquad S_{D\varepsilon} = c_{\varepsilon 2} f_2 \bar{\rho}\frac{\varphi^2}{k}$$

A compressibility correction to the dissipation equation has been developed by Catris and Aupoix [131], which gives the same transport equation as Eq. (2) but with $\varphi = \bar{\rho}\varepsilon$. The diffusion term becomes

$$D_\varepsilon = \frac{\partial}{\partial x_j}\left[\left(\frac{\mu}{\sqrt{\bar{\rho}}} + \frac{\mu_T}{\sigma_\varepsilon\sqrt{\bar{\rho}}}\right)\frac{\partial\sqrt{\bar{\rho}}\varphi}{\partial x_j}\right] \qquad S_{P\varepsilon} = c_{\varepsilon 1} f_1 P_k \frac{\varphi}{k} \qquad S_{D\varepsilon} = c_{\varepsilon 2} f_2 \frac{\varphi^2}{k}$$

The production, and destruction terms are the same form as above but $\varphi = \bar{\rho}\varepsilon$.

Spalart-Allmaras Model

The transport equation for the eddy viscosity was originally developed by Spalart-Allmaras (S-A). Spalart [168] states, "Note that the S-A paper was silent on large density variations, and therefore....". The transport equation is written with the dependent (working) variable $\varphi = \nu$ in the following form, which is appropriate for *S-A model for incompressible flows*:

$$\frac{D\varphi}{Dt} = \frac{\partial\varphi}{\partial t} + \tilde{u}_j\frac{\partial\varphi}{\partial x_j} = D^* + S_P{}^* - S_D{}^* \tag{3}$$

The turbulent eddy viscosity is related to the dependent variable by the relation $\mu_T = \bar{\rho}\varphi f_{v1}$. The diffusion term D^* is

$$D^* = \frac{\partial}{\partial x_j}\left(\mu^*\frac{\partial\varphi}{\partial x_j}\right) + \frac{c_{b2}}{\sigma}\frac{\partial\varphi}{\partial x_j}\frac{\partial\varphi}{\partial x_j} \qquad \mu^* = [(\mu/\bar{\rho}) + \varphi]/\sigma$$

The production term is $S_P{}^* = c_{b1}\tilde{S}\varphi$ and the destruction term is $S_D{}^* = c_{w1}f_w(\varphi/d)^2$. The various terms introduced are defined in the original paper of Spalart and Allmaras. The gas density $\bar{\rho}$ does not appear in the transport equation for φ except in the viscous sublayer. However, the density does appear in the relation for determining the eddy viscosity.

In fluid dynamics codes, the governing equations are generally written in conservation form. The above kinematic eddy viscosity transport Eq. (3) is rewritten in conservation form by multiplying the equation by the density and using the conservation of mass equation to obtain the following *conservation form for the S-A turbulence model*:

$$\bar{\rho}\frac{D\varphi}{Dt} = \frac{\partial}{\partial t}(\bar{\rho}\varphi) + \frac{\partial}{\partial x_j}(\bar{\rho}u_j\varphi) = D + S_P - S_D \tag{4}$$

The diffusion term with a variable density included is

$$D = \frac{\partial}{\partial x_j}\left(\mu_{ef}\frac{\partial\varphi}{\partial x_j}\right) + \frac{c_{b2}}{\sigma}\frac{\partial\varphi}{\partial x_j}\frac{\partial\varphi}{\partial x_j} - \mu^*\frac{\partial\varphi}{\partial x_j}\frac{\partial\bar{\rho}}{\partial x_j}$$

$$\mu_{ef} = \bar{\rho}\ \mu^* = [\mu + \bar{\rho}\varphi]/\sigma$$

The production term is

$$S_P = \bar{\rho} S_P^* = c_{b1} \tilde{S} \bar{\rho} \varphi \tag{5}$$

The destruction term is

$$S_D = \bar{\rho} S_D^* = c_{w1} f_w \bar{\rho} (\varphi / d)^2 \tag{6}$$

The last term in the diffusion term above, which involves the density gradient, is zero for incompressible flows and is usually neglected for compressible flows (see for example: Bardina et al. [91], Roy and Blottner [9], and FLUENT code [165]).

The Spalart-Allmaras model has been modified by Catris and Aupoix [131] to account for compressibility effects. The resulting *Catris and Aupoix equation for the S-A turbulence model for compressible flow* is

$$\frac{D(\bar{\rho}\varphi)}{Dt} = \frac{\partial}{\partial t}(\bar{\rho}\varphi) + u_j \frac{\partial}{\partial x_j}(\bar{\rho}\varphi) = D + S_P - S_D \qquad \varphi = (\mu_T / \bar{\rho}) f_{v1} \tag{7}$$

The diffusion term is

$$D = \frac{\partial}{\partial x_j}\left[\frac{\mu}{\sigma} \frac{\partial(\sqrt{\bar{\rho}}\varphi)}{\partial x_j} + \frac{\sqrt{\bar{\rho}}\varphi}{\sigma} \frac{\partial(\sqrt{\bar{\rho}}\varphi)}{\partial x_j} \right] + \frac{c_{b2}}{\sigma} \frac{\partial}{\partial x_j}(\sqrt{\bar{\rho}}\varphi) \frac{\partial}{\partial x_j}(\sqrt{\bar{\rho}}\varphi)$$

The form of Eq. (7) in conservation form on the left hand side becomes

$$\frac{D(\bar{\rho}\varphi)}{Dt} = \frac{\partial}{\partial t}(\bar{\rho}\varphi) + \frac{\partial}{\partial x_j}(\bar{\rho} u_j \varphi) - \bar{\rho}\varphi \frac{\partial u_j}{\partial x_j} = D + S_P - S_D \tag{8}$$

The production term is defined in Eq. (5) and the destruction term is defined in Eq. (6).

Appendix B: Turbulent Flat Plate Correlations

Correlation of Skin Friction Data

The standard approach for correlation of compressible skin friction on a flat plate is the Van Driest II transformation [115]. This approach transforms the compressible skin friction at a given compressible momentum thickness Reynolds number into the incompressible skin friction at an incompressible momentum thickness Reynolds number. A more complete analysis for the correlation of the skin friction, which was developed by Huang, Bradshaw, and Coakley [71] (HBC) has also been evaluated. The transformation theories transform the experimental compressible skin friction and momentum thickness Reynolds number to incompressible values as follows for the Van Driest II theory

$$C_{fvD} = F_c C_f \qquad F_c \text{ skin friction transformation function}$$

$$Re_{\theta vD} = F_\theta Re_\theta \qquad F_\theta \text{ momentum thickness Reynolds No. transformation function}$$

Therefore if the theory is accurate, the transformed skin friction C_{fvD} and momentum thickness Reynolds number $Re_{\theta vD}$ should be the same as the incompressible values.

$$C_{fvD} \approx C_{f,\,i} \qquad Re_{\theta vD} \approx Re_{\theta,\,i}$$

The transformation functions are given by

$$F_c = rm/(\sin^{-1}\alpha + \cos^{-1}\beta)^2$$

$$F_\theta = \mu_e/\mu_w \qquad F_s = F_\theta/F_c$$

where

$$m = M_e^2(\gamma - 1)/2 \qquad F = T_w/T_e$$

$$r = \text{Recovery factor} = 0.9$$

$$A = \sqrt{rm/F} \qquad B = (1 + rm - F)/F$$

$$\alpha = (2A^2 - B)/\sqrt{4A^2 + B^2}$$

$$\beta = B/\sqrt{4A^2 + B^2}$$

The local incompressible skin friction is evaluated from Karman-Schoenherr relation which is considered the most accurate fit to the incompressible experimental data:

$$C_{f,\,i} = \frac{1}{\log(2Re_\theta|_{inc})[17.075\log(2Re_\theta|_{inc}) + 14.832]}$$

The accuracy of the theory relative to the experimental data is illustrated by plotting the skin friction as a function of momentum thickness Reynolds number for the incompressible and transformed variables. A more sensitive illustration of the accuracy is to use percent error E of experimental skin friction relative to theoretical, which is obtained from

$$E = [(C_{f,\,i}/C_{fvD}) - 1] \times 100$$

Then the percent error E is plotted verses Re_θ. Correlation of the experimental measured skin friction of compressible flows has proven to be reasonably effective with Van Driest II approach. The correlation approach of Huang, Bradshaw, and Coakley [71] gives results of similar accuracy. Squire [72] estimates that the accuracy of the Van Driest II correlation is within ±3% for the flat plate. Based on the sometimes erratic agreement between experiments and the correlation, we feel that this error estimate is somewhat optimistic.

Correlation of Heat Transfer

Reynolds analogy is used to predict the wall heat flux, which is expressed as the Stanton number

$$St = q_w/[\rho_e u_e(H_w - H_{aw})] \qquad C_f = 2\tau_w/\rho_e u_e^2$$

Reynolds analogy (1874) is written in terms of the compressible skin friction

$$2St/C_f = R_{af} = \text{ Reynolds analogy factor}$$

There are several models to predict R_{af} as follows where it is assumed that $Pr = 0.71$:

Reynolds: $R_{af} = 1$

Colburn: $R_{af} = Pr^{-2/3} = 1.26$

Prandtl-Kármán: $R_{af} = [1 + g\sqrt{C_f/2}]^{-1}$ and assume $C_f = 0.004$

Prandtl: $g = 8.7(Pr - 1) = -2.523$ and $R_{af} = 1.13$

Kármán: $g = 5\left\{(Pr-1) + \ln\left[1 + \left(\frac{5}{6}\right)(Pr-1)\right]\right\} = -2.833$ and $R_{af} = 1.15$

Experiments indicate that $0.9 < R_{af} < 1.3$, but may be close to unity for hypersonic flows. There is insufficient reliable experimental data to establish the Reynold analogy factor.

Mean Temperature Profiles

A review of the analysis used to obtain analytical solutions to the boundary layer energy equation are given in the report of Fernholz and Finley [31]. The initial relation developed by Crocco and Busemann assumes that the laminar and turbulent Prandtl numbers are one $(Pr = Pr_T = 1)$. A solution to the total enthalpy energy equation is that the total enthalpy is constant across the boundary layer. Since $\tilde{u} = 0$ and $k = 0$ at the wall and $h = c_p T$, the following relations are obtained for the total enthalpy and the temperature:

$$\begin{gathered} H = h + \tilde{u}^2/2 + k = H_w = h_w \qquad T = T_w - \alpha\tilde{u} - \beta\tilde{u}^2 - \gamma_T k \\ \alpha = 0 \qquad \beta = 1/2c_p \qquad \gamma_T = 1/c_p \end{gathered} \tag{9}$$

The second relation developed by Crocco and Busemann assumes a zero pressure gradient with an isothermal wall and the laminar and turbulent Prandtl numbers are one. The momentum and energy equations are similar, which gives $H = C_1 + C_2\tilde{u}$. With the wall and edge boundary conditions applied, the energy equation in terms of temperature becomes Eq. (9) with the coefficients

$$\alpha = [T_w - T_e - \beta\tilde{u}_e^2 - \gamma_T k_e]/\tilde{u}_e \qquad \beta = 1/2c_p \qquad \gamma_T = 1/c_p \tag{10}$$

Van Driest extended the Crocco analysis for compressible laminar boundary flows to turbulent flows with a variable Prandtl number. The development of this Van Driest [73] temperature relation becomes very complex and not very useful. The mixed Prandtl number was initially introduced in this article by Van Driest and is defined as

$$Pr_m = c_p\left(\frac{\mu + \mu_T}{k + k_T}\right) = \frac{\mu + \mu_T}{(\mu/Pr) + (\mu_T/Pr_T)} \qquad Pr = \frac{c_p\mu}{k} \qquad Pr_T = \frac{c_p\mu_T}{k_T}$$

Fernholz and Finley [31] have presented the work of Walz where the temperature equation is developed for a constant Prandtl number which is restricted to $0.7 < Pr < 1$.

Huang, Bradshaw, and Coakley [71] (HBC) have developed the temperature equation by neglecting the convective terms in the momentum and energy equations. The reduced boundary layer momentum equation with the pressure gradient neglected can be integrated once to obtain

$$(\mu + \mu_T)\frac{d\tilde{u}}{dy} = \tau_w \tag{11}$$

The total enthalpy form of the reduced energy equation can be integrated once to obtain

$$-q + \tilde{u}\tau_w + (\mu + \mu_T)\frac{dk}{dy} = \text{constant}$$

Since at the wall $\tilde{u} = 0$ and $k = c_k y^2 + \ldots$, the constant in the above equation is q_w and the energy equation becomes

$$q = q_w + \tilde{u}\tau_w + (\mu + \mu_T)\frac{dk}{dy} \tag{12}$$

The heat flux normal and near to the wall becomes with the use of the momentum Eq. (11)

$$q = -\left(\frac{\mu + \mu_T}{Pr_m}\right)\frac{\partial h}{\partial y} = -\frac{c_p}{Pr_m}(\mu + \mu_T)\frac{\partial T}{\partial y} = -\frac{c_p\tau_w}{Pr_m}\frac{\partial T}{\partial u} \tag{13}$$

From Eq. (13) and the temperature relation in Eq. (9), the wall heat flux is $q_w = \alpha c_p \tau_w / Pr_m$ and when solved for q_w/τ_w gives

$$q_w/\tau_w = [T_w - T_e - \beta\tilde{u}_e^2 - \gamma_T k_e](c_p/\tilde{u}_e Pr_m)$$

$$\beta\tilde{u}_e^2 = \tilde{u}_e^2/2c_p = mT_e \qquad m = \tilde{u}_e^2/2c_pT_e = \left(\frac{\gamma - 1}{2}\right)M_e^2$$

Using Eq. (12) and Eq. (13), the differential form of the temperature equation becomes

$$dT = -\frac{Pr_m}{c_p}\left[\left(\frac{q_w}{\tau_w} + \tilde{u}\right)d\tilde{u} + dk\right] \tag{14}$$

Integration of this equation with Pr_m constant gives the temperature Eq. (9) with the coefficients

$$\alpha = (Pr_m/c_p)(q_w/\tau_w) \qquad \beta = Pr_m/2c_p \qquad \gamma_T = Pr_m/c_p \tag{15}$$

Eq. (11) and Eq. (12) have been used by HBC with μ and k neglected to obtain the energy Eq. (9) with coefficients given in Eq. (15) where $Pr_m = Pr_T$. The energy equation developed by Fernholz and Finley [31] is essentially the same as given above, except the turbulent Prandtl number in the coefficients α and β is replaced with the recovery factor r. The above coefficient α can also be written as

$$\alpha = [T_w - T_e - \beta\tilde{u}_e^2 - \gamma_T k_e]/\tilde{u}_e$$

For an adiabatic wall $\alpha = 0$ and the above equation with Eq. (15) gives the adiabatic wall temperature $T_{aw} = T_e(1 + Pr_T m + \gamma_T k_e)$ where $Pr_m = Pr_T$. Since the adiabatic wall temperature is defined as $T_{aw} = T_e(1 + rm)$, the recovery factor $r = Pr_T$ for this analysis. The total temperature $T_t = T + \tilde{u}^2/2c_p$ is written in non-dimensional form as $T^* = (T_t - T_w)/(T_{te} - T_w)$ and is plotted as function of $\tilde{u}/\tilde{u}_e$. At the wall $T^* = 0$ and at the edge of the boundary layer $T^* = 1$. When $Pr_T = 1$, the non-dimensional total temperature has a linear variation, $T^* = \tilde{u}/\tilde{u}_e$. When the wall is adiabatic $T_w = T_{aw}$ and the recovery factor equals the turbulent Prandtl number, the non-dimensional total temperature has quadratic variation, $T^* = (\tilde{u}/\tilde{u}_e)^2$.

The Van Driest form of the temperature or density equation with the turbulent kinetic energy neglected is

$$T/T_w = \bar{\rho}_w/\bar{\rho} = 1 + B(u/u_e) - A^2(u/u_e)^2 \tag{16}$$

where

$$A^2 = \beta u_e^2/T_w = Pr_T u_e^2/2c_p T_w \qquad B = -\frac{\alpha u_e}{T_w} = \left(\frac{T_e}{T_w}\right) - 1 + A^2 = -\frac{Pr_T u_e q_w}{c_p T_w \tau_w}$$

In the 1951 paper of Van Driest [73], he assumed that $Pr_T = r = 1$. In a 1955 paper, Van Driest [190] considered a variable Prandtl number and the analysis becomes more complex with the evaluation of a number of integral relations required.

Another form of the temperature or density equation with the turbulent kinetic energy neglected is

$$T/T_w = \bar{\rho}_w/\bar{\rho} = 1 - \bar{\alpha}u^+ - \bar{\beta}u^{+2} \tag{17}$$

where

$$\bar{\alpha} = \alpha u_\tau / T_w = Pr_T q_w u_\tau / c_p T_w \tau_w = Pr_T B_q = [(1 - T_e/T_w)/u_e^+] - \bar{\beta} u_e^+ = 2R^2 H$$

$$\bar{\beta} = \beta u_\tau^2 / T_w = Pr_T u_\tau^2 / 2c_p T_w = Pr_T M_\tau^2 (\gamma - 1)/2 = R^2$$

$$B_q = q_w / \rho_w c_p T_w u_\tau \qquad M_\tau = u_\tau / a_w \qquad H = (q_w/\tau_w)/u_\tau$$

Mean Velocity Profiles

In the *inner region of the turbulent boundary layer*, the total shear stress is approximately constant as given by Eq. (11). The Reynolds stress is written in terms of the eddy viscosity which is approximated with the Prandtl mixing length approach. The total shear stress equation, eddy viscosity μ_T, and mixing length l_m become

$$\bar{\rho} l_m^2 \left(\frac{d\tilde{u}}{dy}\right)^2 + \mu \frac{d\tilde{u}}{dy} - \tau_w = 0 \qquad \mu_T = \bar{\rho} l_m^2 \left|\frac{d\tilde{u}}{dy}\right| \qquad l_m = \kappa y D_f \tag{18}$$

where Van Driest damping function is used in the viscous sublayer and is

$$D_f = 1 - e^{-y^+/A^+} \qquad A^+ = 25.53$$

Introducing inner variables

$$u^+ = \tilde{u}/u_\tau \qquad y^+ = \bar{\rho}_w y u_\tau / \mu_w \qquad u_\tau = \sqrt{\tau_w/\bar{\rho}_w} \qquad l_m^+ = \kappa y^+ D_f ,$$

the total shear stress Eq. (18) becomes

$$\left(a\frac{du^+}{dy^+}\right)^2 + b\frac{du^+}{dy^+} - 1 = 0 \qquad a = l_m^+ \sqrt{\bar{\rho}/\bar{\rho}_w} \qquad b = \mu/\mu_w \tag{19}$$

This equation is solved for the first derivative and then can be integrated numerically to obtain the compressible velocity across the inner layer

$$\frac{du^+}{dy^+} = \frac{2/b}{1 + \sqrt{1 + (2a/b)^2}} \qquad u^+ = \int_0^{y^+} \{(2/b)/[1 + \sqrt{1 + (2a/b)^2}]\} dy^+ \tag{20}$$

Also Eq. (19) can be solved with a velocity transformation by introducing the Van Driest transformed velocity u_c^+ which is defined as

$$\frac{du_c^+}{dy^+} = \sqrt{\bar{\rho}/\bar{\rho}_w}\,\frac{du^+}{dy^+} \qquad \int du_c^+ = \int \sqrt{\bar{\rho}/\bar{\rho}_w}\, du^+ = \int du^+ / \sqrt{T/T_w} , \tag{21}$$

Eq. (19) becomes

$$\left(\bar{a}\frac{du_c^+}{dy^+}\right)^2 + \bar{b}\frac{du_c^+}{dy^+} - 1 = 0 \qquad \bar{a} = l_m^+ \qquad \bar{b} = (\mu/\mu_w)/\sqrt{\bar{\rho}/\bar{\rho}_w} \tag{22}$$

This equation is solved for the first derivative and the transformed velocity becomes

$$\frac{du_c^+}{dy^+} = \frac{2/\bar{b}}{1+\sqrt{1+(2\bar{a}/\bar{b})^2}} \qquad u_c^+ = \int_0^{y^+} \{(2/\bar{b})/[1+\sqrt{1+(2\bar{a}/\bar{b})^2}]\}\,dy^+ \tag{23}$$

The solution of this equation for u_c^+ as a function of y^+ requires a numerical solution since $\bar{b}$ varies across the inner region of the boundary layer.

In the *logarithmic region* $b \to 0$, $a = \kappa y^+$, and solving Eq. (19) for the first derivative gives

$$\frac{du^+}{dy^+} = \sqrt{\bar{\rho}_w/\bar{\rho}}/l_m^+ \qquad l_m^+ = \kappa y^+ \tag{24}$$

For *incompressible flow* (constant density case $\bar{\rho}_w/\bar{\rho} = 1$), the above becomes

$$\int_{u_0^+}^{u^+} du^+ = \int_{y_0^+}^{y^+} \frac{dy^+}{\kappa y^+} \qquad u^+ - u_0^+ = \frac{1}{\kappa}\ln y^+ - \frac{1}{\kappa}\ln y_0^+$$

The incompressible solution becomes

$$u_{inc}^+ = \frac{1}{\kappa}\ln(y^+) + C \qquad C = u_0^+ - \frac{1}{\kappa}\ln(y_0^+) \tag{25}$$

With the velocity $u_0^+ = 0$, the constant $C = -(1/\kappa)\ln(y_0^+)$ and the value of the coordinate $y_0^+ = \exp(-\kappa C)$. Bradshaw suggest that the von Kármán constant $\kappa = 0.41$ and the constant $C = 5.20$, which gives $y_0^+ = 0.1186$. The value of the constants are based on a database of incompressible zero pressure gradient boundary layer experiments. The appropriate values of these constants are still being debated. Eq. (25) is only valid when y^+ is approximately 40 or larger and u_{inc}^+ is 14 or larger.

For *compressible flow in the logarithmic region* $\bar{b} \to 0$, $\bar{a} = \kappa y^+$, and the governing Eq. (23) and solution become

$$\frac{du_c^+}{dy^+} = \frac{1}{\kappa y^+} \qquad u_c^+ = \frac{1}{\kappa}\ln y^+ + C$$
$$C = u_{c0}^+ - \frac{1}{\kappa}\ln(y_0^+) \qquad y_0^+ = \exp[\kappa(u_{c0}^+ - C)] \tag{26}$$

With $u_{c0}^+ = 0$, the coordinate $y_0^+ = \exp(-\kappa C)$ and $C = -(1/\kappa)\ln(y_0^+)$, which are the same as the incompressible values. In the logarithmic region, the transformed compressible velocity u_c^+ becomes the same as the incompressible velocity u_{inc}^+ as given in Eq. (25).

Also for the *compressible flow in the logarithmic region*, the density ratio is obtained from the temperature relation given by Eq. (17) with the turbulent kinetic energy neglected, then Eq. (24) is solved for the velocity u^+ as a function of y^+. The governing equation becomes

$$\int_{u_0^+}^{u^+} \frac{du^+}{\sqrt{1-\bar{\alpha}u^+ - \bar{\beta}u^{+2}}} = \int_{y_0^+}^{y^+} \frac{dy^+}{\kappa y^+}$$

The evaluation of the integrals gives

$$\frac{1}{\sqrt{\bar{\beta}}}\operatorname{asin}\left(\frac{2\bar{\beta}u^+ + \bar{\alpha}}{\sqrt{\bar{\alpha}^2 + 4\bar{\beta}}}\right) - \frac{1}{\sqrt{\bar{\beta}}}\operatorname{asin}\left(\frac{2\bar{\beta}u_0^+ + \bar{\alpha}}{\sqrt{\bar{\alpha}^2 + 4\bar{\beta}}}\right) = \frac{1}{\kappa}\ln(y^+) - \frac{1}{\kappa}\ln(y_0^+) \tag{27}$$

Eq. (27) can be written in the notation of Bradshaw with new variables R and H where $\bar{\alpha} = 2R^2H$, $\bar{\beta} = R^2$, and with the use of Eq. (26) the resulting equation is

$$\frac{1}{R}\operatorname{asin}\left(\frac{Ru^+ + RH}{D}\right) + C_1 = \frac{1}{\kappa}\ln(y^+) + C = u_c^+ \qquad C_1 = u_{c0}^+ - \frac{1}{R}\operatorname{asin}\left(\frac{Ru_0^+ + RH}{D}\right)$$
$$R = u_\tau\sqrt{Pr_T/2c_pT_w} \qquad H = q_w/\tau_w u_\tau \qquad D = \sqrt{1+(RH)^2} \tag{28}$$

From Eq. (25) and Eq. (26) at $y_0^+ = \exp(-\kappa C)$, $u_0^+ = u_{c0}^+ = 0$. The compressible velocity transformation of Van Driest is obtained from Eq. (28) as

$$u_c^+ = \frac{1}{R}\left[\operatorname{asin}\left(\frac{Ru^+ + RH}{D}\right) - \operatorname{asin}\left(\frac{RH}{D}\right)\right] \tag{29}$$

The inverse of this equation has been given by Bradshaw as

$$u^+ = \frac{1}{R}\sin(Ru_c^+) - H[1-\cos(Ru_c^+)] \tag{30}$$

In the original notation, the *Van Driest velocity transformation* is obtained from Eq. (27) where the temperature is given by Eq. (16), $\bar{\alpha} = -Bu_\tau/\tilde{u}_e$, and $\bar{\beta} = (Au_\tau/\tilde{u}_e)^2$, which gives

$$u_c^+ = \frac{\tilde{u}_c}{u_\tau} = \frac{(\tilde{u}_e/u_\tau)}{A}\left\{\operatorname{asin}\left[\frac{2A^2(\tilde{u}/\tilde{u}_e) - B}{\sqrt{B^2+4A^2}}\right] - \operatorname{asin}\left(\frac{-B}{\sqrt{B^2+4A^2}}\right)\right\} = \frac{1}{\kappa}\ln(y^+) + C \tag{31}$$

where A and B are defined after the Van Driest temperature Eq. (16). The velocity ratio is written as follows in the Van Driest article

$$u_e^+ = \tilde{u}_e / u_\tau = 1/\sqrt{(C_f/2)(T_w/T_e)}$$

Also in the Van Driest transformation the turbulent Prandtl number is set equal to one. In the Bradshaw notation $A = R\tilde{u}_e/u_\tau$, $B = -2ARH$, and Eq. (31) is the same as Eq. (29) when the turbulent Prandtl number is one. A plot of $u_c^+ = \tilde{u}_c/u_\tau$ verse y^+ for experimental data or numerical solutions should match Eq. (25), which is the incompressible log-law. Also the above Eq. (31) should approach Eq. (25) as the Mach number at the edge of the boundary layer becomes very small and the temperature becomes uniform across the boundary layer.

The *Fernholz velocity transformation* uses the Prandtl mixing length concept with a recovery factor of $r = 0.896$. The transformation evaluates the integration constant at the lower boundary where $(\tilde{u}/\tilde{u}_e) \approx 0.5$, $u_{c0}^+ \approx 14.5$, and $y_0^+ = \exp[\kappa(u_{c0}^+ - C)] \approx 43$. The von Kármán constant $\kappa = 0.40$ and the constant $C = 5.10$ in the Fernholz analysis. With Fernholz notation the velocity transformation is

$$\tilde{u}_c = \frac{\tilde{u}_e}{b}\text{asin}\left(\frac{2b^2(\tilde{u}/\tilde{u}_e) - a}{d}\right) \tag{32}$$

where the coefficients are

$$a = (1 + rm)(T_e/T_w) - 1 = -Pr_T u_e q_w / c_p T_w \tau_w$$

$$b^2 = rm(T_e/T_w) = r\tilde{u}_e^2/2c_p T_w \qquad d = \sqrt{a^2 + 4b^2}$$

Eq. (32) can be obtained in the Bradshaw notation by starting with Eq. (28) which is

$$u_c^+ = \frac{1}{R}\text{asin}\left(\frac{Ru^+ + RH}{D}\right) + C_1 = \frac{1}{\kappa}\ln(y^+) + C \tag{33}$$

where C_1 is defined in Eq. (28) and C is defined in Eq. (26). The coefficients in the Bradshaw form of the Fernholz velocity transformation are

$$R = u_\tau b/\tilde{u}_e = u_\tau\sqrt{r/2c_p T_w} \qquad H = q_w/\tau_w u_\tau$$

$$RH = -a/2b \qquad D = d/2b = \sqrt{1 + (RH)^2}$$

Fernholz has shown for an adiabatic wall $(H = 0)$, that C_1 is small and can be neglected in Eq. (33). The Van Driest transformation given in Eq. (29) is the same as the Fernholz Eq. (33) if $r = Pr_T$ and $\text{asin}(RH/D)$ is neglected in the Van Driest transformation.

In the *outer region of the turbulent boundary layer*, the similarity of the velocity profiles is obtained with the use of the velocity defect $(\tilde{u}_{ce} - \tilde{u}_c)/u_\tau$. The velocity defect outside the viscous sublayer is approximated as

$$(\tilde{u}_{ce} - \tilde{u}_c)/u_\tau = -\frac{1}{\kappa}\ln(y/\delta) + \frac{\Pi}{\kappa}w(y/\delta) \tag{34}$$

Fernholz and Finley [31] has shown the above can be approximated as

$$U_D = (\tilde{u}_{ce} - \tilde{u}_c)/u_\tau = -4.70\ln(y/\Delta^*) - 6.74 \qquad \Delta^* = \delta\int_0^1 U_D\, d(y/\delta) \tag{35}$$

Fernholz and Finley [31] use this relation to assess the accuracy of flat plate turbulent boundary layers in the outer region.

Huang, Bradshaw, and Coakley [71] have obtain the transformed velocity from the wall to the edge of the boundary by taking into account the viscous sublayer and by including a wake function. This procedure gives the skin friction, velocity, and temperature profiles as a function of the Reynolds number. It has been developed as a 7 step procedure with iteration of the solution until converged. The procedure is described for the case when the momentum thickness Reynolds number is used and the momentum thickness is specified. The following properties are specified:

θ	Boundary layer momentum thickness
$\bar{\rho}_e$	Density at edge of boundary layer
c_p	Specific heat at constant pressure
Pr_T	Turbulent Prandtl number
p	Pressure across boundary layer
T_w	Temperature of the wall
$\tilde{u}_e$	Velocity at the edge of the boundary layer
μ_w	Viscosity at the wall is determined from Sutherland or Keyes viscosity law with the specified wall temperature

From the above specified properties, the following parameters are calculated:

$\mu_w = \mu(T_w)$ = Function of viscosity law (Sutherland or Keyes)

$\bar{\rho}_w = p/RT_w$

$T_e = p/R\bar{\rho}_e$

$\mu_e = \mu(T_e)$

The solution procedure is as follows:

1. Guess the ***thickness ratio*** θ/δ and the ***wall friction velocity*** $u_\tau = \sqrt{\tau_w/\rho_w}$; then determine the boundary layer thickness $\delta = \theta/(\theta/\delta)$. The thickness ratio for incompressible flow is estimated as $\theta/\delta \approx 7/72$ while for compressible flow the relation developed by Smits and Dussauge [191] (see page 194) can be used.

2. Calculate the momentum thickness Reynolds numbers $Re_\theta = \bar{\rho}_e \tilde{u}_e \theta/\mu_e$ and $Re_{\theta w} = \bar{\rho}_e \tilde{u}_e \theta/\mu_w = (\mu_e/\mu_w) Re_\theta$. Then determine the wall function $\Pi(Re_\theta)$ from Figure 1a in the Huang et al. paper or use Cebeci-Smith correlation.

3. Calculate the non-dimensional boundary layer thickness $\delta^+ = y_e^+ = \bar{\rho}_w u_\tau \delta/\mu_w$ and wall density $\bar{\rho}_w = p/RT_w$. Then determine the law-of-the-wall profile from the wall $(y^+ = 0)$ to the edge of the boundary layer $(y^+ = \delta^+)$ by numerical evaluation of the following relation:

$$u_{cb}^+ = \int_0^{y^+} \frac{2dy^+}{1 + \sqrt{1 + 4(l^+)^2}} \qquad l^+ = \kappa y^+ (1 - e^{-y^+/A^+}) \qquad A^+ = 25.53 \qquad \kappa = 0.41$$

4. Obtain compressible velocity at the edge of the boundary layer, $\eta = y^+/\delta^+ = 1$.

$$u_e^+ = (1/R)\sin(Ru_{ce}^+) - H[1 - \cos(Ru_{ce}^+)]$$

$$u_{ce}^+ = u_{cb}^+(\eta) + (\Pi/\kappa) w(\eta) \qquad \eta = 1 \qquad w(1) = 2$$

5. ***Update shear velocity*** $u_\tau = \tilde{u}_e/\tilde{u}_e^+$ and local skin friction $c_f = 2(T_e/T_w)(u_\tau/\tilde{u}_e)^2$.

6. Tabulate the transformed velocity, the compressible velocity, and the temperature across the boundary layer using the following relations

$$u_c^+ = u_{cb}^+(\eta) + (\Pi/\kappa) w(\eta) \qquad u^+ = (1/R)\sin(Ru_c^+) - H[1 - \cos(Ru_c^+)]$$

$$T = T_w(1 - \bar{\alpha} u^+ - R^2 u^{+2}) \qquad \bar{\alpha} = 2R^2 H$$

$$R = u_\tau \sqrt{Pr_T/2c_p T_w} \qquad H = [(1 - T_e/T_w)/(R^2 u_e^+) - u^+]/2$$

7. Update the thickness ratio

$$\theta/\delta = \int_0^1 \frac{\bar{\rho} u^+}{\bar{\rho}_e u_e^+} \left(1 - \frac{u^+}{u_e^+}\right) d\eta \qquad \bar{\rho}/\bar{\rho}_e = T_e/T$$

Steps 1 to 7 are repeated until the solution converges.

Appendix C: Turbulent Sharp Cone to Flat Plate Transformations

Cone to Flat Plate transformation

Theories for cone to flat plate Mangler transformation are usually of the form

$$(C_f)_{Cone}/(C_f)_{FlatPlate} = (St)_{Cone}/(St)_{FlatPlate} = G(Re, M_e, T_e/T_e)$$

The Mangler transformation parameter G for compressible flow could be a function of the boundary layer edge Reynolds number based on x or θ, M_e, and T_w/T_e. Below is a brief indication of some of the contributions to this issue.

Van Driest [74] (1952) has developed a simple rule for transforming local flat plate skin friction and heat transfer to cones at zero angle of attack for fully turbulent boundary layers (no transition from laminar flow) in supersonic/hypersonic flows. His method is different than the standard approach. The flat plate compressible skin friction is determined from Van Driest II theory, which gives $(C_f)_{FlatPlate} = F(Re_x, M_e, T_w/T_e)$. Van Driest determined that the cone compressible skin friction is determined from $(C_f)_{Cone} = F(Re_x/2, M_e, T_w/T_e)$ where the flat plate skin friction relation is evaluated at one half the edge Reynolds number. The transformation parameter $G = F(Re_x/2, M_e, T_w/T_e)/(F(Re_x, M_e, T_w/T_e))$ with $G = 1.14$ at $Re_x = 10^5$ and $G = 1.08$ at $Re_x = 10^8$.

Seiff [231] (1954) has taken into account that the turbulent boundary layer begins down stream on the flat plate and has determined the effective or virtual origin of the turbulent boundary layer. It is assumed that the boundary layer is initially laminar and instantaneously transitions to turbulent flow at x_{tr}, which must be specified. The Blasius relation for incompressible skin friction is transformed to a compressible skin friction relation which is used with the Karman momentum-integral relation for axisymmetric boundary layer flow. The combined relation is a differential equation for the compressible skin friction which is integrated downstream from the transition location to obtain the local cone skin friction $(C_f)_{FlatPlate} = F_{Cone}(x_{tr}, M_e, T_w/T_e)$. For the case of fully turbulent flow on the cone and flat plate, transformation parameter $G = 1.17$ where the edge Reynolds number, edge Mach number, and wall temperature ration are the same for the cone and flat plate.

Reshotko and Tucker [232] (1957) use the compressible turbulent boundary layer integral equations for momentum thickness Theta and form factor $H = \delta^*/\theta$, which are transformed into incompressible form with the Dorodnitsyn transformation. The compressible shear stress (skin friction) is required in these equations and is determined from the Ludwieg-Tillmann incompressible skin friction relation which is transformed with the Eckert reference enthalpy method (variables with subscript r). The compressible skin friction is of the form $C_f = 2\tau_w/\rho_e u_e^2 = K_0(\rho_r u_e \theta/\mu_r)^m$ where $m = 0.268$ and K_0 is function of T_e/T_r and the form factor H. For the flat plate, the investigation gives the momentum thickness and skin friction as

$$\theta_{FlatPlate} = 0.0259 K_T x^{0.823} \qquad (C_f)_{FlatPlate} = 0.086 K_f x^{-0.220}$$

For the cone, the investigation gives the momentum thickness and skin friction as

$$\theta_{Cone} = 0.0135 K_T x^{0.823} \qquad (C_f)_{Cone} = 0.102 K_f x^{-0.220}$$

Where K_T and K_f are a function of T_e/T_r, T_0/T_e, and $M_e \rho_0 a_0/\mu_0$. The authors obtain for the momentum thickness, skin friction, and heat transfer ratios as

$$\theta_{Cone}/\theta_{FlatPlate} = 0.521$$
$$G = (C_f)_{Cone}/(C_f)_{FlatPlate} = St_{Cone}/St_{FlatPlate} = 1.192$$

where the boundary layer edge properties and stagnation conditions on the cone and flat plate are the same.

Bertram and Neal [233] (1965) investigated the influence of the location of the virtual origin of the turbulent boundary layer and the relationship of the results obtained on cones to those obtained on flat plates. Since the theories usually assume the origin of the turbulent boundary layer is at the tip of the cone while most experiments have laminar flow near the tip with transition occurring at x_{tr} from the tip. The authors use the Mangler transformation to transform the cone boundary layer equations into the flat plate boundary layer equation. The details of the development of the theory is not presented, only the final results are given in an appendix. The authors assume the virtual origin is at the location where the peak shear stress or peak heating occurs. One transformation presented is applied to data obtained on cones to change the results to the values that would be obtained with the flow turbulent from the cone tip. The following Reynolds are defined with the distance on the cone from the virtual origin $x_v = x - x_{tr}$, the distance on the flat plate from the virtual origin $\xi_v = \xi - \xi_{tr}$, and the parameter $Re_{ue} = \rho_e u_e/\mu_e$.

$$Re_{xv} = Re_{ue} x_v \qquad Re_{\xi v} = Re_{ue} \xi_v \qquad Re_x = Re_{ue} x \qquad R_x^* = Re_{xtr}/Re_{xv}$$

The ratio of the local skin friction on a truncated cone (TC) to that on a pointed cone is

$$G^* = (C_f Re_{xv})_{TC}/(C_f Re_x)_{Cone} = \{1 + R_x^* - R_x^* [R_x^*/(1 + R_x^*)]^{n/(n-1)}\}^{-1/n}$$

The ratio of the local skin friction on a truncated cone to that on a flat plate is

$$(C_f Re_{xv})_{TC}/(C_f Re_{\xi v})_{FlatPlate} = [(2n-1)/(n-1)]^{1/n} G^*$$

The authors suggest $n = 4$ for turbulent cone flow.

Tetervin [234] (1970) has extended the Mangler transformation to compressible boundary layer flows. The flat plate incompressible skin friction is obtained from the Ludwieg-Tillmann relation which is modified to compressible flow with the Eckert reference enthalpy method. The compressible wall shear stress becomes

$$2\tau_w/\rho_r u_e^2 = k(Re_\theta)^{-m} \qquad Re_{\theta r} = \rho_r u_e \theta/\mu_r \qquad m = 0.268$$

$$k = 0.246e^{-1.561H_i}(\rho_r/\rho_e)^{1-m}(\mu_r/\mu_e)^m$$

The transformed flat plate compressible skin friction becomes

$$C_f = k(Re_{\theta e})^{-m} \qquad Re_{\theta e} = \rho_e u_e \theta/\mu_e$$

The ratio of the axisymmetric to flat plate skin friction as given by Tetervin is

$$G = (C_f)_{Cone}/(C_f)_{FlatPlate} = [(x/\xi)(r_w/L)^{m+1}(Re_\xi/Re_x)]^{m/(m+1)}$$

$$Re_\xi = \rho_e u_e \xi/\mu_e \qquad Re_x = \rho_e u_e x/\mu_e$$

The Mangler transform of the turbulent boundary layer equations gives the distance x along the axisymmetric body as a function of the distance ξ along the flat plate as

$$\xi = \int_0^x (r_w/L)^{m+1} dx \qquad L = \text{Reference length}$$

For a cone $(r_w/L) = a(x/L)$ where $a = \sin\theta_c$ and

$$\xi/L = [a^{m+1}/(m+2)](x/L)^{m+2}$$

The above equation for a cone with $\xi = x$ becomes

$$G = (C_f)_{Cone}/(C_f)_{FlatPlate} = (2+m)^{m/(m+1)} = 1.189$$

If $(C_f)_{Cone} = (C_f)_{FlatPlate}$, then the above equation becomes

$$Re_\xi/Re_x = 1/(m+2) = 0.441$$

White [235], [75] (1973, 1977) has developed the Cone Rule with the Karman momentum-integral equation for axisymmetric flow $(j = 1)$ which is

$$\frac{d\theta}{dx} + j\frac{\theta}{r_w} = \frac{C_f}{2}$$

The compressible skin friction is approximated as $C_f = K(Re_\theta)^{-m} = A\theta^{-m}$ where $A = K(\rho_e u_e/\mu_e)^{-m}$. For a flat plate $(j = 0)$ the solution of the integral equation gives the momentum thickness and skin friction as

$$\theta_{FlatPlate} = [(1+m)A\xi/2]^{1/(1+m)} \qquad C_f = A[(1+m)A\xi/2]^{-m/(1+m)}$$

For a cone (j = 1) the solution of the integral equation gives the momentum thickness and skin friction as

$$\theta_{Cone} = \left[\frac{(1+m)A\xi}{2(2+m)}\right]^{1/(1+m)} \qquad C_f = A\left[\frac{(1+m)A\xi}{2(2+m)}\right]^{-m/(1+m)}$$

The G transformation becomes with the cone and flat plate locations the same $(\xi = x)$

$$G = (C_f)_{Cone}/(C_f)_{FlatPlate} = (2+m)^{m/(1+m)}$$

The skin friction relation becomes with $m = 1/4$, $(C_f)_{Cone}/(C_f)_{FlatPlate} = 1.176$ and $(Re_\xi)_{Cone} = (Re_x)_{FlatPlate}$. If $(C_f)_{Cone} = (C_f)_{FlatPlate}$, then $\xi = (2+m)x$ and $(Re_\xi)_{Cone} = (2+m)(Re_x)_{FlatPlate}$. The constant K in the skin friction relation has been determined by Young [236] and is given on page 158 in his book. In the development of the above relation, it is assumed that the turbulent boundary layer begins at the tip of the cone and the leading edge of the flat plate.

Zoby, Moss, and Sutton [237] (1981) have determined the power law velocity profile exponent as a function of the momentum thickness Reynolds number.

$$u/u_e = (y/\delta)^{1/n} \qquad n = 12.67 - 6.6\log(Re_\theta) + 1.21[\log(Re_\theta)]^2$$

The skin friction relation parameter is obtained from $m = 2/(n+1)$.

Seiler, Werner, and Patz [238] (2002) have used the Hantzsche and Wendt transformations to first transform the compressible boundary layer equations on a cone (in spherical coordinates) to a new set of cone transformed governing equations. The compressible boundary layer equations on a flat plate are transformed to a new set of flat plate transformed governing equations. The transformed governing equations for the cone and the flat plate are of the same form. This approach needs further development to determine Mangler transformation parameter G.

Zoby et al. [76],[77],[237]: In a NASA Technical Note Zoby and Sullivan predicted the heating rate (Stanton number) on axisymmetric sharp-cones at zero angle of attack and compared the results to six a supersonic flight experiments. The flat plate heat rate is obtained from the Colburn form of Reynolds analogy, which is expressed as

$$St_e = \frac{1}{2} C_{fe} Pr^{-2/3} \qquad Pr = 0.71$$

The incompressible skin-friction for a flat plate is obtained from the Blasius or Schultz-Grunow relations, which are of the form $(C_{fe})_{FlatPlate}$ = function of the surface distance Reynolds number $(Re_x)_{FlatPlate}$. The incompressible Reynolds number is modified for compressible flow with the Eckert reference-enthalpy method. The cone inviscid flow conditions at the edge of the boundary layer are obtained from the Sims tables. The cone Reynolds number $(Re_x)_{Cone}$ is related to the flat plate Reynolds number by the Van Driest relation $(Re_x)_{Cone} = 2(Re_x)_{FlatPlate}$. The calculated heat rates differ from the experimental heat rates by approximately 20% or less. In a synoptic journal article, Zoby and Graves [77] (1977) compared a larger experimental turbulent heating database including wind tunnel and flight experiments (no references for database) with prediction using the transformation to an incompressible plane approach as investigated by Peterson [197] (1963).

The compressible cone skin friction is transformed to compressible skin friction on a flat plate with the relations

$$(C_{fc})_{Cone} = G(C_{fc})_{FlatPlate} \qquad (Re)_{Cone} = (Re)_{FlatPlate}$$

where the Reynolds number is held constant. The geometric parameter G has been given by Whites cone rule (page 561) to have a value between 1.087 and 1.176. Zoby, Moss, and Sutton [237] have shown that G is a function of the momentum thickness Reynolds number, $G = 1.201$ at $Re_\theta = 10^4$ and $G = 1.123$ at $Re_\theta = 10^5$.

From the Colburn Reynolds analog given above for the compressible flow, the geometric transformation for the Stanton number is $(St_{ec})_{Cone} = G(St_{ec})_{FlatPlate}$. Since no value of G is specified in this article, it is assumed that $G = 1$. The compressible flat plate Stanton number and Reynolds number are transformed to incompressible flat plate values with the relations

$$St_{ei} = F_c St_{ec} \qquad Re_{Li} = F_L Re_{Le} \qquad L = x \text{ or } \theta$$

The length scale in the Reynolds number is the distance along the surface s in this article. The prediction of the incompressible Stanton number as a function of incompressible Reynolds number is obtained from the Colburn Reynolds analogy given above where the incompressible skin friction is obtained from one of three relation investigated. With the Van Driest II transformation, Van Driest skin friction relation, and with all of the experimental database used, the rms error of the transformed experimental data relative to the incompressible prediction is between 17.7% to 23% depending on surface distance used in the Reynolds number.

In the paper by Zoby, Moss and Sutton, the skin friction is evaluated from $C_f/2 = C_1(Re_\theta)^{-m}$.

Hopkins et al. [128],[129] (1969, 1971): The investigation of Hopkins and co-workers on the correlation of skin friction and heat transfer for zero pressure-gradient flows at hypersonic Mach numbers uses mainly flat plate data but includes cones and hollow cylinder flows. This work has already been discussed in the flat plate case. The initial work was documented in a NASA technical note [128] and the complete investigation in a journal article [129]. The cone data base is from the experiments of Mateer (see cone experimental database). The correlation of heat transfer as a function of wall-temperature ratio for Mach 4.9 to 7.4 includes all three geometries and shows no influence of geometries on the correlation. There is no indication that the cone data has been transformed to flat plate data (geometry transformation is discussed below in the Zoby section). This investigation does not resolve the appropriate geometry transformation for cones and the Reynolds analogy factor for cones and flat plates.

Holden [48] (1977) has correlated his experimental heat transfer data into incompressible form where the incompressible Stanton number St_i is plotted as a function of the incompressible Reynolds number Re_{xi}. The best documentation of this work is given in Holden [44] (1991). Holden uses the Bertram and Neal cone to flat plate transformation to transform the experimental data to incompressible flat plate Stanton number. It appears that the Reynolds analogy factor has been set to one. In the Bertram and Neal transformation theory the virtual origin of the turbulent must be specified and no information is given on this issue. The experimental data is correlated into reasonable agreement with the incompressible curve, but there is significant scatter of the data about the curve.

References (Authors' note: some references below are not cited in the text)

1. G. S. Settles and L. J. Dodson, "Hypersonic Shock/Boundary-Layer Interaction Database," NASA CR 177577, April 1991.

2. G. S. Settles and L. J. Dodson, "Hypersonic Turbulent Boundary-Layer and Free-Shear Layer Database," NASA CR177610, April 1993.

3. G. S. Settles and L. J. Dodson, "Hypersonic Shock/Boundary-Layer Interaction Database: New and Corrected Data," NASA CR 177638, April 1994.

4. Gary S. Settles and Lori J. Dodson, "Supersonic and Hypersonic Shock/Boundary-Layer Interaction Database," *AIAA Journal*, Vol. 32, pp. 1377-1383, July 1994.

5. Wilcox, D. C., *Turbulence Modeling for CFD*, 2nd Ed., DCW Industries, Inc. 5354 Palm Drive, La Canada, CA 91011, 1998.

6. Menter, F. R., "Eddy Viscosity Transport Equations and Their Relation to the $k-\varepsilon$ Model," *Journal of Fluids Engineering*, Vol. 119, No. 4, 1997, pp. 876-884.

7. Spalart, P. R., and Allmaras, S. R., "A One-Equation Turbulence Model for Aerodynamic Flows," AIAA Paper 92-0439, 1992.

8. Spalart, P. R., and Allmaras, S. R., "A One-Equation Turbulence Model for Aerodynamic Flows," *La Recherche Aerospatiale*, No. 1, 1994, pp. 5-21.

9. Roy, C. J., and Blottner, F. G., "Further Assessment of One- and Two-Equation Turbulence Models for Hypersonic Transitional Flows," AIAA Paper 2001-0210, January 2001.

10. Jones, W. L., and Launder, B. E., "The Prediction of Laminarization with a Two-Equation Model of Turbulence," *International Journal of Heat and Mass Transfer*, Vol. 15, 1972, pp. 301-314.

11. Launder, B. E., and Sharma, B. I., "Application of the Energy Dissipation Model of Turbulence to the Calculation of Flow Near a Spinning Disk," *Letters in Heat and Mass Transfer*, Vol. 1., No. 2, 1974, pp. 131-138.

12. Roy, C. J., and Blottner, F. G., "Methodology for Turbulence Model Validation: Application to Hypersonic Flows," *Journal of Spacecraft and Rockets*, Vol. 40, No. 3, May-June 2003, pp. 313-325.

13. Menter, F. R., "Two-Equation Eddy-Viscosity Turbulence Models for Engineering Applications," *AIAA Journal*, Vol. 32, No. 8, Aug. 1994, pp. 1598-1605.

14. Robinson, D. F., Harris, J. E., and Hassan, H. A., "Unified Turbulence Closure Model for Axisymmetric and Planar Free Shear Flows," *AIAA Journal*, Vol. 33, No. 12, December 1995, pp. 2324-2331.

15. Robinson, D. F., and Hassan, H. A., "Further Development of the k-ζ (Enstrophy) Turbulence Closure Model," *AIAA Journal*, Vol. 36, No. 10, October 1998, pp. 1825-1833.

16. McDaniel RD, and Hassan HA. Study of transition in a high disturbance environment. Journal of Aircraft, Vol. 38, No. 6, pp. 1051-1055.

17. Craft, T. J., Launder, B. E., and Suga, K., "Prediction of Turbulent Transitional Phenomena with a Nonlinear Eddy-Viscosity Model," *International Journal of Heat and Fluid Flow*, Vol. 18, No. 1, 1997, pp. 15-28.

18. Cebici, T., and Bradshaw, P., "Ch. 6: Uncoupled Turbulent Boundary Layers," *Physical and Computational Aspects of Convective Heat Transfer*, Springer-Verlag, New York, 1984, p. 173.

19. Marvin, J. G., "Perspective on Computational Fluid Dynamics Validation," *AIAA Journal*, Vol. 33, No. 10, 1995, pp. 1778-1787.

20. Marvin, J. G., and Huang, G. P., "Turbulence Modeling - Progress and Future Outlook," in *Computational Fluid Dynamics Review 1998, Vol. II*, edited by M. Hafez and K. Oshima, World Scientific, 1998, pp. 891-906.

21. Moore, J. G., and Moore, J., "Realizeability in Two-Equation Turbulence Models," AIAA Paper 99-3779, June 1999.

22. Roache, P. J., "Ch. 3: A Methodology for Accuracy Verification of Codes: the Method of Manufactured Solutions," *Verification and Validation in Computational Science and Engineering*, Hermosa Publishers, New Mexico, 1998.

23. P. Knupp, K. Salari, in: K.H. Rosen (Ed.), Verification of Computer Codes in Computational Science and Engineering, Chapman and Hall/CRC, Boca Raton, FL, 2003.

24. Roache, P. J., "Perspective: A Method for Uniform Reporting of Grid Refinement Studies," *ASME Journal of Fluids Engineering*, Vol. 116, No. 3, 1994, pp. 405-413.

25. Carpenter, M. H., and Casper, J. H., "Accuracy of Shock Capturing in Two Spatial Dimensions," *AIAA Journal*, Vol. 37, No. 9, 1999, pp. 1072-1079.

26. Roy, C. J., "Grid Convergence Error Analysis for Mixed-Order Numerical Schemes," *AIAA Journal*, Vol. 41, No. 4, 2003, pp. 595-604.

27. C. J. Roy, C. C. Nelson, T. M. Smith, and C. C. Ober, "Verification of Euler / Navier-Stokes Codes using the Method of Manufactured Solutions," *International Journal for Numerical Methods in Fluids*, Vol. 44, No. 6, 2004, pp. 599-620.

28. Craft, T. J., Launder, B. E., and Suga, K., "Prediction of Turbulent Transitional Phenomena with a Nonlinear Eddy-Viscosity Model," *International Journal of Heat and Fluid Flow*, Vol. 18, No. 1, 1997, pp. 15-28.

29. Cebici, T., and Bradshaw, P., "Ch. 6: Uncoupled Turbulent Boundary Layers," *Physical and Computational Aspects of Convective Heat Transfer*, Springer-Verlag, New York, 1984, p. 173.

30. H. H. Fernholz and P. J. Finley, "A Critical Compilation of Compressible Turbulent Boundary Layer Data," AGARDograph No. 223, 1977.

31. H. H. Fernholz and P. J. Finley, "A Critical Commentary on Mean Flow Data for Two-Dimensional Compressible Turbulent Boundary Layers," AGARDograph No. 253, May 1980.

32. H. H. Fernholz and P. J. Finley, "A Further Compilation of Compressible Boundary Layer Data with a Survey of Turbulence Data," AGARDograph No. 263, November 1981.

33. G. T. Coleman and J. L. Stollery, "Heat Transfer from Hypersonic Turbulent Flow at a Wedge Compression Corner," *Journal of Fluid Mechanics*, Vol. 56, pp. 741-752, 1972.

34. M. I. Kussoy and C. C. Horstman, "Documentation of a Two- and Three Dimensional Hypersonic Shock Wave/Turbulent Boundary Layer Interaction Flows," NASA TM 101075, January 1989.

35. M. S. Holden, A. G. Havener, and C. H. Lee, "Shock Wave/Turbulent Boundary Layer Interaction in High-Reynolds Number Hypersonic Flows," Calspan-University of Buffalo Research Center, CUBRC-86681, Buffalo, NY, 1986.

36. M. S. Holden, "Experimental Studies of Quasi-Two-Dimensional and Three-Dimensional Viscous Interaction Regions Induced by Skewed-Shock and Swept-Shock Boundary Layer Interactions," AIAA Paper 1984-1677, 1984.

37. M. I. Kussoy and C. C. Horstman, "An Experimental Documentation of a Hypersonic Shock-Wave Turbulent Boundary Layer Interaction Flow - With and Without Separation," NASA TM X-62412, Feb. 1975.

38. M. I. Kussoy and C. C. Horstman, "Intersecting Shock-Wave/Turbulent Boundary-Layer Interactions at Mach 8.3," NASA TM 103909, Feb. 1992.

39. C. H. Law, "3D Shock Wave-Turbulent Boundary Layer Interactions At Mach 6," Aeronautical Research Laboratory, ARL TR 75-0191, 1975.

40. M. I. Kussoy and C. C. Horstman, “Documentation of a Two- and Three Dimensional Shock Wave/Turbulent Boundary Layer Interaction Flows at Mach 8.2,” NASA TM 103838, May 1991.

41. M. I. Kussoy and C. C. Horstman, “Three-Dimensional Shock-Wave/Turbulent Boundary-Layer Interaction,” *AIAA Journal*, Vol. 31, pp. 8-9, 1993.

42. M. S. Holden and J. R. Moselle, “A Database of Aerothermal Measurements in Hypersonic Flow for CFD Validation,” AIAA Paper 1992-4023, July 1992.

43. M. S. Holden, “Experimental Studies of the Effects of Asymmetric Transition on the Aerothermal Characteristics of Hypersonic Blunted Slender Cones,” AIAA Paper 1985-0325, January 1985.

44. M. S. Holden, “Studies of the Mean and Unsteady Structure of Turbulent Boundary Layer Separation in Hypersonic Flow,” AIAA Paper 1991-1778, June 1991.

45. Holden et al? An experimental investigation of turbulent boundary layers at high mach number a reynolds numbers. Calspan Report No. AB-5072-A-1, also NASA CR-112147, 1972.

46. M. S. Holden, “A Database of Aerothermal Measurements in Hypersonic Flows in “Building Block” Experiments for CFD Validation,” AIAA paper 2003-1137, January 2003.

47. Holden MS. Shock wave-turbulent boundary layer interaction in hypersonic flow. AIAA Paper 1972-0074, 1972.

48. Holden MS. Shock wave-turbulent boundary layer interaction in hypersonic flow. AIAA Paper 1977-0045, 1977.

49. H. G. Hornung, “28th Lanchester Memorial Lecture- Experimental Real-Gas Hypersonics,” *The Aeronautical Journal*, pp. 379-389, December 1988.

50. Hans Groenig and Herbert Olivier, “Experimental Hypersonic Flow Research in Europe,” *JSME International Journal*, Series B, Vol. 41, No. 2, pp. 397-407,1998.

51. F. Grasso, G. Leone, and J. M. Delery, “Validation Procedure for the Analysis of Shock-Wave/Boundary-Layer Interaction Problems,” *AIAA Journal*, Vol. 32, pp. 1820-1827, 1994.

52. J.-A. Desideri, R. Glowinski, and J. Periaux (Editors), *Hypersonic Flows for Reentry Problems, Volumes I and II*, Springer-Verlag, 1991.

53. D. Kumar and J. L. Stollery, “Hypersonic Control Flap Effectiveness,” *The Aeronautical Journal*, pp. 197-208, June/July 1996.

54. G. T. Coleman and J. L. Stollery, “Incipient Separation of Axially Symmetric Hypersonic Turbulent Boundary Layers,” *AIAA Journal*, Vol. 12, pp. 119-120, 1974.

55. K. Kontis and J. L. Stollery, “Incipient Separation on Flared Bodies at Hypersonic Speeds,” *The Aeronautical Journal*, pp 405-414, September 1999.

56. Babinsky H, Edwards JA. On the incipient separation of a turbulent hypersonic boundary layer. Aeronautical Journal 1996; 100(996):209-214.

57. Babinsky H, A study of roughness in turbulent hypersonic boundary-layers, Ph.D. Thesis, Cranfield University, College of Aeronautics, December 1993.

58. M. S. Holden, “Viscous Interactions at Hypersonic Speeds,” AFOSR TR 86-2072, Oct. 1986.

59. M. I. Kussoy and K. C. Horstman, “Intersecting Shock-Wave/Turbulent-Boundary-Layer Interactions,” *AIAA Journal,* Vol. 31, pp. 2197-2203, 1993.

60. M. I. Kussoy, K. C. Horstman, and C. C. Horstman, “Hypersonic Crossing Shock-Wave/ Turbulent-Boundary-Layer Interactions,” *AIAA Journal*, Vol. 31, pp. 8-9, 1993 (see also AIAA Paper 1993-0781).

61. G. T. Coleman, G. M. Elfstrom, and S. L. Stollery, “Turbulent Boundary Layers at Supersonic and Hypersonic Speeds,” AGARD-CP-93, January 1972.

62. E. J. Hopkins, E. R. Keener, T. E. Polek, and H. A. Dwyer, “Hypersonic Turbulent Skin-Friction and Boundary-Layer Profiles on Nonadiabatic Flat plates,” *AIAA Journal*, Vol. 10, pp. 40-48, Jan. 1972.

63. E. R. Keener and E. J. Hopkins, “Turbulent Boundary Layer velocity Profiles on a Non-Adiabatic Flat Plate at Mach 6.5,” NASA TN D-6907, 1972.

64. F. Grasso and D. Falconi, “High-Speed Turbulence Modeling of Shock-Wave/Boundary-Layer Interaction,” *AIAA Journal*, Vol. 31, pp. 1199-1206, 1993.

65. D. J. Mee, “Boundary-Layer transition Measurements in Hypervelocity Flows in a Shock Tunnel,” *AIAA Journal,* Vol. 40, pp. 1542-1548, August 2002.

66. John J. Bertin, Anthony Martellucci, and Richard D. Neumann, “Developing a Data Base for the Calibration and Validation of Hypersonic CFD Codes - Sharp Cones,” AIAA Paper 93-3044, 1993.

67. L. B. Lin and J. K. Harvey, “Experimental Study of the Hypersonic Turbulent Boundary Layer on a Cold Slender Cone,” *Journal of Thermophysics,* Vol. 3, pp. 105-111, April 1989.

68. R. Hillier, D. C. Kirk, M. Sell and S. Soltani, “Studies of Hypersonic Viscous Flows,” in AGARD Conference Proceedings 514, *Theoretical and Experimental Methods in Hypersonic Flows*, May 4-8, 1992.

69. P. D. Germain and H. G. Hornung, “Transition on a Slender Cone in Hypervelocity Flow,” *Experiments in Fluids*, Vol. 22, pp. 1883-190, 1997.

70. Philippe H. Adam and Hans G. Hornung, “Enthalpy Effects on Hypervelocity Boundary-Layer Transition: Ground Test and Flight Data,” *Journal Spacecraft and Rockets,* Vol. 34, pp. 614-619, Sept.-Oct. 1997.

71. P. G. Huang, P. Bradshaw, and T. J. Coakley, “Skin Friction and Velocity Profile Family for Compressible Turbulent Boundary Layers,” AIAA Journal, Vol. 31, pp. 1600-1604, September 1993.

72. Squire, L. C., “The Accuracy of Flat Plate, Turbulent Skin Friction at Supersonic Speeds,” *The Aeronautical Journal,* Vol. 104, No. 1036, 2000, pp. 257-263.

73. Van Driest, E. R., “Turbulent Boundary Layer in Compressible Fluids,” *Journal of the Aeronautical Sciences,* Vol. 18, 1951, pp. 145-160.

74. E. R. Van Driest, "Turbulent Boundary Layer on a Cone in a Supersonic Flow at Zero Angle of Attack," *Journal of the Aeronautical Sciences*, Vol. 19, pp. 55-57,72, 1952.

75. Frank M. White, *Viscous Fluid Flow*, McGraw-Hill Book Company, New York, 1974.

76. E. V. Zoby and E. M. Sullivan, "Correlation of Free-Flight Turbulent Heat-Transfer Data from Axisymmetric Bodies with Compressible Flat-Plate Relations," NASA TN D-3802, 1967.

77. Ernest V. Zoby and Randolph A. Graves Jr., "Comparison of Turbulent Prediction Methods with Ground and Flight Test Heating Data," *AIAA Journal*, Vol. 15, pp. 901-902, July 1977.

78. Roy, C. J., and Blottner, F. G., "Further Assessment of One- and Two-Equation Turbulence Models for Hypersonic Transitional Flows," AIAA Paper 2001-0210, Jan. 2001.

79. S. K. Lele, "Compressible Effects on Turbulence," in *Annual Review of Fluid Mechanics*, Vol. 26, 1994.

80. G. N. Coleman, J. Kim and R. D. Moser, "A Numerical Study of Turbulent Supersonic Isothermal-Wall Channel Flow," *Journal of Fluid Mechanics*, Vol. 305, pp. 159-183, 1995.

81. Nateri K. Madavan, "Direct Numerical Simulation of Transitional and Turbulent Flow over a Heated Flat Plate Using Finite-Difference Schemes," NASA-CR-197753, Jan. 1995.

82. Chien JY. Predictions of channel boundary-layer flows with a low-reynolds-number turbulence model. AIAA Journal 1982; 20(1):33-38.

83. So RM, Zhang HS, Speziale CG. Near-wall modeling of the dissipation rate equation. AIAA Journal 1991; 29(12):2069-2076.

84. T. J. Coakley and P. G. Huang, "Turbulence Modeling For High Speed Flows," AIAA Paper 92-0436, 1992.

85. Vuong ST, Coakley TJ. Modeling of turbulence for hypersonic flows with and without separation. AIAA Paper 1987-0286, 1987.

86. T. J. Coakley, C. C. Horstman, J. G. Marvin, J. R. Viegas, J. E. Bardina, P. G. Huang, and M. I. Kussoy, "Turbulence Compressibility Corrections," NASA Technical Memorandum 108827, May 1994.

87. B. Aupoix and S. Viala, "Compressible Turbulent Boundary Layer Modeling," FED-Vol. 224, *Transitional and Turbulent Compressible Flows*, ASME, 1995.

88. C. C. Horstman, "Prediction of Hypersonic Shock-Wave/Turbulent-Boundary-Layer Interaction Flows," AIAA Paper 87-1367, 1987.

89. C. C. Horstman, "Hypersonic Shock-Wave/Turbulent-Boundary-Layer Interaction Flows," *AIAA Journal*, Vol. 30, pp. 1480-1481, June 1992.

90. P. G. Huang and T. J. Coakley, "Turbulence Modeling for Complex Hypersonic Flows," AIAA Paper 93-0200, 1993.

91. J. E. Bardina, P. G. Huang, and T. J. Coakley, "Turbulence Modeling Validation, Testing, and Development," NASA TM-110446, April 1997.

92. J. E. Bardina, P. G. Huang, and T. J. Coakley, “Turbulence Modeling Validation,” AIAA Paper 97-2121, 1997.

93. T-H Shih, W. W. Liou, A. Shabbir, Z. Yang, and J. Zhu, “A New $k-\varepsilon$ Eddy Viscosity Model for High Reynolds Number Turbulent Flows,” *Computers Fluids*, Vol. 24, pp. 227-238, 1995.

94. William W. Liou and P. G. Huang, “Calculations of Oblique Shock Wave/ Turbulent Boundary-Layer Interactions with New Two-Equation Turbulence Models,” FED-Vol. 224, *Transitional and Turbulent Compressible Flows*, ASME 1995.

95. Elfstrom GM. Turbulent hypersonic flow at a wedge-compression corner. Journal of Fluid Mechanics 1972; 53(1):113-127.

96. Robert P. Nance and H. A. Hassan, “Turbulence Modeling of Shock-Dominated Flows with a $k-\zeta$ Formulation,” AIAA Paper 99-0153, January 15-18, 1999.

97. U. Goldberg, P. Batten, S. Palaniswamy, S. Chakravarthy, and O. Peroomian, “Hypersonic Flow Predictions Using Linear and Nonlinear Turbulence Closures,” *Journal of Aircraft*, Vol. 37, pp. 671-675, July-August 2000.

98. Horstman CC. Hypersonic shock-wave/turbulent-boundary-layer interaction flows. AIAA Paper 1991-1760, 1991.

99. Coratekin T, van Keuk J, Ballmann J. Performance of upwind schemes and turbulence models in hypersonic flows. AIAA Journal 2004; 42(5):945-957.

100. Marvin JG, and Coakley TJ. Turbulence modeling for hypersonic flows. NASA TM-101079, 1989.

101. Hillier R, Kirk D, Soltani S. Navier-stokes computations of hypersonic flows. International Journal of Numerical Methods for Heat and Fluid Flow 1995; 5(3):195-211.

102. Mikulla V, Horstman CC. Turbulence measurements in hypersonic shock-wave boundary-layer interaction flows. AIAA Journal 1976; 14(5):568-575.

103. J. E. Bardina and T. J. Coakley, “Three-Dimensional Navier-Stokes Simulation with Two-equation Turbulence Models of Intersecting Shock-Waves/Turbulent Boundary Layer at Mach 8.3,” AIAA Paper 94-1905, 1994.

104. N. Narayanswami, C. C. Horstman, and D. D. Knight, “Computation of Crossing Shock/ Turbulent Boundary Layer Interaction at Mach 8.3,” *AIAA Journal*, Vol. 31, pp. 1369-1376, August 1993 (see also AIAA Paper 1993-0779).

105. Brian R. Smith, “Prediction of Hypersonic Shock-Wave/Turbulent Boundary-Layer Interactions,” *Journal of Spacecraft and Rockets*, Vol. 33, pp. 614-619, Sept.-Oct. 1996 (also AIAA Paper 95-0232).

106. Alexander Wiedermann, “Blunt-Fin Induced Interaction of Wall Shear Layers in Supersonic Flow,” *Fluid Dynamics Research*, Vol. 21, pp. 221-232, 1997.
Also Goldberg [97] has used this flow geometry.

107. D. Barberis and P. Molton, “Shock Wave-Turbulent Boundary Layer Interaction in a Three Dimensional Flow,” AIAA Paper 95-0227, January 9-12, 1995.

108. Kussoy MI, Kim K-S, Horstman KC. An experimental study of a three-dimensional shock wave/turbulent boundary-layer interaction at a hypersonic mach number. AIAA Paper 1991-1761, 1991.

109. Bardina J, Coakley T, Marvin J. Two-equation turbulence modeling for 3-d hypersonic flows. AIAA Paper 1992-5064, 1992.

110. M. A. Leschziner, P. Batten, and H. Loyau, "Modeling Shock-Affected Near-Wall Flows with Anisotropy-Resolving Turbulence Closures," *International Journal of Heat and Fluid Flow*, Vol. 21, pp. 239-251, 2000.

111. Knight DD, Horstman CC, Monson DJ. The hypersonic shock wave-turbulent boundary layer interaction generated by a sharp fin at Mach 8.2. AIAA Paper 1992-0747, 1992.

112. J. R. Edwards and S. Chanda, "Comparison of Eddy Viscosity-Transport Turbulence Models for Three-Dimensional, Shock-Separated Flowfields," *AIAA Journal*, Vol. 34, pp. 756-763, 1995.

113. J. D. Brown, J. L. Brown, and M. I. Kussoy, "A Documentation of Two- and Three-Dimensional Shock-Separated Turbulent Boundary Layers," NASA TM 101008, July 1988 (also AIAA Paper 87-0553).

114. D. Gaitonde, J. S. Shang, and J. R. Edwards, "The Computed Structure of a 3-D Turbulent Interaction Caused by a Cylinder/Offset Flare Junction," AIAA Paper 95-0230, Jan. 1995.

115. E. R. Van Driest, "Problem of Aerodynamic Heating," *Aeronautical Engineering Review*, Vol. 15, pp. 26-41, Oct. 1956.

116. Mee DJ. Boundary-layer transition measurements in hypervelocity flows in a shock tunnel. AIAA Journal 2002; 40(8):1542-1548.

117. Coakley TJ, Viegas JR, Huang PG, Rubesin MW. An assessment and application of turbulent models for hypersonic flows. 9th National Aero-Space Plane Technology Symposium, Paper No. 106, November 1990.

118. G. A. Alexopoulos and H. A. Hassan, "$k-\zeta$ (Enstophy) Compressible Turbulence Model for Mixing and Wall Bounded Flows," *AIAA Journal*, Vol. 35, pp. 1221-1224, 1997.

119. Kimmel, R. L., "Experimental Transition Zone Lengths in Pressure Gradient in Hypersonic Flow," in *Transitional and Turbulent Compressible Flows 1993*, edited by L. D. Kral and T. A. Zang, FED-Vol. 151, ASME, 1993, pp. 117-127.

120. Kimmel, R. L., "The Effects of Pressure Gradients on Transition Zone Length in Hypersonic Boundary Layers," *Journal of Fluids Engineering*, Vol. 119, No. 1, 1997, pp. 36-41.

121. Eric S. Warren, Julius E. Harris, and H. A. Hassan, "Transition Model for High-Speed Flow," *AIAA Journal*, Vol. 33, pp. 1391-1397, 1995.

122. R. D. McDaniel, R. P. Nance, and H. A. Hassan, "Transition Onset Prediction for High-Speed Flow," *Journal of Spacecraft and Rockets*, Vol. 37, pp. 304-309, May-June 2000.

123. Daniel C. Reda and John D. Murphy, "Shock Wave/Turbulent Boundary-Layer Interactions in Rectangular Channels," *AIAA Journal*, Vol. 11, pp. 139-140, Feb. 1973.

124. Daniel C. Reda and John D. Murphy, "Sidewall Boundary Layer Influence on Shock Wave/Turbulent Boundary-Layer Interactions," *AIAA Journal*, Vol. 11, pp. 1367-1368, Feb. 1973.

125. P. Krogmann and E. Schulein, "Documentation of Two-Dimensional Impinging Shock/ Turbulent Boundary Layer Interaction Flow," DLR IB 223-96 A 49, 1996.

126. Nagano, Y., and Hishida, M., "Improved Form of the $k-\varepsilon$ Model for Wall Turbulent Shear Flows." *Journal of Fluids Engineering*, Vol. 109, June 1987, pp. 156-160.

127. Van Driest, E. R., "On Turbulent Flow Near a Wall," *Journal of the Aeronautical Sciences*, Vol. 23, 1036, Nov. 1956, pp. 1007-1011.

128. J. E. Hopkins, M. W. Rubesin, M. Inouye, E. R. Keener, G. G. Mateer, and T. E. Polek, "Summary and Correlation of Skin-Friction and Heat-Transfer Data for a Hypersonic Turbulent Boundary Layer on Simple Shapes," NASA TN D-5089, 1969 (also *AIAA Journal*, "Hypersonic Turbulent Skin-Friction and Boundary-Layer Profiles on Nonadiabatic Flat Plates," Vol. 10, Jan. 1972, pp. 40-48.)

129. E. J. Hopkins and M. Inouye, "An Evaluation of Theories for Predicting Turbulent Skin Friction and Heat Transfer on Flat Plates at Supersonic and Hypersonic Mach Numbers," *AIAA Journal*, Vol. 9, pp. 993-1003, June 1971.

130. P. Bradshaw, B. E. Launder, and J. L. Lumley, "Collaborative Testing of Turbulence Models," *Journal of Fluids Engineering*, Vol. 118, pp. 243-247, June 1996.

131. S. Catris and B. Aupoix, "Improved Turbulence Models for Compressible Boundary Layers," AIAA Paper 98-2696, June 1998.

132. Wilcox DC. Turbulence Modeling for CFD, 1st Ed., DCW Industries, Inc. 5354 Palm Drive, La Canada, CA 91011, 1988.

133. J. E. Bardina, "Three-Dimensional Navier-Stokes Method with Two-Equation Turbulence Models for Numerical Simulation of Hypersonic Flows," AIAA Paper 94-2950, 1994.

134. T. J. Garrison, G. S. Settles, N. Narayanswami, and D. D. Knight, "Laser Interferometer Skin-Friction Measurements of Crossing-Shock-Wave/Turbulent-Boundary-Layer Interactions," *AIAA Journal*, Vol. 32, pp. 1234-1241, June 1994.

135. Doyle D. Knight, T. J. Garrison, G. S. Settles, A. A. Zheltovodov, A. Maksimov, A. M. Shevchenko, and S. S. Vorontsov, "Asymmetric Crossing-Shock-Wave/Turbulent-Boundary-Layer Interaction," *AIAA Journal*, Vol. 33, pp. 2241-2249, 1995.

136. C. W. Albertson and R. L. Ash, "Compressible Equilibrium Turbulent Boundary Layers at Non Adiabatic Wall Conditions," *AIAA Journal*, Vol. 29, No. 10, October 1991, pp. 1573-1580.

137. C. W. Albertson, "Evaluation of Equilibrium Turbulence for a Hypersonic Boundary Layer at Nonadabatic Wall Conditions," M.S. Thesis, Old Dominion University, Norfolk, VA, July 1989, also available as NASA TM-101663, Nov. 1989.

138. Alexander Wiedermann, "Blunt-Fin Induced Interaction of Wall Shear Layers in Supersonic Flow," Fluid Dynamics Research, Vol. 21, pp. 221-232, 1997.

139. U. C. Goldberg, "Towards a Pointwise Turbulence Model for Wall-Bounded and Free Shear Flows," *ASME Journal of Fluids Engineering*, Vol. 116, pp. 72-76, 1994.
See Goldberg et al.[97] the cubic eddy viscosity form of this model.

140. Menter, F. R., Grotjans, H., and Unger, F., "Numerical Aspects of Turbulence Modeling for the Reynolds Averaged Navier-Stokes Equations," *Computational Fluid Dynamics Lecture Series* 1997-02, von Karman Institute for Fluid Dynamics, March 3-7, 1997.

141. Roy, C. J., and Blottner, F. G., "Assessment of One- and Two-Equation Turbulence Models for Hypersonic Transitional Flows," AIAA Paper 2000-0132, January 2000.

142. Roy, C. J., and Blottner, F. G., "Assessment of One- and Two-Equation Turbulence Models for Hypersonic Transitional Flows," *Journal of Spacecraft and Rockets*, Vol. 38, No. 5, September-October 2001, pp. 699-710.

143. Zoby, E. V., and Sullivan, E. M., "Correlation of Free-Flight Turbulent Heat-Transfer Data from Axisymmetric Bodies with Compressible Flat-Plate Relationships," NASA Technical Note D-3802, Jan. 1967.

144. Zoby, E. V., and Graves, R. A., "Comparison of Turbulent Prediction Methods with Ground and Flight Test Heating Data," *AIAA Journal*, Vol. 15, No. 7, 1977, pp. 901-902.

145. M. Martin, G. Weits, U. Piomelli, and G. Candler, "Large-Eddy Simulation Over a Hypersonic Elliptical Cross-Section Cone," AIAA Paper 2000-2311, June 19-22, 2000. (do not have this)

146. H. S. Zhang, R. M. C. So, C. G. Speziale, and Y. G. Lai, "Near Wall Two-Equation Model for Compressible Turbulent Flows," *AIAA Journal*, Vol. 31, pp. 196-199, 1993.

147. T. J. Craft, B. E. Launder, and K. Suga, "Development and Application of a Cubic Eddy-Viscosity Model of Turbulence," *International Journal of Heat and Fluid Flow*, Vol. 17, pp. 108-115, 1996.

148. D. F. Robinson, J. E. Harris, and H. A. Hassan, "Unified Turbulence Closure Model for Axisymmetric and Planar Free Shear Flows," *AIAA Journal*, Vol. 33, pp. 2325-2331, 1995.

149. Jeffrey K. Wideman, James L. Brown, John B. Miles, and Oktay Ozcan, "Skin-Friction Measurements in Three-Dimensional, Supersonic Shock-Wave/Boundary-Layer Interaction," *AIAA Journal*, Vol. 33, pp. 805-811, 1995.

150. . D. F. Robinson and H. A. Hassan, "Further Development of the $\boldsymbol{k} - \zeta$ (Enstrophy) Turbulence Closure Model," *AIAA Journal*, Vol. 36, pp. 1825-1833, 1998.

151. L. D. Kral, "Recent Experience with Different Turbulence Models Applied to the Calculation of Flow Over Aircraft Components," *Progress in Aerospace Sciences*, Vol. 34, pp. 481-541, 1998.

152. Roger L. Kimmel, Jonathan Poggie and Stephen N. Schwoerke, "Laminar-Turbulent Transition in a Mach 8 Elliptic Cone Flow," *AIAA Journal*, Vol. 37, pp. 1080-1087, September 1999.

153. M. S. Holden, "Turbulent Boundary Layer Development on Curved Compression Surfaces," Calspan Report No. 7724-1, 1992.

154. B. E. Launder, “The Modeling of Turbulent Flows with Significant Curvature or Rotation,” in *Modeling Complex Turbulent Flows*, Edited by Manuel D. Salas, Jerry N. Hefner, and Leonidas Sakell, Kuwer Academic Publishers, 1999.

155. Horstman and Owen, AIAA Journal

156. Mikulla V, and Horstman CC. The measurement of shear stress and total heat flux in a nonadiabatic turbulent hypersonic boundary layer. AIAA Paper 75-0119, 1975.

157. Mikulla V, and Horstman CC. Turbulence stress measurements in a nonadiabatic hypersonic boundary layer. AIAA Journal, V. 13, No. 12, 1975, pp. 1607-1613.

158. Goldberg U. Hypersonic flow heat transfer prediction using single equation turbulence models. ASME Journal of Heat Transfer, V. 123, Feb. 2001, pp. 65-69.

159. Coleman GT. Hypersonic turbulent boundary layer studies. Ph.D. Thesis, Dept. of Aeronautics, Univ. of London, London, 1973.

160. Rodi W. Experience with two-layer models combining the k-ε model with a one-equation model near the wall. AIAA Paper 1991-0216, Jan. 1991.

161. Holden MS, Bergman RC, Harvey J, Duryea GR, Moselle JR. Studies of the structure of attached and separated regions of viscous/inviscid interaction and the effects of combined surface roughness and blowing in high Reynolds number hypersonic flows. AFOSR-89-0033TR, 1988.

162. Holden MS. Experimental database from CUBRC studies in hypersonic laminar and turbulent interacting flows including flowfield chemistry, Prepared for RTO code validation of DSMC and Navier-Stokes code validation studies, Calspan-University at Buffalo Research Center, Buffalo, NY, June 2000, pp. 105-114.

163. Smith BR. A near wall model for the k-l two equation turbulence model. AIAA Paper 1994-2386, June 1994.

164. Marvin JG, Horstman CC, Rubesin MW, Coakley TJ, and Kussoy MI. An experimental and numerical investigation of shock-wave induced turbulent boundary-layer separational hypersonic speeds,” AGARDograph-CPP-168, May 1975.

165. Fluent 6.1 User's Guide, Vols. 1-3, 2003.

166. Oberkampf, WL, and Aeschliman, DP. Joint computational/experimental aerodynamics research on a hypersonic vehicle, part 1: experimental results. AIAA Journal, V. 9, No. 3, 1995, pp. 432-437.

167. P. G. Huang, P. Bradshaw, and T. J. Coakley, “Turbulence Models for Compressible Boundary Layers,” *AIAA Journal*, Vol. 32, pp. 735-740, April 1994

168. P. R. Spalart, “Trends in Turbulence Treatments,” AIAA 2000-2306, June 19-22, 2000.

169. Sebastein Deck, P. Duveau, P. d’Espiney, and P. Guillen, “Development and Application of Spalart-Allmaras One Equation Turbulence Model to Three-Dimensional Supersonic Complex Configurations,” *Aerospace Science and Technology*, Vol. 6, pp. 171-183, 2002.

170. H. H. Fernholz and P. J. Finley, “Incompressible Zero-pressure-Gradient Turbulent Boundary Layer: Assessment of the a Data,” *Progress in Aerospace Sciences*, Vol. 32, pp 245-311, August 1996.

171. F. K. Hill, “Boundary-Layer Measurements in Hypersonic Flow,” *J. of the Aeronautical Sciences*, Vol. 23, pp. 35-42, Nov.-Dec. 1956. (F&F 5901)

172. F. K. Hill, “Turbulent Boundary Layer Measurements at Mach Number 8 to 10,” *Physics of Fluids*, Vol. 2, 1959, pp. 668-680,

173. . E. M. Winkler and M. H. Cha, “Investigation of Flat Plate Hypersonic Turbulent Boundary Layers With heat Transfer at a Mach Number of 5.2,” NOL NAVORD Report 6631, 1959; also Trans. ASME, Series E, Vol. 83, pp. 323-329, 1961.

174. D. R. Moore, “Velocity Similarity in the Compressible Turbulent Boundary layer With Heat Transfer,” University of Texas Defence Research Laboratory, Report DRL 480, 1962.

175. D. R. Moore and J. Harkness, “Experimental Investigation of the Compressible Turbulent Boundary layer at Very High Reynolds Numbers,” *AIAA Journal*. Vol. 3, No. 4, April 1965, pp. 631-638

176. R. D. Watson, J. E. Harris, and J. B. Andeps, “Measurements in a Transitional/Turbulent Mach 10 Boundary layer at High Reynolds Numbers,” AIAA Paper 73-165, 1973.

177. R. D. Watson, “Characteristics of Mach 10 Transitional and Turbulent Boundary Layers,” NASA TP-1243, Nov. 1, 1978, also “Wall Cooling Effects on Hypersonic Transitional/Turbulent Boundary Layers at High Reynolds Numbers,” *AIAA Journal*, Vol. 15, pp. 1455-1461, Oct. 1977.

178. A. J. Laderman and A. Demetriades, “Mean and Fluctuating Flow Measurements in the Hypersonic boundary Layer Over a Cooled Wall,” Journal of Fluid Mechanics, Vol. 63, pp. 121-144, 1974, (F&F 7403) also “Investigation of the Structure of a Cooled Wall Turbulent Supersonic Boundary Layer,” Aeronautics Publication No. U-6370.

179. J. E. Hopkins, and E. R. Keener, “Studies of Surface Pitots for Measuring Turbulent Skin Friction at Supersonic Mach Numbers,” NASA TN D-3478, 1966.

180. E. J. Hopkins, E. R. Keener, “Pressure-Gradient Effects on Hypersonic Turbulent Skin-Friction and Boundary-Layer Profiles,” *AIAA Journal*, Vol. 10, pp. 1141-1142, Sept. 1972.

181. F. K. Owen, C. C. Horstman, “On the Structure of Hypersonic Turbulent Boundary Layers,” *Journal of Fluid Mechanics*, Vol. 53, pp. 611-636, June 1972.

182. C. C. Horstman and F. K. Owen, “Turbulent Properties of a Compressible Boundary Layer,” *AIAA Journal*, Vol. 10, pp. 1418-1424, Nov. 1972.

183. F. K. Owen, C. C. Horstman, and M. I. Kussoy, “Mean and Fluctuating Flow Measurements on a Fully-Developed, Non-Adiabatic Hypersonic Boundary Layer,” *Journal of Fluid Mechanics*, Vol. 70, No. 2, pp. 393-413, 1975.

184. J. E. Hopkins, E. R. Keener, and P. T. Louie, “Direct Measurements of Turbulent Skin Friction on a Non-Adiabatic Flat Plate at Mach Number 6.5 and Comparisons with Eight Theories,” NASA TN D-5675, 1969.

185. C. W. Albertson and R. L. Ash, “Compressible Equilibrium Turbulent Boundary Layers at Non Adiabatic Wall Conditions,” *AIAA Journal*, Vol. 29, No. 10, October 1991, pp. 1573-1580.

186. C. W. Albertson, “Evaluation of Equilibrium Turbulence for a Hypersonic Boundary Layer at Nonadabatic Wall Conditions,” M.S. Thesis, Old Dominion University, Norfolk, VA, July 1989, also available as NASA TM-101663, Nov. 1989.

187. M. S. Holden, “Turbulent Boundary layer Development on Curved Compression Surfaces,” Calspan report No. 7724-1, 1992.

188. H. Yan, D. Knight, and A. A. Zheltovodov, “Large Eddy Simulation of Supersonic Flat Plate Boundary Layer Using MILES Technique,” *Journal of Fluid Engineering*, Vol. 124, No. 4, pp. 868-875, 2002 (also H. Yan, D. Knight, and A. A. Zheltovodov, “Large Eddy Simulation of Supersonic Flat Plate Boundary Layer Part I,” AIAA 2002-0132, January 14-17, 2002).

189. M. P. Martin, “Preliminary DNS Database of Hypersonic Turbulent Boundary Layers,” AIAA 2003-3726, June 22-26, 2003.

190. E. R. Van Driest, “The Turbulent Boundary layer With Variable Prandtl Number,” in *50 Jahre Grenzschichtforschung*, Edited by H. Gortler and W. Tollmien, Friedr. Vieweg & Sohn, Braunschweig, 1955.

191. . A. J. Smits and Jean-Paul Dussauge, *Turbulent Shear layers in Supersonic Flow,* American Institute of Physics, Woodbury, N. Y., 1996.

192. Dean R. Chapman and R. H. Kester, “Measurements of Turbulent Skin friction on Cylinders in Axial Flow at Subsonic and Supersonic Velocities,” *Journal of the Aeronautical Sciences,* Vol. 20, pp. 441-448, July, 1953.

193. R. K. Lobb, E. M. Winkler, J. Persh, “Experimental Investigation of Turbulent Boundary layers in Hypersonic Flow,” U.S. Naval Ordnance Laboratory, Report 3380, 1955 also *Journal of the Aeronautical Sciences,* Vol. 22, 1955, pp. 1-9, 1955.

194. D. Coles, “Measurements in the Boundary Layer on a Smooth Flat Plate Boundary-Layer at Jet Propulsion Laboratory,” Jet Propulsion Lab., California Institute of Technology, Pasadena, CA, Report 20-71, 1953; also *Journal of the Aeronautical Sciences*,” Vol. 21, No. 7, July. 1955, pp. 433-448.

195. S. C. Sommer and B. J. Short, “Free-Flight Measurements of Turbulent Boundary-Layer Skin Friction in the Presence of Severe Aerodynamic Heating at Mach Numbers from 2.8 to 7.0,” NACA TN 3391, 1955; also *Journal of the Aeronautical Sciences*, Vol. 23, No. 6, June 1956, pp. 536-542.

196. R. H. Korkegi, “Transition Studies and Skin-Friction Measurements on an Insulated Flat Plate at a Mach Number of 5.8,” *Journal of the Aeronautical Sciences*,” Vol. 23, No. 2, Feb. 1956, pp. 97-107.

197. J. B. Peterson, Jr., A Comparison of Experimental and Theoretical Results for the Compressible Turbulent-Boundary-Layer Skin Friction with Zero Pressure Gradient, NASA Technical Note D-1795, March 1963

198. F. W. Matting, D. R. Chapman, T. R. Nyholm, and A. G. Thomas, "Turbulent Skin Friction at High Mach Numbers and Reynolds Numbers in Air and Helium," NASA TR R-82, 1961

199. R. E. Wilson, "Turbulent Boundary-Layer Characteristics at Supersonic Speeds - Theory and Experiments," *Journal of the Aeronautical Sciences*, Vol. 17, pp. 585-594, September 1950.

200. J. E. Wallace and E. J. McLaughlin, "Experimental Investigation of Hypersonic Turbulent Flow and Laminar Leeward-Side Flow on Flat Plates," Cornell Aeronautical Lab., Buffalo, N.Y., Technical Report AFFDL-TR-66-63, Vol. 1, July 1966.

201. F. L. Young and E. J. McLaughlin, "Experimental Investigation of the Effects of Surface Roughness on Compressible Turbulent Boundary Layer Skin Friction and heat Transfer," Defence Research Lab., University of Texas, Austin, Texas, Report DRL-532, CR-21, 1965.

202. L. Neal Jr., "A Study of the Pressure, Heat transfer, and Skin Friction on Sharp and Blunt Flat Plates at Mach Number 6.8," NASA TN D-3312, 1966.

203. S. Catris and B. Aupoix, "Density Corrections for Turbulence Models," *Aerospace Science Technology*, Vol. 4, pp. 1-11, 2000.

204. A. L. Kistler, "Fluctuation Measurements in Supersonic Turbulent Boundary Layers," Ballistic Research Laboratories, Report 1052, 1958 and *Physics of Fluids*, Vol. 2, 1959.

205. . R. C. Hasting and W. G. Sawyer, "Turbulent Boundary Layers on a Large Flat Plate at M = 4," R.A.C., Technical Report 70040 and R&M 3678, 1970.

206. D. G. Mabey, H. U. Meier, and W. G. Sawyer, "Experimental and Theoretical Studies of the Boundary layer on a Flat Plate at Mach Numbers from 2.5 to 4.5," RAE TR 74127, 1974.

207. D. G. Mabey, "Some Observations on the Wake Component of the Velocity Profiles of Turbulent Boundary Layers at Subsonic and Supersonic Speeds," RAE TR 77-004.

208. R. L. Richmond, "Experimental Investigation of Thick, Axially Symmetric Boundary Layers on Cylinders at Subsonic and Hypersonic Speeds," Guggenheim Aeronautics Lab., Cal Tech, Pasadena, CA, Hypersonic Research Project Memo 39, 1957.

209. J. L. Sims, Tables for Supersonic Flow Around Right Circular Cones, NASA SP-3004, Jan. 1, 1964.

210. C. B. Rumsey and D. B. Lee, Measurements of Aerodynamic Heat Transfer and Boundary-Layer Transition on a 15 Degree Cone in Free Flight at Supersonic Mach Numbers Up to 5.2, NASA Technical Note D-888, August 1961.

211. C. F. Merlet and C. B. Rumsey, "Supersonic Free-Flight Measurement of Heat Transfer and Transition on a 10 Degree Cone Having a Low Temperature Ratio, NASA Technical Note D-951, August 1961.

212. R. L. Wright and E. V. Zoby, Flight Boundary-Layer Measurements on Slender Cone at Mach 20, AIAA Paper 77-719, June 1977.

213. P. C. Stainback, M. C. Fischer, and Wagner, Effects of Wind-Tunnel Disturbances on Hypersonic Boundary Transition, AIAA Paper Number 72-181, January 17-19, 1972

214. Kuei-Yuan Chien, Hypersonic, Turbulent Skin-Friction and Heat-Transfer Measurements on a Sharp Cone, AIAA Journal, Vol. 12, pp. 1522-1526, Nov. 1974

215. K. F. Stetson, Mach 6 Experiments of Transition on a Cone at Angle of Attack, J. Spacecraft, Vol. 19, pp. 397-403, September-October 1982.

216. K. F. Stetson, E. R. Thompson, J. C. Donaldson, and L. G. Siler, Laminar Boundary Layer Stability Experiments on a Cone at Mach 8, Part 1: Sharp Cone, AIAA Paper 83-1761, July 12-14, 1983.

217. P. A. Deman, J. K. Harvey, and R. Hillier, Hypersonic Boundary Layer and Base Flow Workshop Test Problem 1 and 2, pp. 43-56 in Reference [52].

218. S. G. Mallinson, R. Hillier, A. P. Jackson, D. C. Kirk, S. Soltani, and M. Zanchetta, Gun Tunnel Flow Calibration: Defining Input Conditions for Hypersonic Flow Computations, Shock Waves, Vol.10, pp. 313-322, 2000.

219. S L. Lawrence, Hypersonic Cone Flow Predictions Using an Implicit Upwind Space-Marching Code, pp. 75-91.

220. Same as 100 S. P. G. Dinavahi, Comparison of Two Transition Models, in Instability and Transition, Edited by M. Y. Hussaini and R. G. Voigt, Springer-Verlag, 1989.

221. R. Abgrall and J. A. Desideri, M. Mallet, J. Periaux, P. Perrier, and B. Stoufflet, The European Hypersonic Data Base: A New CFD Validation Tool for the Design of Space Vehicles, AIAA Paper 93-3045, July 6-9, 1993

222. G. G. Mateer and H. K. Larson, "Unusual Boundary-Layer Transition Results on Cones in Hypersonic Flow," *AIAA Journal*, Vol. 7, pp. 660-666, April 1969.

223. G. G. Mateer, Effects of Wall Cooling and Angle of Attack on Boundary-Layer Transition on Sharp Cones at Mach = 7.4, NASA Technical Note D-6908, August 1972.

224. G. G. Meeter, The Effect of Angle of Attack on Boundary-Layer Transition on Cones, *AIAA Journal,* Vol. 10, August 1972.

225. M. S. Holden, D. Bower, and K. Chadwick, Measurements of Boundary Layer Transition on Cones at Angle of Attack for Mach Numbers from 11 to 13, AIAA 95-2294, June 19-22, 1995.

226. F.-J. Chen, M. R. Malik, and I. E. Beckwith, Boundary-Layer Transition on a Cone and Flat Plate at Mach 3.5, *AIAA Journal*, Vol. 27, pp. 687-693, 1989.

227. J. T. Lachowicz, N. Chokani, and S. P. Wilkinson, Hypersonic Boundary-Layer Stability Over a Flared Cone in a Quiet Tunnel, AIAA Paper number 96-0782, 1996.

228. J. T. Lachowicz, N. Chokani, and S. P. Wilkinson, Boundary-Layer Stability Measurements in a Hypersonic Quiet Tunnel, *AIAA Journal*, Vol. 34, pp. 2496-2500, December 1996.

229. C. D. Pruett and C-L Chang, Spatial Direct Numerical Simulation of High-Speed Boundary-Layer Flows Part II: Transition on a Cone in Mach 8 Flow, Theoretical and Computational Fluid Dynamics, Vol. 7, pp. 397-424, 1995.

230. C. D. Pruett, Direct Numerical Simulation of Hypersonic Boundary-Layer Flow on a Flared Cone, Theoretical and Computational Fluid Dynamics, Vol. 11, pp. 49-67, 1998.

231. Alvin Seiff, Examination of the Existing Data on the Heat Transfer of Turbulent Boundary Layers at Supersonic Speeds From the Point of View of Reynolds Analogy, NACA Technical Note 3284, August 1954.

232. Eli Reshotko and M. Tucker, "Approximation Calculation of the Compressible Turbulent Boundary Layer With Heat Transfer and Arbitrary Pressure Gradient," NACA TN 4154, December 1957.

233. M. H. Bertram and L. Neal, Recent Experiments in Hypersonic Turbulent Boundary Layers, NASA Technical Memorandum X-56335, 1965.

234. Neal Tetervin, "A Transformation Between Axisymmetric and Two-Dimensional Turbulent Boundary Layers," *AIAA Journal*, Vol. 8, pp. 985-987, May 1970.

235. F. M. White, R. C. Lessmann and G. H. Christoph, "Analysis of Turbulent Skin Friction in Thick Axisymmetric Boundary Layers," *AIAA Journal*, Vol. 11, pp. 821-825, June 1973.

236. A. D. Young, *Boundary Layers*, AIAA Education Series, AIAA, Washington D. C., 1089.

237. E. V. Zoby, J. N. Moss, and K. Sutton, Approximate Convective-Heating Equations for Hypersonic Flows, *J. Spacecraft*, Vol. 18, pp. 64-70, January-February 1981.

238. F. Seiler, U. Werner, and G. Patz, Ground Testing Facility for Modeling Real Projectile Flight Heating in Earth Atmosphere, *Journal of Thermophysics and Heat Transfer*, Vol. 16, pp. 101-108, January-March 2002.

239. S. P. G. Dinavahi, "Comparison of Two Transition Models," pages 453-462 in *Instability and Transition (Volume II)*, Editors M. Y. Hussaini and R. G. Voigt, Springer-Verlag, 1989.

240. S. A. McKeel, R. W. Walters, and K. M. Chadwick, Investigation into Transition Modeling, AIAA Paper 95-1746, In AIAA CFD Conference Papers, pp 1126-1138, June 19-22, 1995.

241. P. E. Rodi and D. S. Dolling, "An Experimental/Computational Study of Sharp Fin Induced Shock Wave/Turbulent Boundary Layer Interactions at Mach 5," AIAA Paper 92-0749, Jan. 1992

Figures

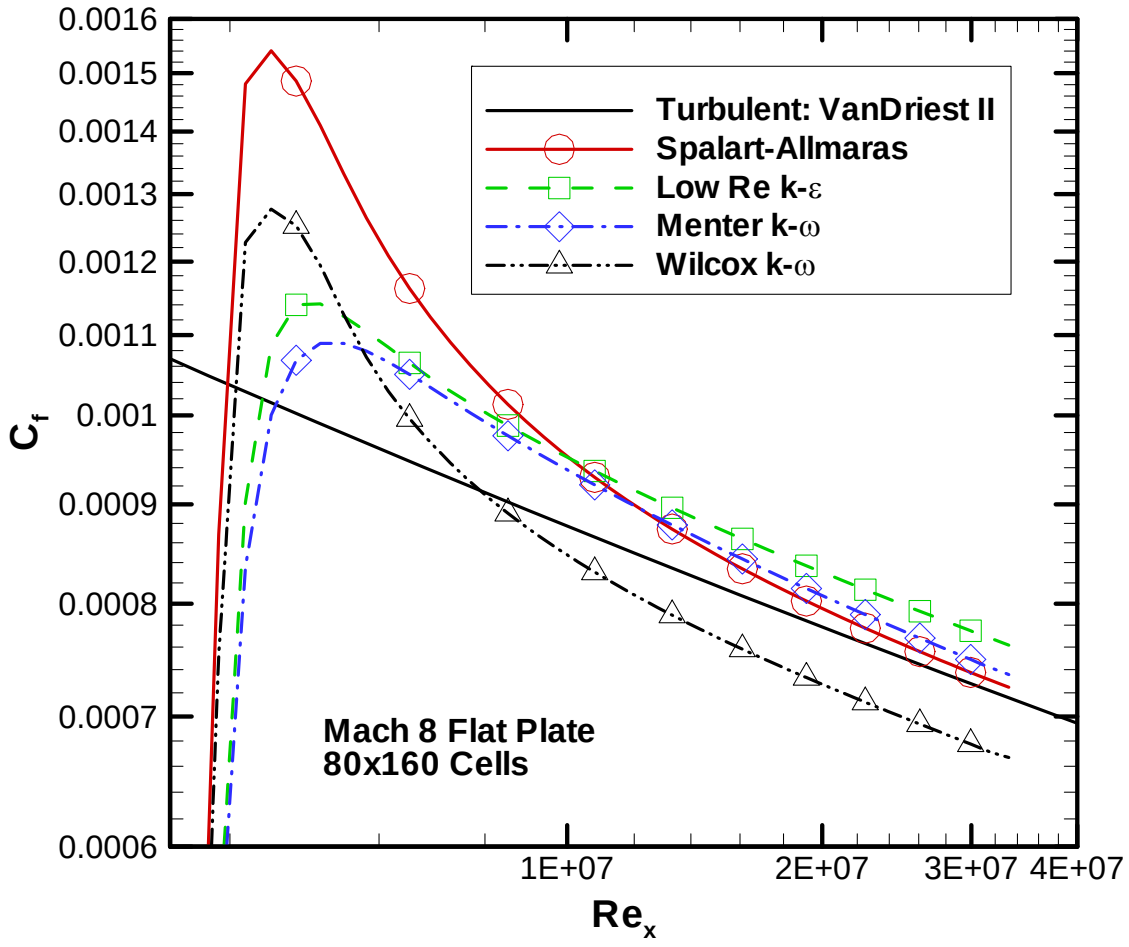

Fig. 1: Skin friction turbulence model comparisons (enlarged view) for Case 9: Flat Plate/ Cylinder (correlation is Van Driest II [115]).

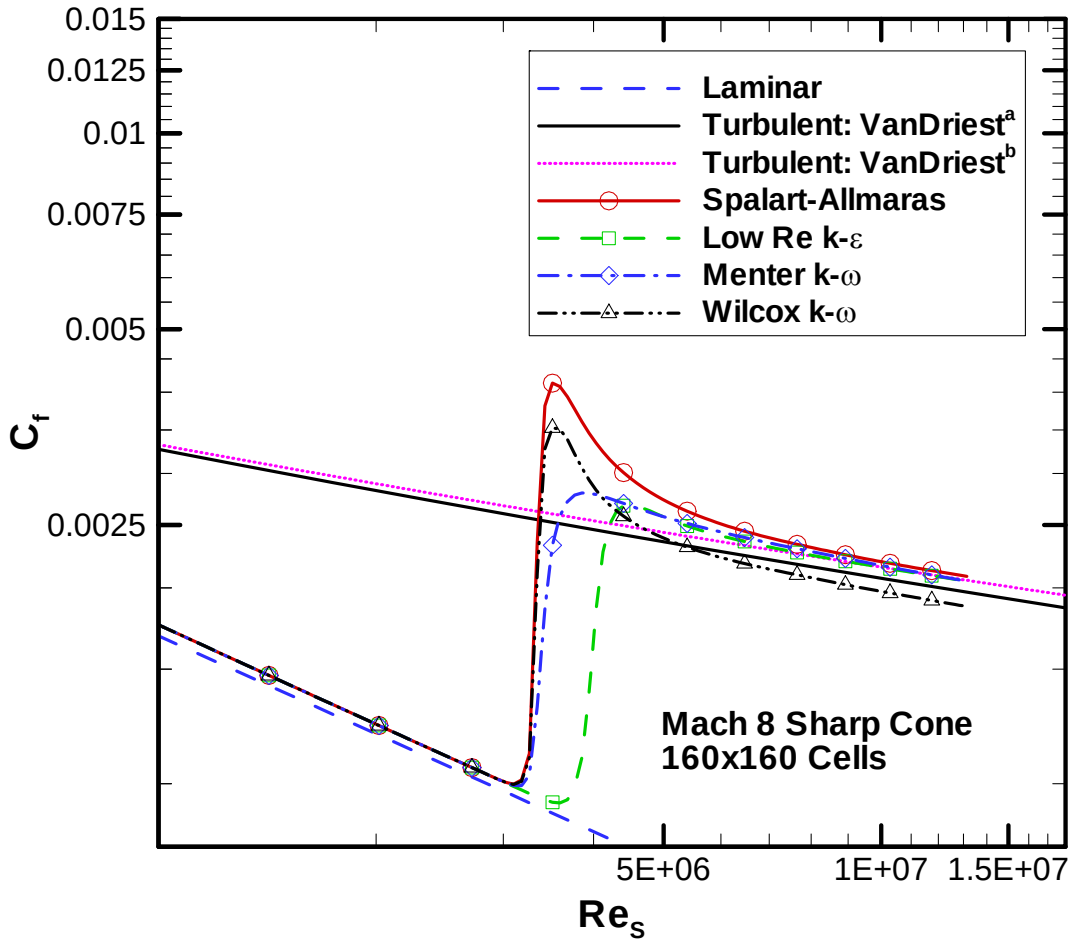

Fig. 2: Skin friction turbulence model comparisons for Case 10: Sharp Circular Cone (correlations are Van Driest[a] [74] and White's cone rule[b] [75]).

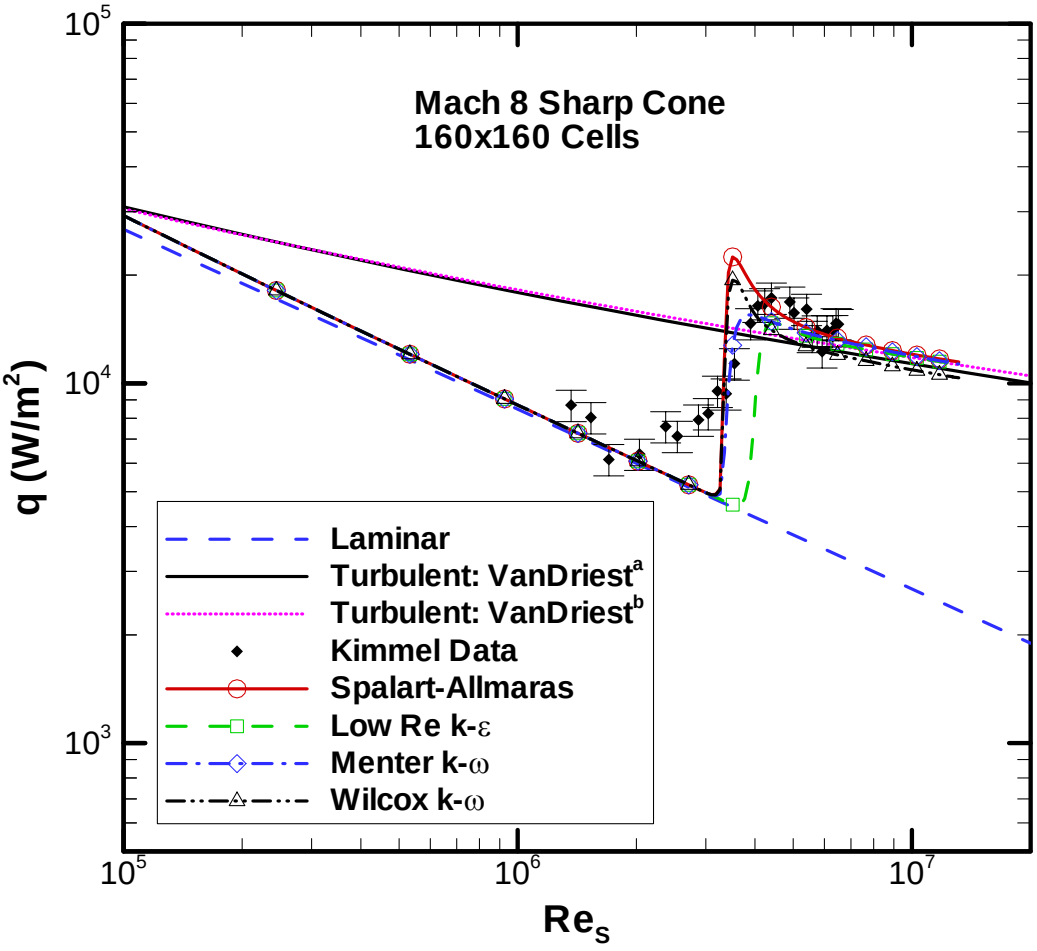

Fig. 3: Surface heat flux turbulence model comparisons for Case 10: Sharp Circular Cone (correlations are Van Driest[a] [74] and White's cone rule[b] [75] and experiment by Kimmel [119], [120]).

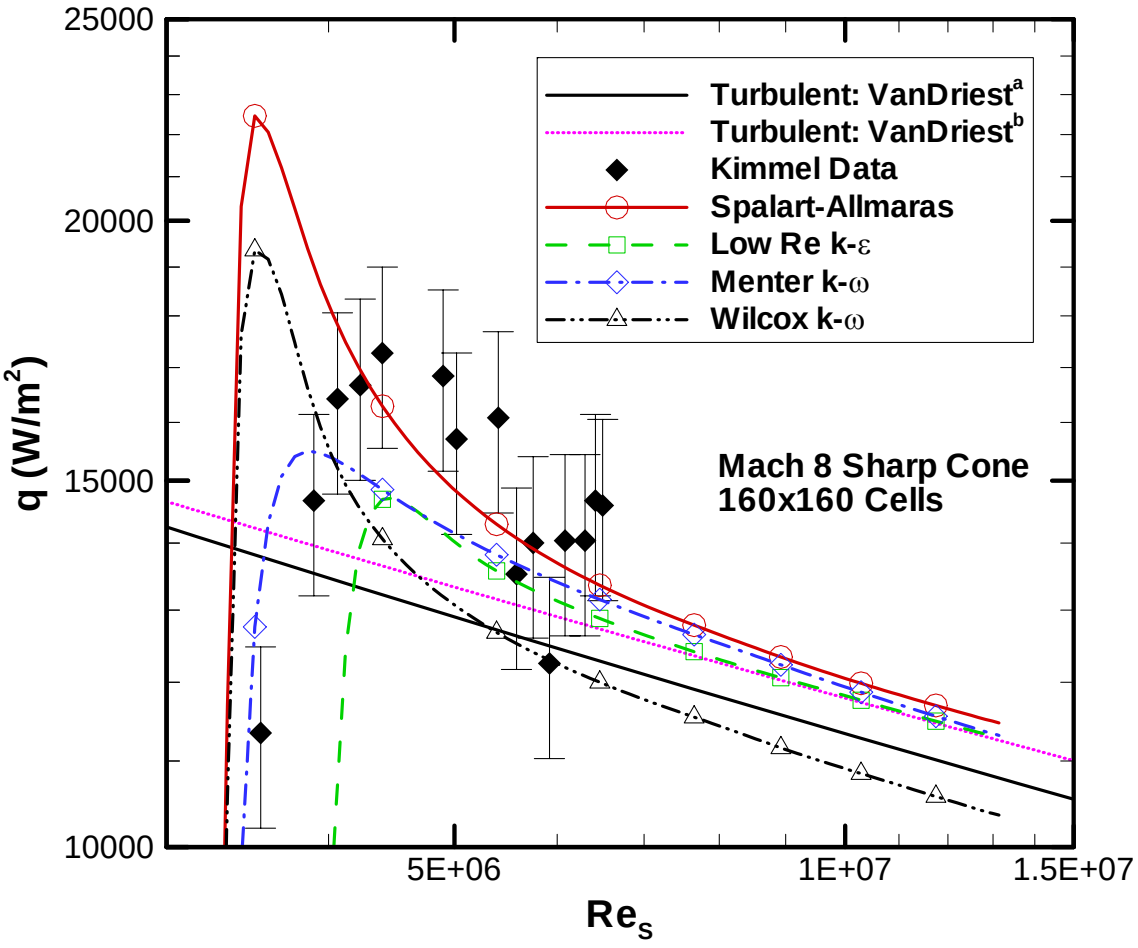

Fig. 4: Surface heat flux turbulence model comparisons (enlarged view) for Case 10: Sharp Circular Cone (correlations are Van Driest[a] [74] and White's cone rule[b] [75] and experiment by Kimmel [119], [120]).

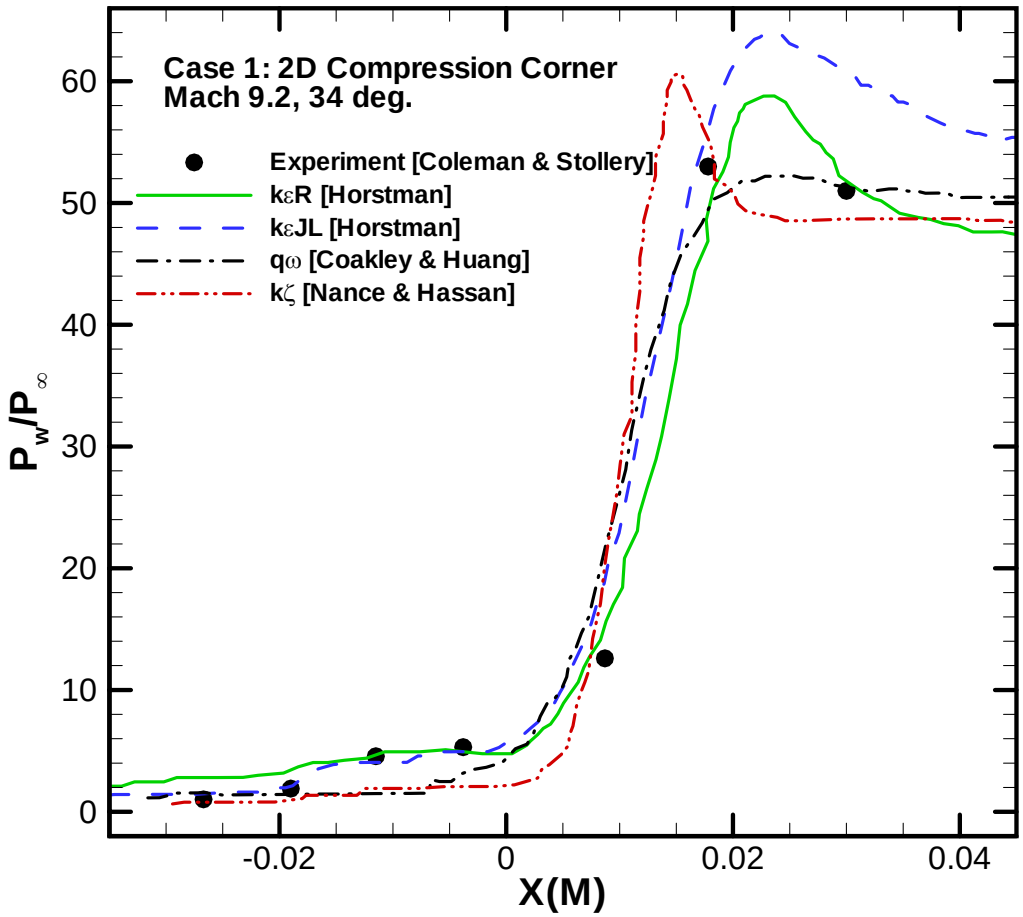

Fig. 5: Surface pressure turbulence model comparisons (part 1) for Case 1: 2D Compression Corner at 34 deg (experiment by Elfstrom [95]).

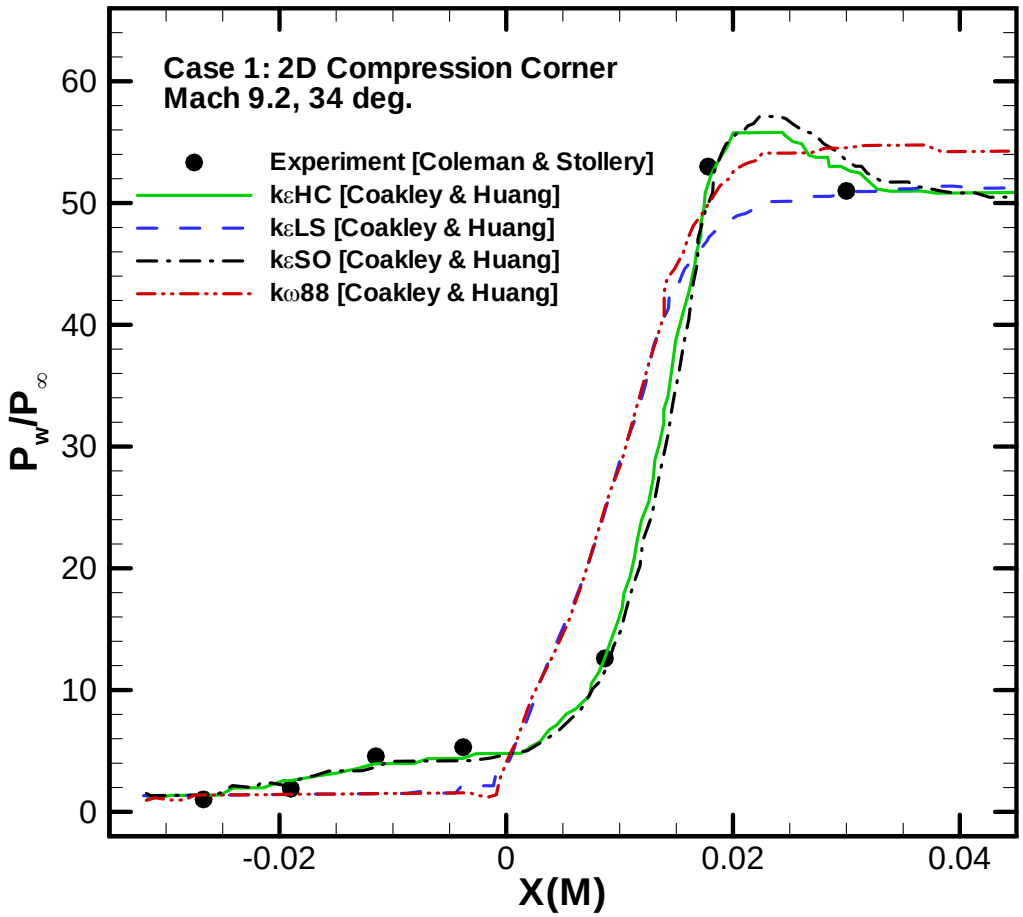

Fig. 6: Surface pressure turbulence model comparisons (part 2) for Case 1: 2D Compression Corner at 34 deg (experiment by Elfstrom [95]).

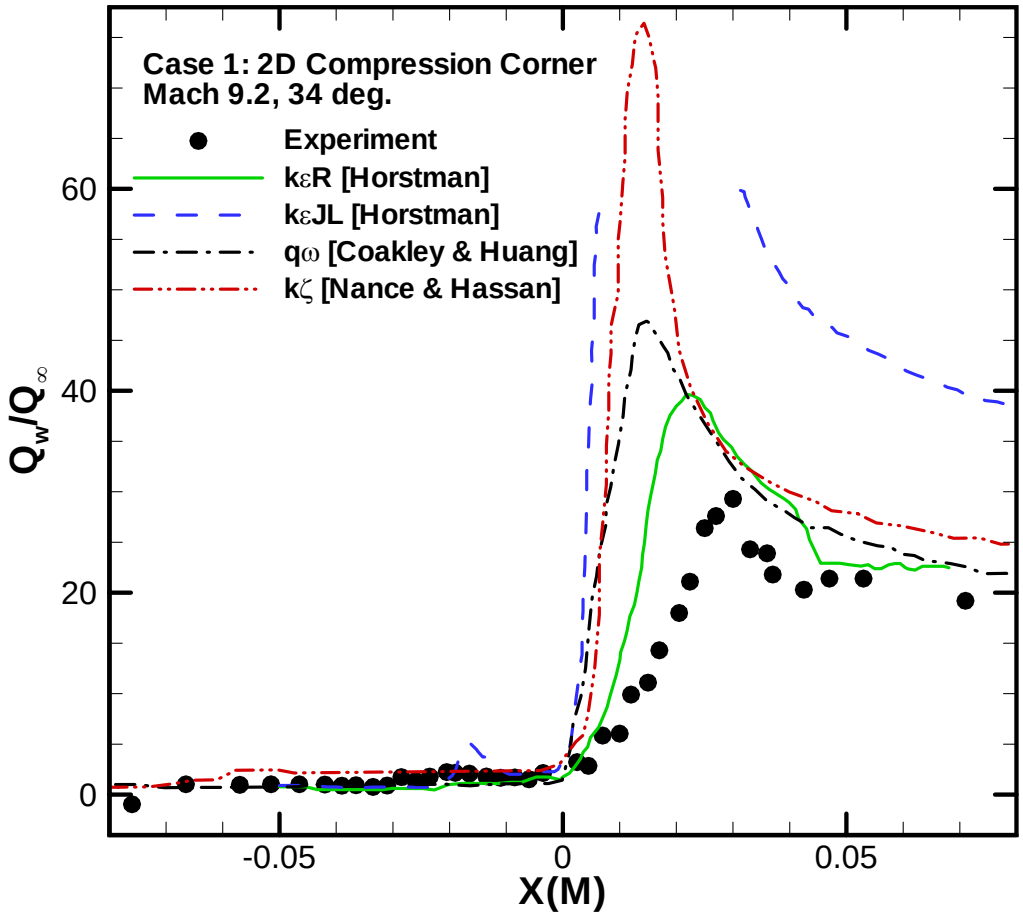

Fig. 7: Surface heat flux turbulence model comparisons (part 1) for Case 1: 2D Compression Corner at 34 deg. (experiment by Coleman and Stollery [33]).

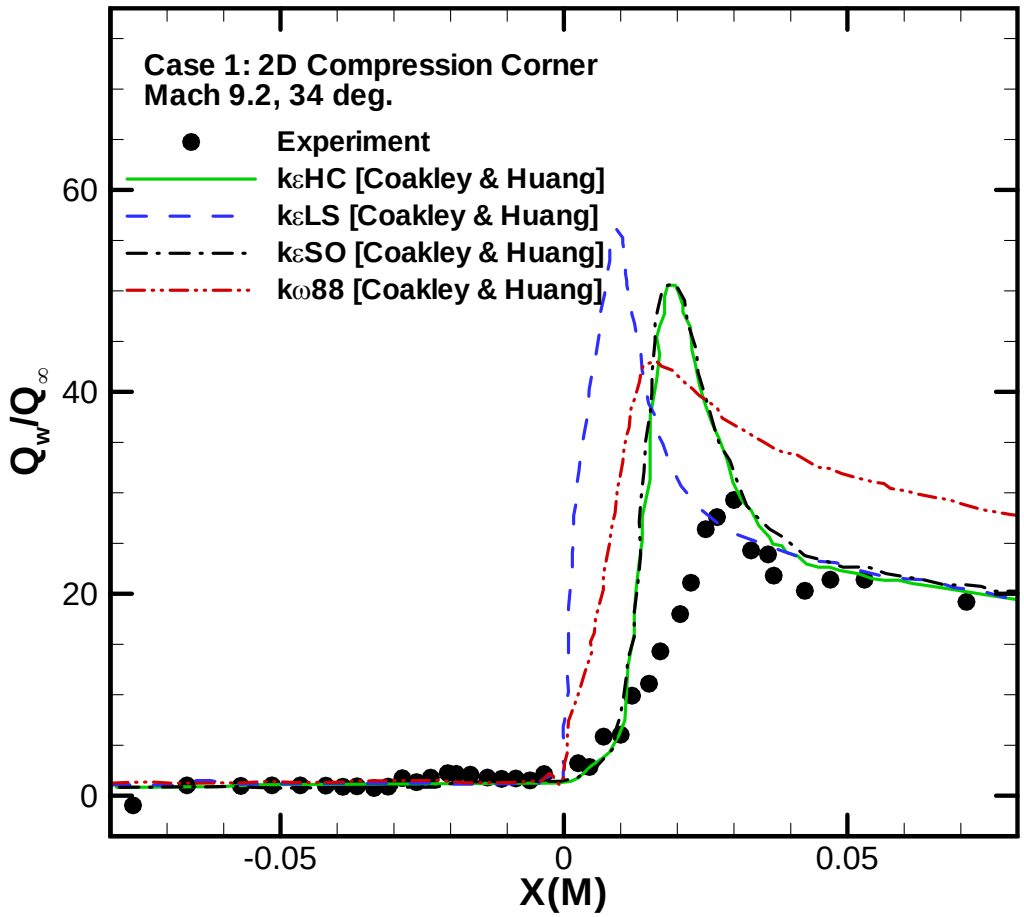

Fig. 8: Surface heat flux turbulence model comparisons (part 2) for Case 1: 2D Compression Corner at 34 deg. (experiment by Coleman and Stollery [33]).

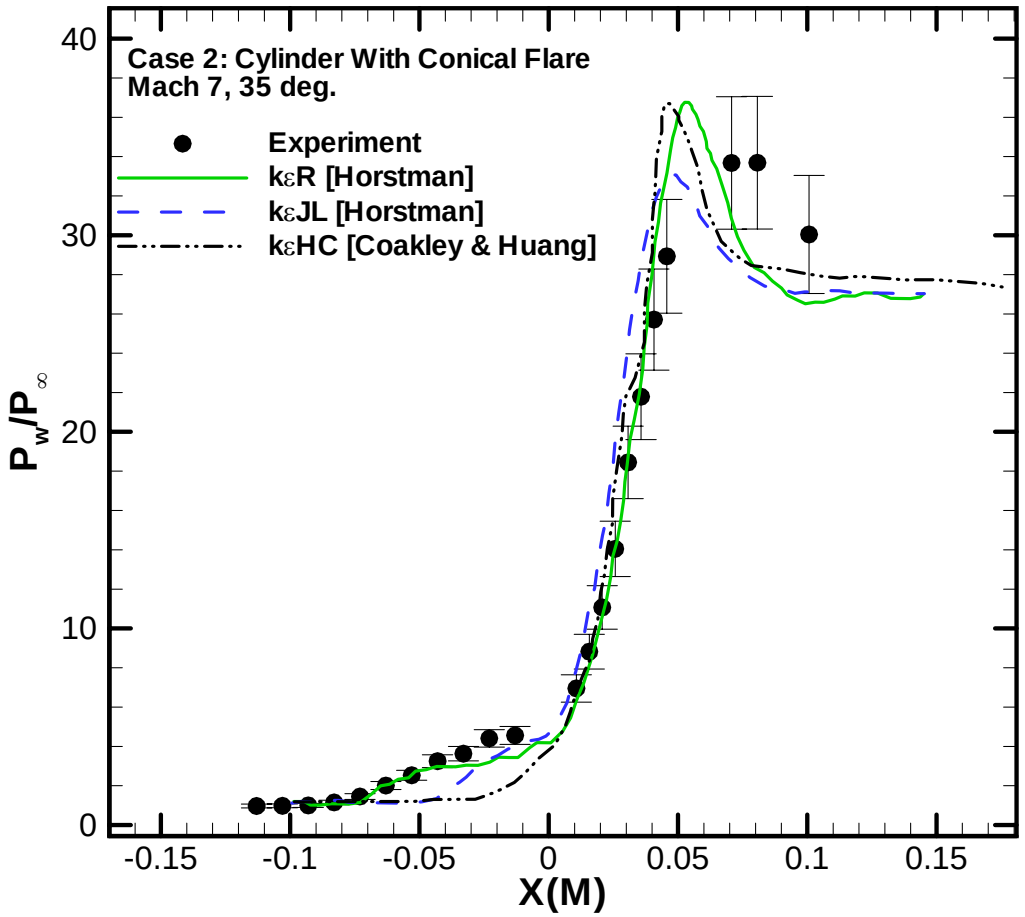

Fig. 9: Surface pressure turbulence model comparisons (part 1) for Case 2: Cylinder with Conical Flare at 35 deg. (experiment by Kussoy and Horstman [34]).

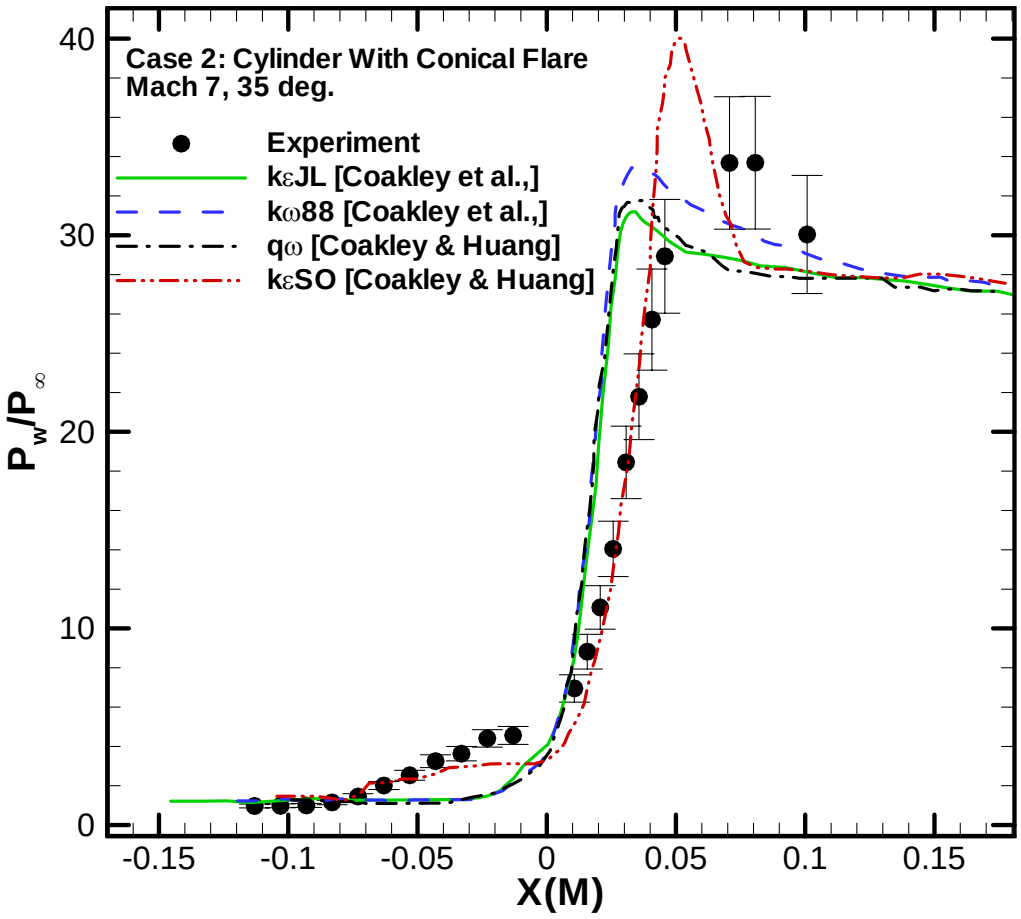

Fig. 10: Surface pressure turbulence model comparisons (part 2) for Case 2: Cylinder with Conical Flare at 35 deg. (experiment by Kussoy and Horstman [34]).

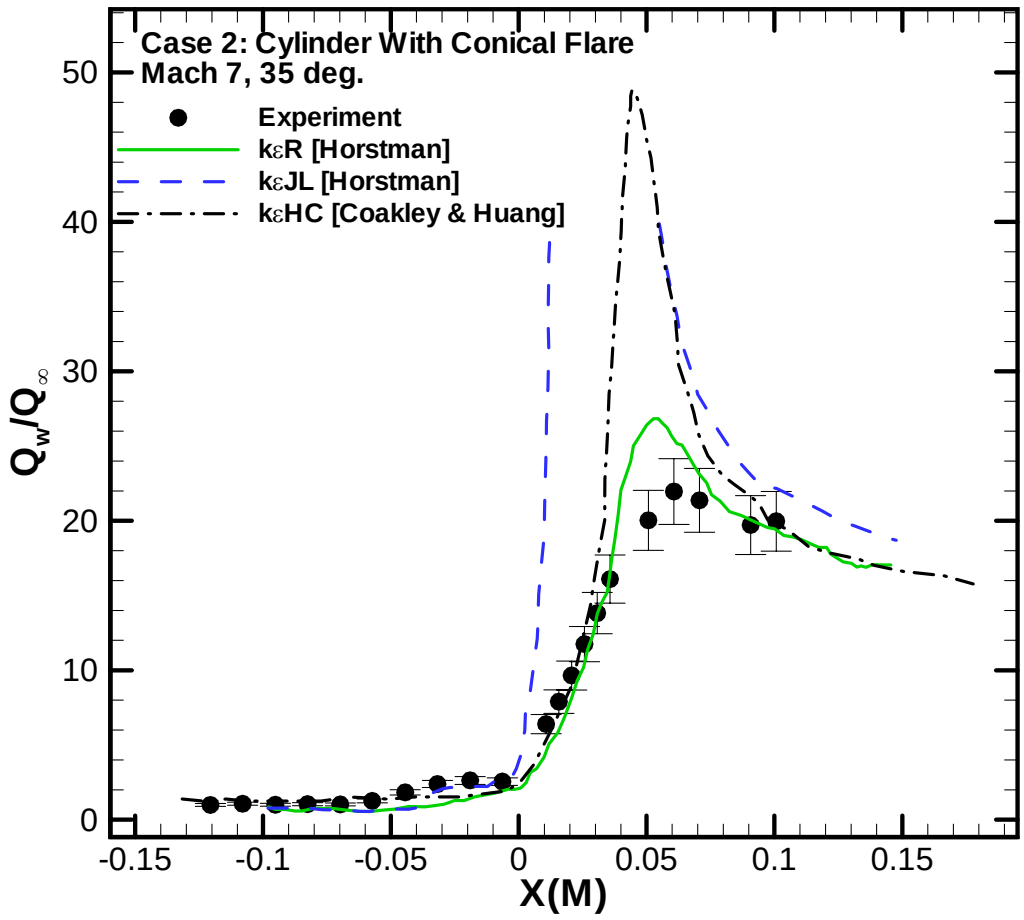

Fig. 11: Surface heat flux turbulence model comparisons (part 1) for Case 2: Cylinder with Conical Flare at 35 deg. (experiment by Kussoy and Horstman [34]).

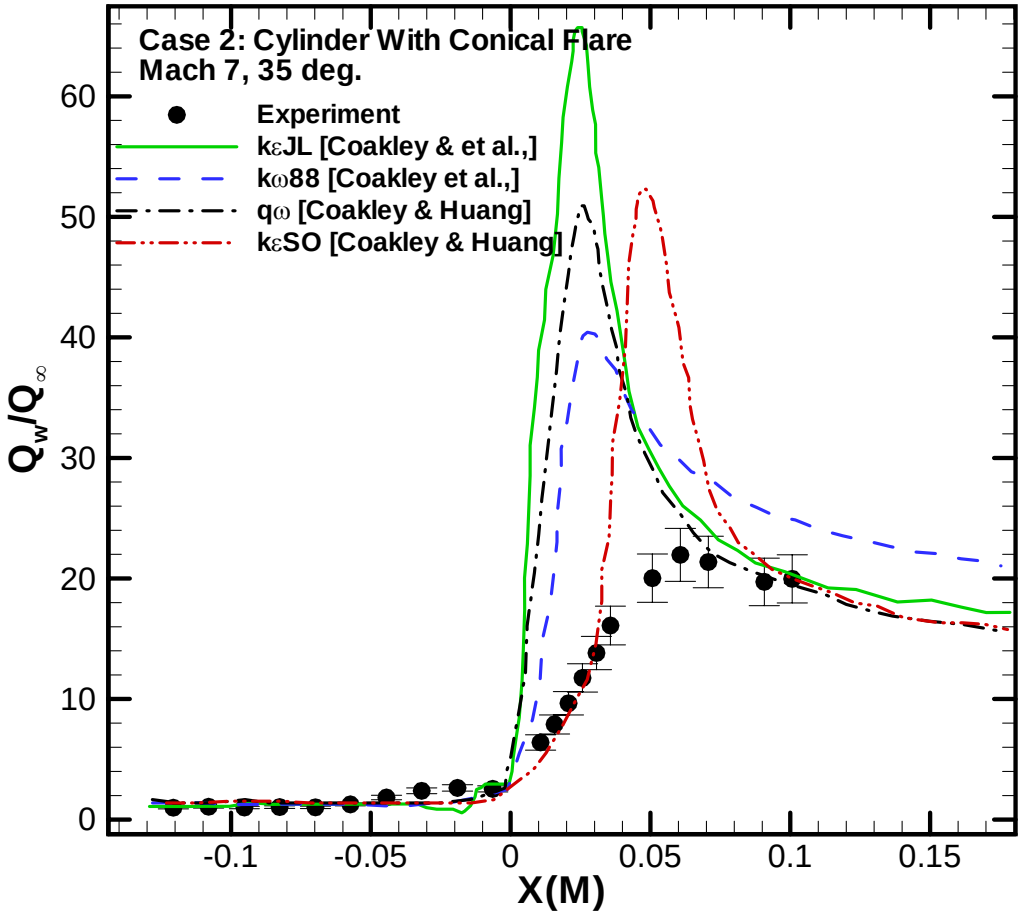

Fig. 12: Surface heat flux turbulence model comparisons (part 2) for Case 2: Cylinder with Conical Flare at 35 deg. (experiment by Kussoy and Horstman [34]).

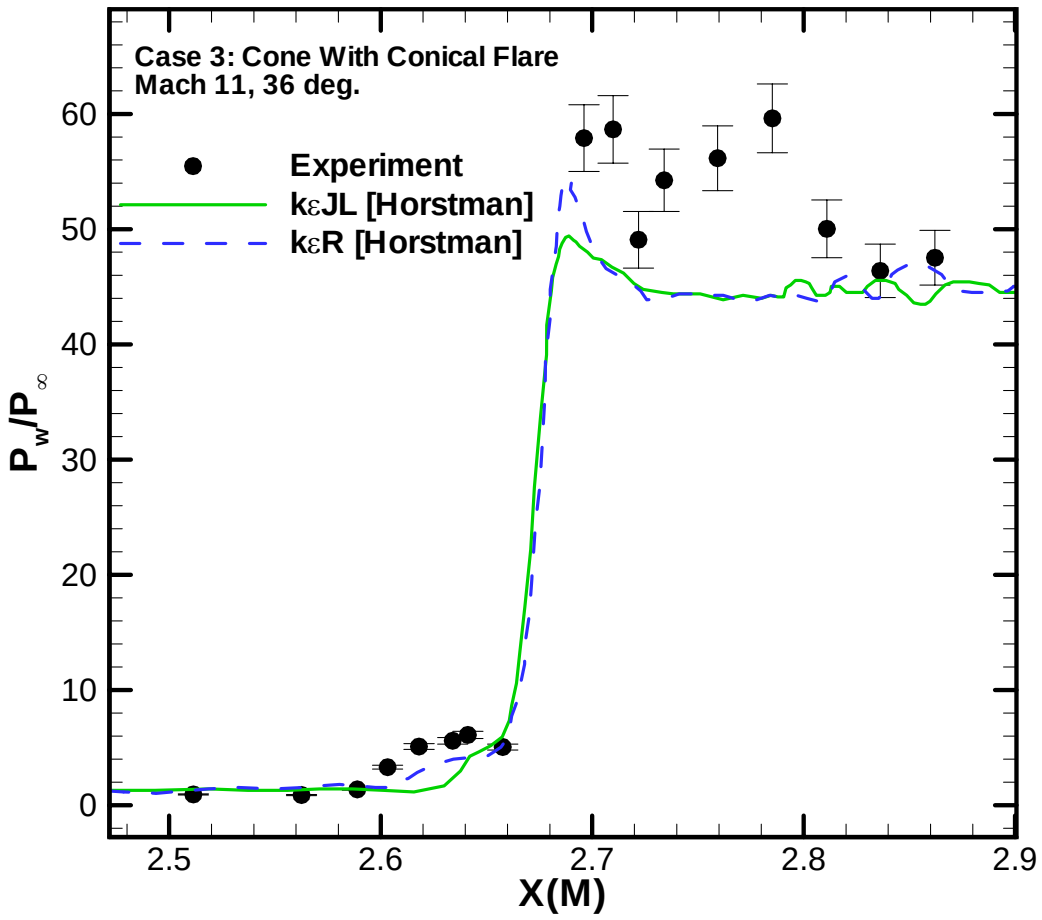

Fig. 13: Surface pressure turbulence model comparisons for Case 3: Cone with Conical Flare at 36 deg. (experiment by Holden [44]).

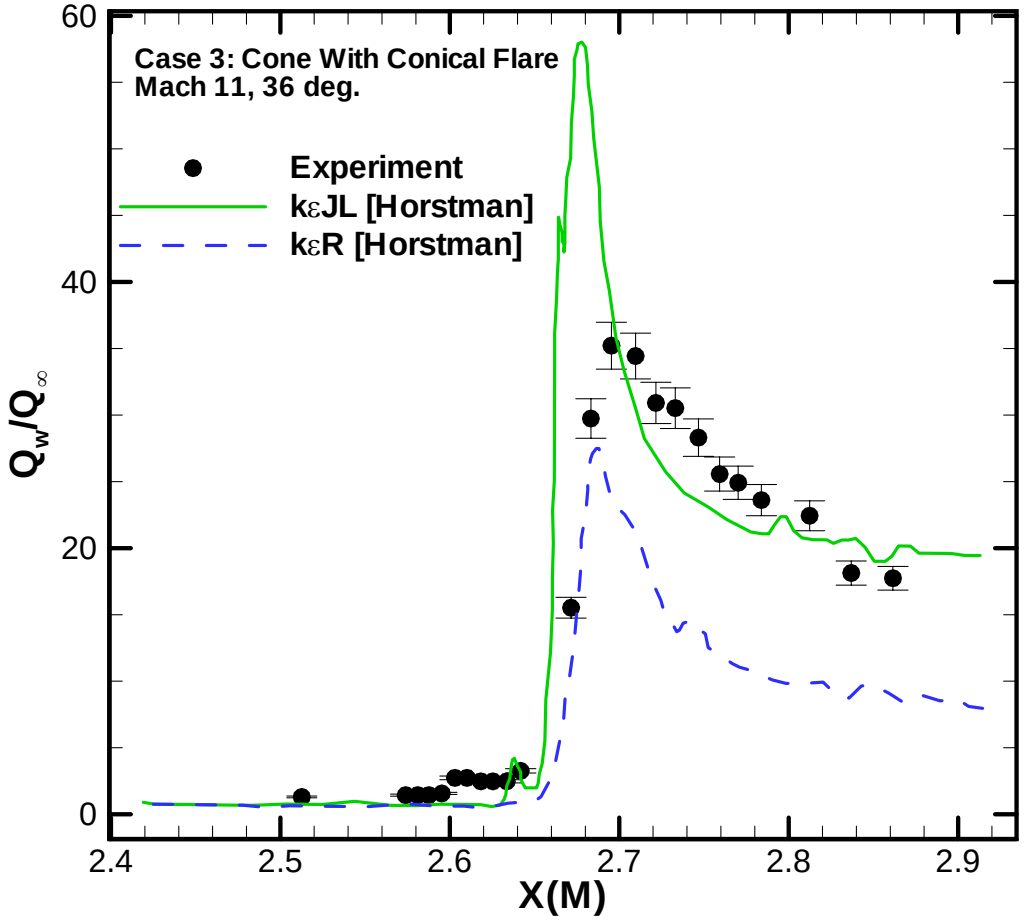

Fig. 14: Surface heat flux turbulence model comparisons for Case 3: Cone with Conical Flare at 36 deg. (experiment by Holden [44]).

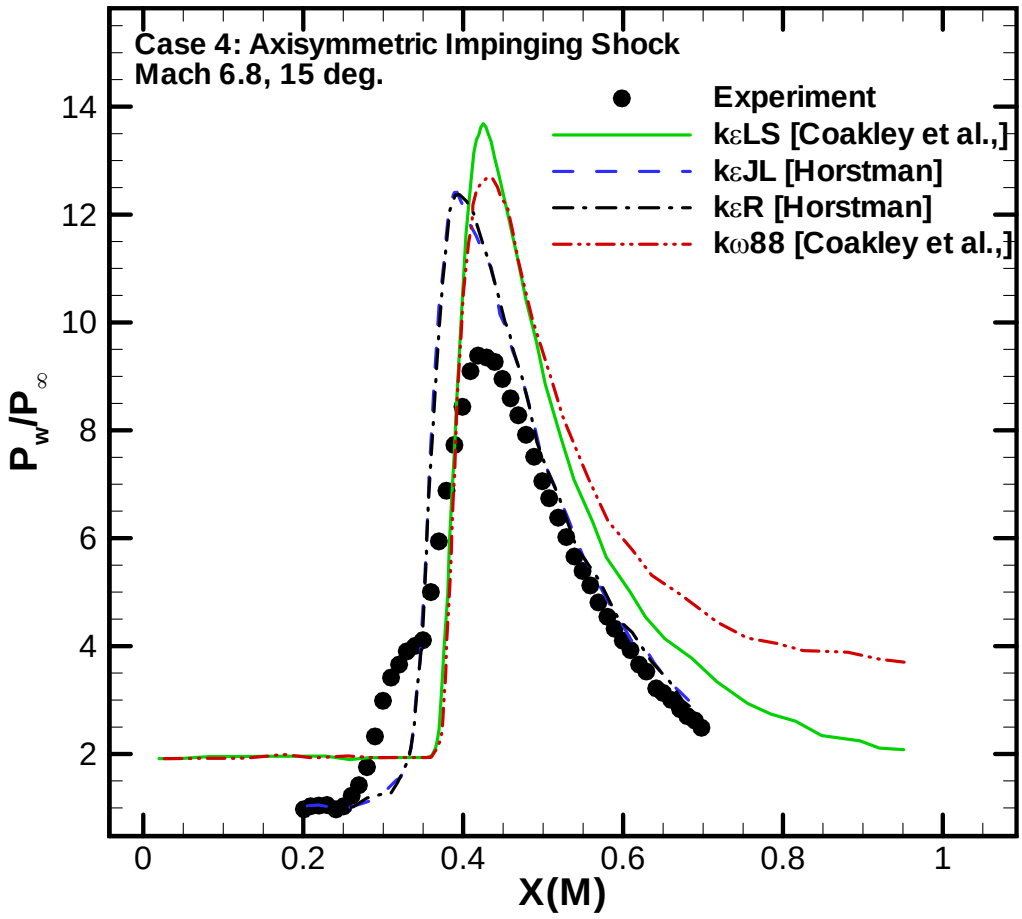

Fig. 15: Surface pressure turbulence model comparisons for Case 4: Axisymmetric Impinging Shock at 15 deg. (experiment by Kussoy and Horstman [37], [164]).

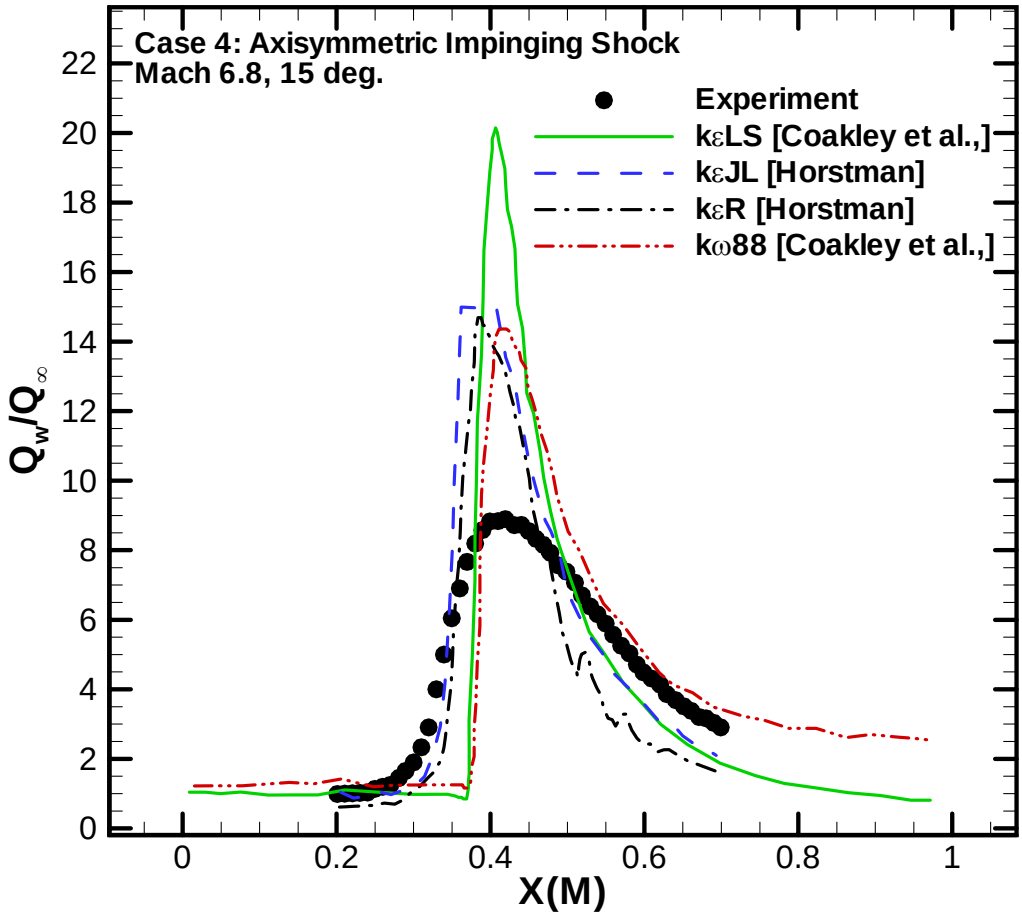

Fig. 16: Surface heat flux turbulence model comparisons for Case 4: Axisymmetric Impinging Shock at 15 deg. (experiment by Kussoy and Horstman [37], [164]).

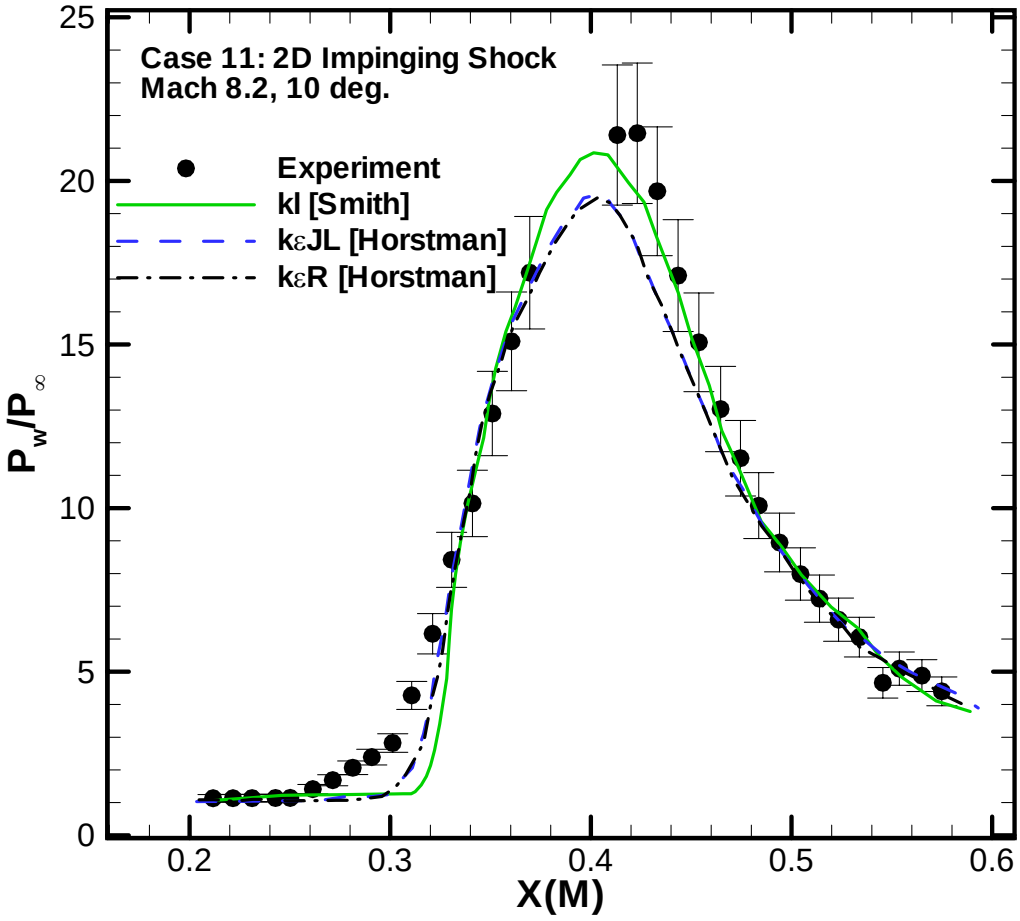

Fig. 17: Surface pressure turbulence model comparisons for Case 11: 2D Impinging Shock at 10 deg. (experiment by Kussoy and Horstman [40]).

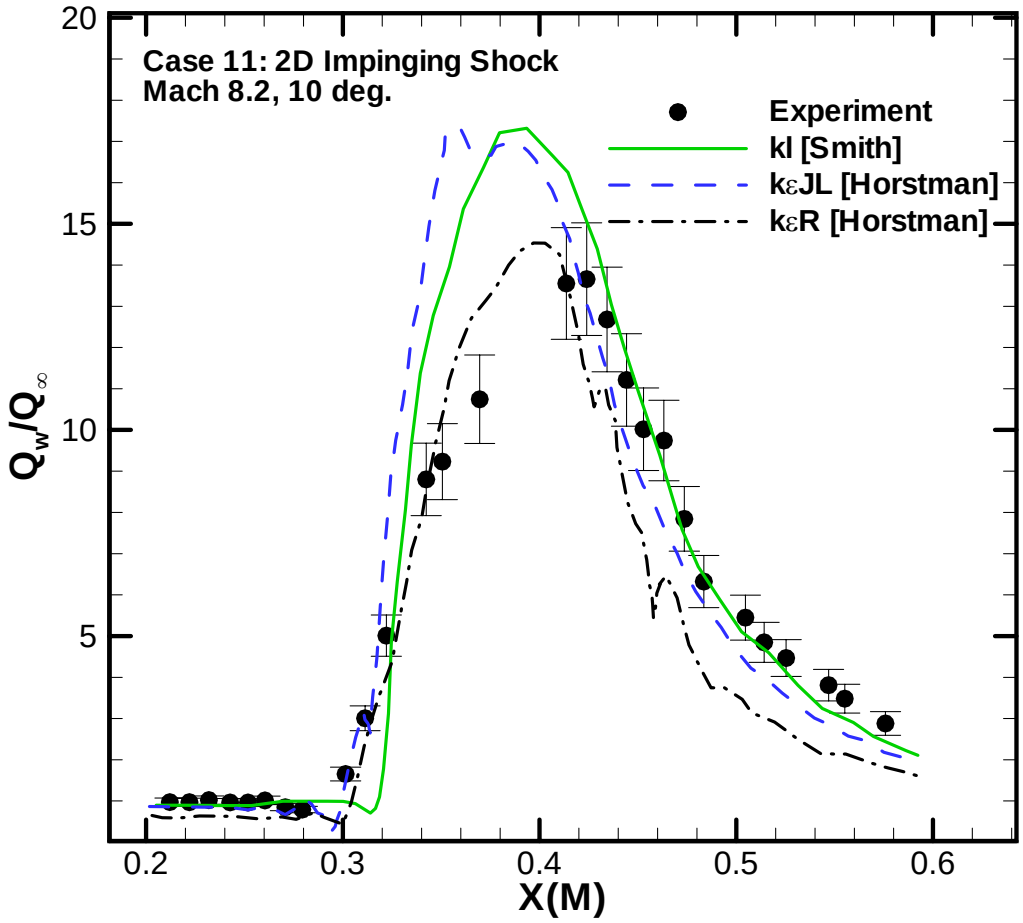

Fig. 18: Surface heat flux turbulence model comparisons for Case 11: 2D Impinging Shock at 10 deg. (experiment by Kussoy and Horstman [40]).